NASA CR-72602
TRW ER-7419

NONDESTRUCTIVE FLAW DEFINITION TECHNIQUES FOR CRITICAL DEFECT DETERMINATION

By

FRANK J. SATTLER

TRW Inc.
Equipment Group
Materials Technology

Prepared for

NATIONAL AERONAUTICS AND SPACE ADMINISTRATION

NASA Lewis Research Center
Contract NAS 3-11221

Project Managers
Raymond F. Lark
Richard N. Johnson

NASA CR-72602
TRW ER-7419

FINAL REPORT

NONDESTRUCTIVE FLAW DEFINITION TECHNIQUES FOR CRITICAL DEFECT DETERMINATION

by

Frank J. Sattler

prepared for

National Aeronautics and Space Administration

January 1970

Contract NAS 3-11221

Technical Management
NASA Lewis Research Center
Cleveland, Ohio
Chemical Rocket Division

Raymond F. Lark
Richard N. Johnson

TRW Equipment Group
Materials Technology
23555 Euclid Avenue
Cleveland, Ohio 44117

FOREWORD

This final report summarizes all work performed under NASA Lewis Research Center Contract NAS 3-11221 from May 1, 1968 to September 30, 1969.

Mr. Richard N. Johnson and Raymond F. Lark of NASA-LeRC were project managers. Mr. Frank J. Sattler of TRW was program manager.

Other TRW personnel involved in this work were:

J.M. Gerken (Welding)
R.V. Heckman (Specimen Preparation)
C.R. Honeycutt (Data Analysis)
E.A. Steigerwald (Fracture Mechanics Consultation)

ACKNOWLEDGEMENTS

The weld specimens were prepared by J.B. Bell. Particular credit should go to E.J. Hotko who prepared the fatigue cracked specimens and performed the radiographic, tensile tests and data correlations; and to J. Touhalisky who performed the penetrant and ultrasonic inspections. K.J. Hannah of Automation Industries authored the original report on the delta technique included as part of this report.

ABSTRACT

The accuracy of radiographic, penetrant, ultrasonic shear-wave and ultrasonic delta inspection methods were evaluated on defect specimens made from 2014 and 2219 aluminum, and 5Al-2.5Sn and 6Al-4V titanium alloys. The accuracies of these test methods are compared for these alloys at nominal section thicknesses of 0.020, 0.125, 0.500 and 1.000-inches. The penetrant test method provided the most accurate test to determine defect length in all but the 0.5 and 1.0-inch aluminum specimens. Radiographic inspections provided the best accuracy in the 0.5 and 1.0-inch aluminum specimens. None of the test methods had sufficient accuracy in determining critical crack depths as determined from fracture toughness calculations. The effects of stress conditions on the detectability of defect dimensions was evaluated. Fracture toughness calculations were made from the defect dimensions and tensile test data on the specimens.

SUMMARY

This program was initiated to evaluate nondestructive testing methods capable of detecting critical-defect dir sions in aluminum and titanium alloys. The critical-defect dimensions are used calculate fracture toughness data for materials in determining the effects of defects on the material's performance. The object of this work was to determine the ability of conventional nondestructive tests to detect and to evaluate the defect dimensions. The work included a review of nondestructive tests applicable to tight defects such as incomplete weld penetration and fatigue cracks. A study was conducted of the effect of stress states on ultrasonic shear-wave measurements. Ultrasonic shear and delta tests were performed on the defect specimens, along with fluorescent penetrant and radiographic tests. Tensile tests were performed on the defect specimens to reveal the actual defect geometries and to determine fracture toughness values for the specimens. The actual defect measurement data were correlated with the various NDT measurements for various thicknesses (0,020, 0.125, 0.500 and 1.0-inch 2014-T6 and 2219-T87 aluminum, and 0.020, 0.125 and 0.500-inch extra low interstitial 5Al-2.5Sn and 6Al-4V titanium) of four alloys.

Analysis of the nondestructive test results showed that fluorescent penetrants provided the most accurate test method for determining crack length in 0.020 and 0.125-inch aluminum and in all of the titanium alloy thicknesses. The 3σ variation for the penetrant tests ranged between $\pm$0.021 and $\pm$0.067-inch for these specimens. No penetrant indications were obtained from the fatigue cracks in the 0.5 and 1.0-inch aluminum specimens. Ultrasonic shear-wave tests provided the best 3σ limits ($\pm$0.246-inch) on the 0.5-inch aluminum specimens; and radiographic tests provided a $\pm$0.164-inch 3σ limit on the 1.0-inch aluminum specimens. The maximum actual crack length at zero indicated length with the given 3σ limit variation was much larger for these latter two test methods. The results for crack-length determinations are not adequate for the 0.5 and 1.0-inch aluminum specimens. For crack depth measurements, although the accuracies in some instances were lower than those for the best crack-length measurements, the accuracy combined with the maximum possible actual depth for zero indicated depth for the ultrasonic tests were not adequate to define the depth, compared to the crack depths calculated from fracture toughness theory. When broken in the tensile tests, the 2219 aluminum specimen fatigue cracks revealed delaminations perpendicular to the fatigue cracks. These defects undoubtedly were responsible for the poor test accuracy in the two ultrasonic tests.

The ultrasonic shear-wave tests performed on defects under varying stress revealed rather large changes in the indicated signals. For the aluminum specimens, the ultrasonic signals showed a decrease in signal strength from a zero stress condition to applied compressive stress levels of about 1/2 the yield stress. When these signals were compared with signals from artifical notches, the variation between the smallest and largest notch-depth signals was in the same range of signal variation as that resulting from stress variation. The ratio of notch depths (largest to the smallest) was 6:1. A large variation in signal amplitude occurred for a titanium specimen stressed in tension and compression. Two gain settings were necessary on the ultrasonic instrument to cover the full range of signal amplitudes. These tests may help

to explain the low accuracies developed in the ultrasonic tests, since any residual stresses on the defects will vary the defect's response.

Present nondestructive tests are of limited use for critical crack measurements. Improved testing techniques are necessary in order to achieve better measurement accuracy.

TABLE OF CONTENTS

TABLE OF CONTENTS (Cont'd.)

I - INTRODUCTION

The inability of conventional design approaches, such as maximum tensile or shear strength to predict failure, has led to the development and application of fracture mechanics theory. Fracture mechanics provides a quantitative method for evaluating material reliability in the presence of defects of known size and distribution. On the basis of this theory, the contribution of specimen geometry to notch strength can be predicted, and the fracture toughness, as determined from laboratory tests, can be used to evaluate material performance in full-size structures.

Through the use of fracture mechanics theory and fracture toughness determinations, a material's propensity to fail in a brittle manner can be determined. It is possible to predict with this theory, the size of defects which will cause failure in a structure. Knowing these defect sizes, meaningful acceptance or rejection criteria can be established for a particular thickness of material, taking into account its fracture toughness properties. However, it is of utmost importance to characterize completely the defects present in a structure in order to accurately predict its performance. For this latter reason, nondestructive test methods capable of resolving critical size defects are a necessity. A further requirement is for nondestructive test methods which will accurately define the defect geometry so that critical length and depth variables can be differentiated. Many types of nondestructive tests have been developed to find defects but little attention has been paid to determining their precise dimensions and shapes.

Nondestructive tests have been utilized by Packman, et al (1)* to measure critical flaw dimensions in materials. This work reviewed several nondestructive test methods and detailed their utility in finding cracks of critical size. The evaluation of radiographic, ultrasonic, penetrant and magnetic particle methods to determine crack length was performed in this study on 4330 steel and 7075 aluminum. The inability of nondestructive tests to determine accurate crack lengths below 0.1-inch was reported.

Since titanium and aluminum alloys are potentially useful for pressure vessel applications, nondestructive tests on these materials to define defect geometry are of considerable interest. This program to study the applicability of nondestructive tests in revealing critical defects was initiated in May of 1968; first to define applicable test methods, and then, to evaluate the most promising test techniques. In order to evaluate the test methods, weld and crack defect specimens were prepared in 2219-T87 and 2014-T6 aluminum and ELI** 6Al-4V and 5Al-2.5Sn titanium alloys. In order to accomplish the program objectives, the following tasks were performed:

---

* - numbers in parentheses refer to references listed in References.

** - extra low interstitial.

1. Conduct a review and preliminary evaluation of nondestructive tests applicable to tight defects.

2. Fabricate defect specimens.

3. Perform nondestructive tests on defect specimens.

4. Evaluate effects of stress state on defect measurement.

5. Perform tensile tests for fracture toughness determinations.

6. Evaluate and correlate test data.

II - NDT SURVEY AND SPECIMEN FABRICATION

Many types of nondestructive tests are employed in industry to detect material inhomogenieties such as cracks, voids, inclusions or other material variability. These test methods utilize some type of probing medium which interacts with the material inhomogeniety, resulting in an alteration of probing energy or probing matter. The inspection is completed by detecting the alterations and determining what has been its cause. Available nondestructive tests range from simple visual tests to very elaborate techniques utilizing automated systems. A wealth of information is available on various testing techniques and is compiled in two volumes of the Nondestructive Testing Handbook (2).

Additional information has been generated since these books were printed and is available in the publication Materials Evaluation, or its predecessor, the Nondestructive Testing Journal, publications of the American Society for Nondestructive Testing. The large number of available testing methods indicate that no one method has solved all quality control problems. Indeed, the wide variety of engineering materials in use present a large range of physical variability, so that testing techniques which work well for one material, often fail on another. Quite often different types of defects will cause sufficient test variability to render an inspection method unreliable for a particular type of defect.

Finding defects on the one hand, and determining their size and shape on the other, can be two different problems. Almost all of the test methods available are orientation sensitive. Testing techniques, in general, have a maximum sensitivity to defects oriented in a particular plane. This is true for radiographic as well as ultrasonic tests. Penetrant tests are limited to surface defects or surface connected defects.

In evaluating any nondestructive test, it is important that realistic defects be used so that they represent not only possible structural defects but ones that also tax the detection capabilities of the test methods. The most common types of defects encountered in cryogenic tanks and pressure vessels are cracks and weld defects. Among the most difficult types of defects to detect in materials are fatigue cracks initiated by sharp stress risers and lack of penetration in welds. This section will review possible nondestructive test methods and will describe some preliminary experiments performed to select optimum conventional test methods; a description of the test specimens which were produced with specific defects is also included.

A. Nondestructive Test Review

1. Penetrants

Penetrant testing is one of the oldest nondestructive tests in use today. This inspection method is very sensitive for detection of surface defects such as cracks, pores, seams, laps and folds. Two types of penetrant inspection are in common usage. Dye penetrants are applied to structures when reduced sensitivity can be tolerated because of the ease of using this inspection method. Fluorescent penetrant methods are used for very critical inspections where extreme sensitivity is desirable.

Penetrants are applied to the surface of test objects and are drawn into small surface openings by capillary action. Excessive penetrant is washed away after a suitable exposure time. The part is dried and a developer is applied which pulls residual penetrant from the cavities; in some inspections, the developer may be omitted. The developer acts as a blotter pulling penetrant from the cavities and spreading it out from the defect edges. Fluorescent penetrant oils contain particles which emit visible light when they absorb ultraviolet radiations, providing for increased contrast against an otherwise dark background. Micro size cracks as well as grain boundary porosity have been detected with fluorescent penetrant methods.

There are many factors which influence the sensitivity of this test method. These include the surface condition of the part and the crack, the capillarity of the penetrant, the wetting ability of the penetrant, and the dimensions and shape of the defect. All these factors influence the detectability of a given defect, in addition to the variability of inspection personnel. There are many penetrants and their associated emulsifiers and developers available on the market from many different manufacturers.

Evaluation of penetrants is an arduous and difficult process where no concrete quantitative methods of comparison have been developed and accepted. Each manufacturer has devised tests for the evaluations of their own penetrants. Many different types of cracked block samples have been used by various individuals with varying degrees of success. Crack blocks have limited use since it is almost impossible to wash the penetrant from a crack once it has penetrated. This condition then limits accurate comparison of one penetrant against another since the crack is not always the same in replicate specimens.

The principles of penetrant usage have been detailed by Betts (3), Thomas (4) and many others. One of the most comprehensive studies of penetrant penetration was conducted by McCauley and Van Winkle (5) under Air Force sponsorship. They defined two relationships which are used to indicate the penetrant penetrability. One of these is the free energy of immersion, which is equal to the surface tension at a vapor-liquid interface times the cosine of the contact angle (θ). This theory presumes that the penetrant covering the surface of the part decreases surface energy and penetrates cracks. This quantity, the static penetrability parameter, is reported to be a measure of the force that drives penetrants into cracks, dislodging entrapped air and absorbing it at the interface.

The other relationship which was obtained from the work of McCauley, et.al., was that of a crack detection efficiency of the penetrant. This relationship was established by using cracked chromium test plates and counting the cracks in a given area under high magnification. Skoglund and Magdalin (6) have questioned the use of either of these parameters in evaluating penetrants since neither coefficient relates to the other. They point out that other researchers have argued that penetration is based on the interaction of the penetrant with the walls of the crack and not merely on the separation of the walls of the crack as the McCauley and VanWinkle work suggests. The Air Force work and other sources suggest that some media penetrate into tighter cracks more readily than in wider cracks. The validity of the latter idea is not confirmed by experimental studies on cracked specimens since finer cracks are more difficult to detect than their wider counterparts in the same plates. Skoglund and Magdalin have suggested and utilized a Gallespian approach to evaluating penetrants. They point out that penetrability implies an equilibrium of the

forces involved in penetration. The force which places the penetrant into a crack and the resisting forces are at equilibrium. They also point out that the resisting forces are greater in very narrow sections of the crack or in tight cracks. Viscosity is stated to have little effect on the penetration since it is a dynamic force having no influence on the static system in equilibrium. Work must be done in order to compress the air in a crack and they feel that, to a large extent, this is the resisting force in penetration. They point out though that it is not obvious what force actually resists the penetration process at equilibrium. They concluded that the Gallespian approach appears very promising in evaluating penetrants although the application of this approach to actual cracks is not straight forward. A mathematical treatment of the parameters involved in penetrant testing, performed by Campbell and McMaster (7), suggests that the present achievable penetrant sensitivities are limited not by the penetrants but by the developers. They suggest that defects which do not have oxide coatings are much more difficult to detect than those with such coatings.

With all the conflicting information in the literature, it is difficult to select any one set of tests in order to evaluate penetrants. This was pointed out by Lomerson (8) who used statistical methods to evaluate penetrant sensitivity and reproducibility. This investigation revealed that some penetrants give rather large differences in the sensitivity at a given confidence level. This was also true of the inspectors who interpreted the actual indications. Although there were definite differences in penetrants brought out in this study, no brand names were listed identifying the penetrants.

For this present study, in order to select a suitable penetrant for fatigue-cracked specimens, evaluations were made of Magnaflux ZL-22 and ZL-30A and Tracer Tech P-151 penetrants. ZL-22 is a standard commercial penetrant widely used in the aircraft industry. Preliminary data on the detectability of cracks by penetrants were obtained using the three penetrants, one commercial developer and an experimental developer listed in Table I. For this work, three chromium-plated crack panels per Military Standard I-8963 containing fine, medium and coarse cracks were utilized. It was hoped that a suitable penetrant for dectection of surface cracks could be determined by this set of tests. Figure I shows the results of a series of these tests using the three penetrants and the Magnaflux ZP-4 developer. From these photographs, one might judge the ZL-22 penetrant to have better resolution capabilities. However, this was not confirmed on other sets of tests with the experimental developer and on the other two cracked panels, nor is it consistent with practical knowledge of these penetrants. From these evaluations, it was impossible to determine the optimum penetrant and developer for detecting the very tight, deep cracks of the type encountered in the fatigue-cracked specimens. No further analytical tests were made at this point since the crack panels were not representative of conditions encountered in the fatigue-cracked specimens.

2. Radiation Test Evaluation

The ability of short wavelength radiation to be attenuated by materials is the basis for many different radiation tests. The absorption of X and Gamma radiations is a function of the energy of the particular photons and the nuclear structure and density of the material. Many types of recording media may be used to detect the changes in radiation intensity. Among the more common methods are film, image intensifiers, fluoroscopic screens and

TABLE I

PENETRANTS AND DEVELOPERS FOR EVALUATION TESTS
ON
CRACKED CHROMIUM-PLATED TEST PANELS WITH EMULSIFIER

Penetrant	Developer
ZL-30A*	X
ZL-30A*	ZP-4*
ZL-22*	X
ZL-22*	ZP-4*
P-151**	X
P-151**	ZP-4*

* - Magnaflux Corporation Products
** - Tracer Tech Corporation Product

Penetration Time - 10 minutes
Emulsification Time - 30 seconds

X - Cabosil Silica

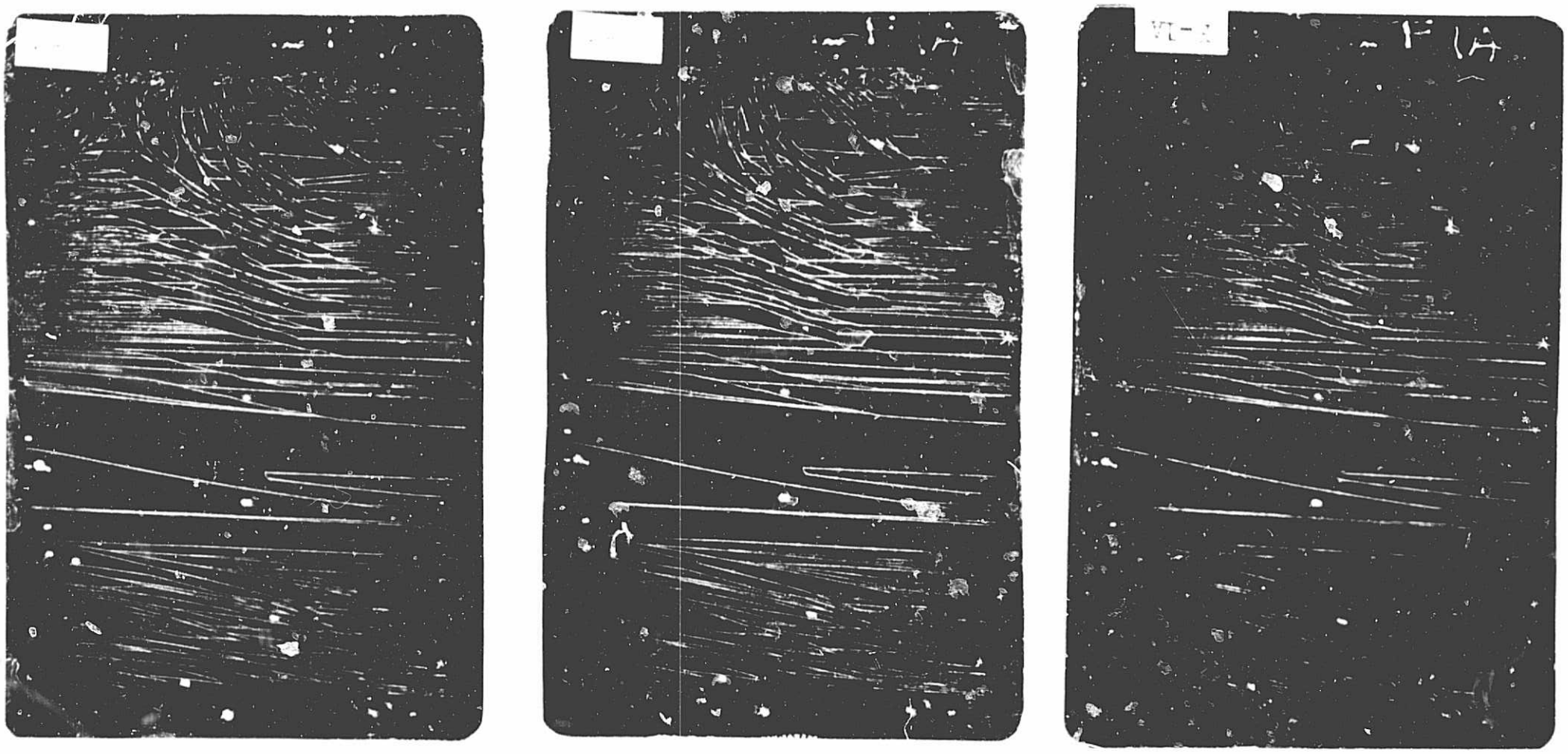

Figure 1. Fluorescent penetrant indications on a fine crack chromium coated test panel utilizing Magnaflux ZP-4 Developer. a) Magnaflux ZL-30A, b) Magnaflux ZL-22, and c) Tracer Tech P-151.

ion chamber and scintillation detectors. In general, the shorter the radiation wavelength, the greater will be its penetrating power. The basic law for radiation attenuation is given by the following equation:

$$I = I_o e^{-\mu x} \qquad (1)$$

I = transmitted radiation intensity through absorber

I_o = radiation intensity with no absorber

μ = linear attenuation coefficient

x = attenuating thickness

e = base of the natural logarithms

This equation which holds for monochromatic sources of radiation is approached in the case with isotopes and is a close approximation to the conditions which exist in X and gamma radiography.

Defects are revealed in radiographic testing by detecting changes in material density or thickness; the size discontinuity that can be detected is a function of both contrast and geometrical considerations. These two factors interact to produce the wide range of sensitivities available in the many radiographic tests. Radiographs with high contrast will not reveal small defects if the sharpness is poor and vice versa.

Image sharpness is a function of geometrical considerations, the resolution capability of the radiation detector and scattered radiation effects (9). The resolving power of radiographic film is determined by the grain size of the emulsion, while scattered radiation reduces image sharpness by the fogging of detail. Geometrical sharpness is derived directly from exposure geometry and the size of the focal spot or isotope source used in the radiographic procedure (10,11). The effects of the focal spot size on geometrical sharpness are related directly to the distance from defect to film, and to the size of the focal spot; the sharpness is also inversely proportional to the focus-film distance. Thin specimens result in very good geometric-sharpness values regardless of the focal-spot size. The thicker the section being radiographed, the poorer the sharpness becomes with a fixed focus and focal distance.

X-ray image contrast is one of the most important and least understood variables in radiography. A simple definition of contrast is the percentage change in thickness of the object under study that can be visualized in the radiographic image. The smaller this contrast value, the better the image quality. Material contrast is a function of both the linear attenuation coefficient (μ) and the thickness being radiographed. For a fixed source of low voltage radiation energy, contrast will increase with increasing thickness. If the thickness is fixed, increased contrast must be obtained by increasing the linear attenuation coefficient which is accomplished by lowering the radiation energy. No fixed standard is in use to evaluate radiographic techniques, other than the use of radiographic penetrameters. A method has been suggested for analysis of contrast, but as yet has little practical

application because the measurement is difficult and no correlations exist for the values generated (12).

In the present investigation, 6Al-4V and 5Al-2.5Sn titanium, up to one-half inch thick, was to be utilized, as well as, 2219 and 2014 aluminum in sizes up to one-inch thick. These thicknesses for both alloys required low-voltage X-ray techniques. Several types of radiation detection systems were investigated in order to determine the relative merits of each system. The X-ray methods investigated were: 1) conventional X-ray film, 2) microradiographic film, and 3) vidicon X-ray television-imaging systems. Other imaging methods such as direct fluoroscopic and fluoroscopic image-enhancement methods were not considered because of the known lower resolution capabilities of these methods. In this investigation, only the techniques which give optimum resolution were considered. Only X-ray techniques with the greatest resolution capabilities have any hope of visualizing a tight crack or incomplete weld penetration. In order to obtain optimum resolution and contrast, beryllium window X-ray units with small focal spots are mandatory (13).

a. Vidicon Image Enlargement System

The evaluation of the capability of the vidicon television image enlargement system developed at Ohio State University was conducted on various thicknesses of aluminum and titanium alloys. This system provides direct conversion and enlargement of the X-ray image into a video signal with an approximate 30X display on a 17-inch television monitor. The evaluations were performed with Military Standard 453 radiographic penetrameters and wire-mesh screens having 40, 100, 200 and 320 mesh per inch; the three larger-mesh screens were brass, while the 320 mesh was stainless steel with 0.0015-inch wire. Photographs showing the comparative resolution capabilities through 3/8" of 6 Al-4V titanium alloy are shown in Figure 2. The 320 mesh screen is not visible in the television system image while the 200 mesh is barely visible. In Figure 2b, the enlargement of a conventional film radiograph made with Eastman Kodak Industrial X-ray Film, Type R single emulsion, on the same thickness of titanium provides better contrast and detail since all of the screens are resolved clearly. The small wire-mesh screens were also used on 0.2-inch thick 2219 aluminum for comparison purposes. Figure 3a shows that the photograph of the television X-ray image does not reveal the image of the 200 mesh screen very well. Figure 3b shows the comparison results with conventional R single emulsion radiographic film revealing even the 320 mesh grid. The images are a little sharper and more contrasting with both radiographic methods using the aluminum because of the lower density and thickness of the aluminum specimen in comparison to the titanium. The thinner the section, the better the performance of the X-ray image system. However, since section thicknesses of up to 0.500-inch of titanium and 1.0-inch of aluminum were to be radiographed, the decreased sensitivity eliminated the use of the television image system for any work on the larger thicknesses. Since these defects were detectable with other NDT methods, it was felt that the application of the television image system would have only limited use in achieving the program objectives.

b. Radiographic Film Evaluations

Two other X-ray film recording media were investigated. These two methods involved the use of Eastman Kodak Type SA-413 spectrographic film and high resolution plates used for microradiographic work. The type

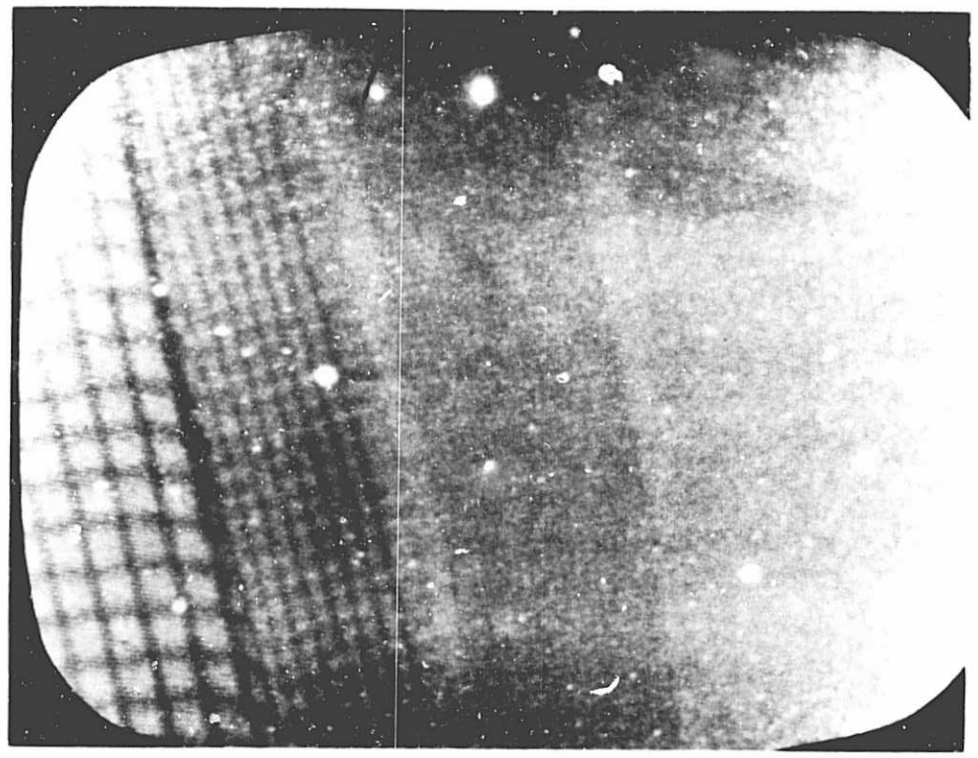

a)

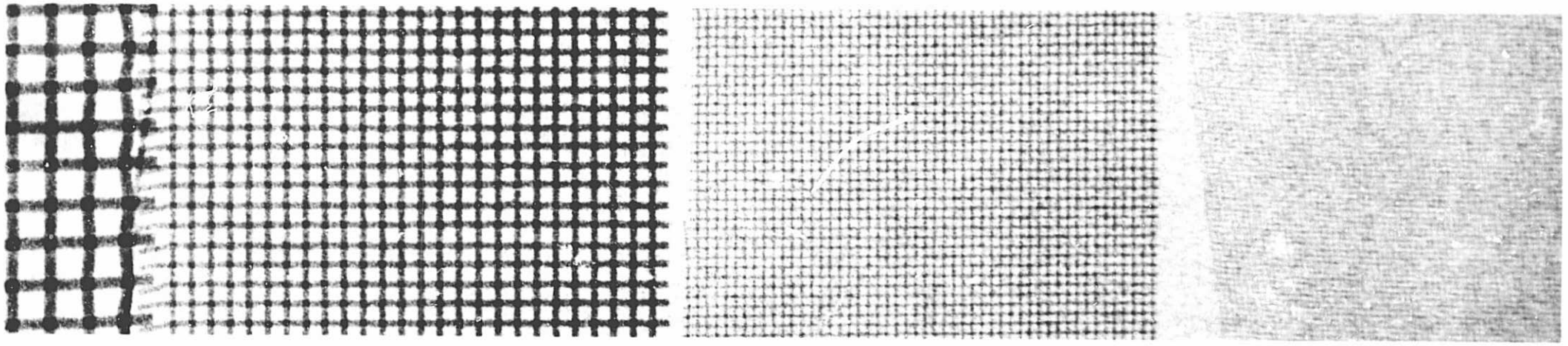

b)

Figure 2. Radiographic images of 40, 100, 200 and 320 mesh wire screens on 0.375 inches of titanium at 8X.

a) Ohio State University Television X-ray Image System
b) Conventional radiograph made with Eastman Kodak Industrial X-ray Film, Type R single emulsion

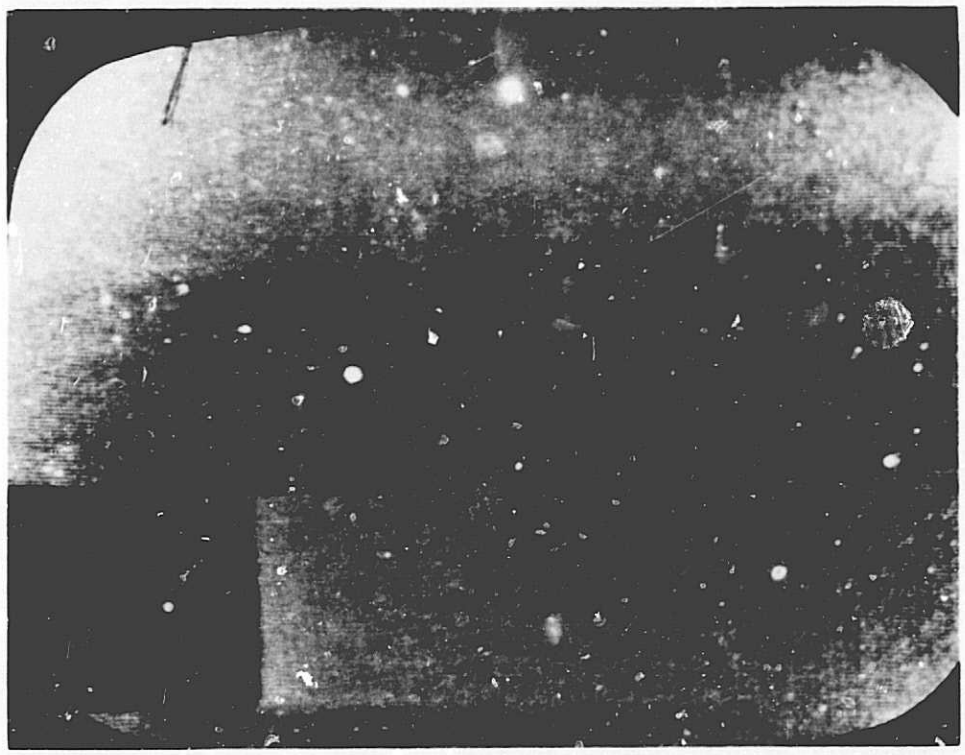

a

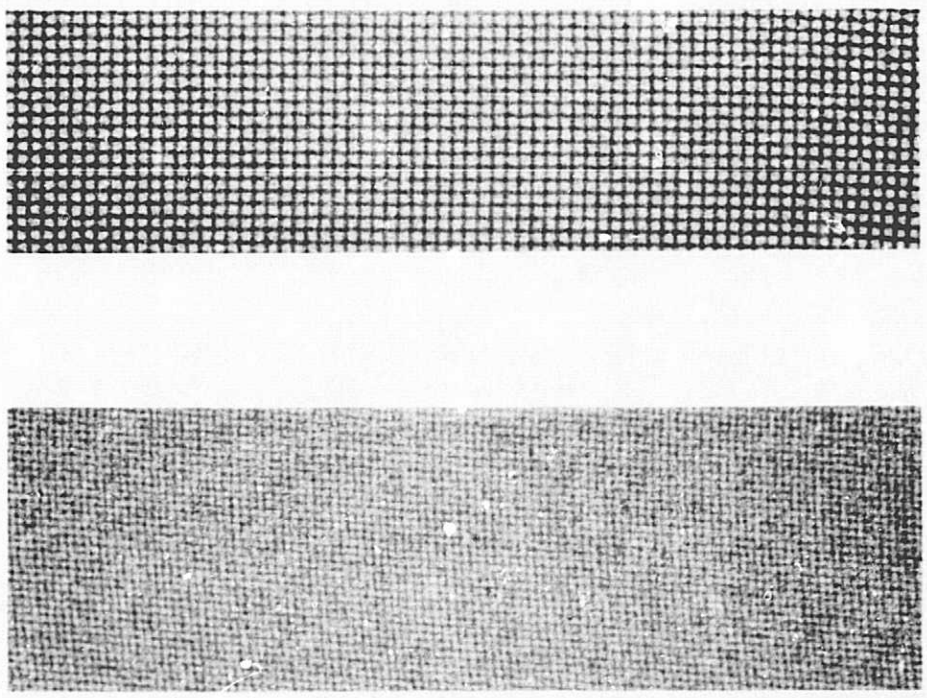

b

Figure 3. Radiographic images of 200 mesh wire screen on 0.200-inch 2219 Al at 8X.

a) Ohio State University Television X-ray Image System
b) Conventional Radiograph made with Eastman Kodak Industrial X-ray Film, Type R single emulsion with 320 mesh grid also included

SA-413 film was found to be limited in resolution and contrast. Use of the high resolution plates was limited to the thinner sections of material by the extremely long exposures necessary for this film. Some excellent radiographic images were obtained on the 0.020-inch specimens, but as the section thicknesses increased, the energy of the X-ray source had to be raised in order to reduce the exposure time to respectable levels. This produced a reduction in the amount of image contrast, and limited the usefulness of this high resolution film.

c. Summary Radiation Tests

From these evaluations, it was concluded that the Eastman Kodak Type R film would offer the best overall sensitivity for the radiation test that could be obtained on the weld and fatigue specimens. However, there are certain advantages to the television X-ray image system such as moving the defect in the beam to optimize the angle with the detector and the radiation source. Nevertheless, the unit is still only partially applicable to most of the specimens being investigated.

High resolution X-ray films are also made by other manufacturers and should give comparable results to Type R film. Eastman Kodak Type R film is available in single emulsion sheets which is necessary for any subsequent enlargement.

3. Ultrasonic Testing

a. Review

Ultrasonic testing employs piezoelectric transducers to convert high-frequency electrical signals into mechanical vibrations. The mechanical wave is coupled into the material under test and serves as the probing energy medium. The use of ultrasonics for materials inspection was first performed by Sokolow in 1929 utilizing what has become known as the through transmission method (14). In the United States, Firestone patented the first pulse-echo flaw detection and measuring instrument in 1942 (15). These two test methods, with many refinements, are generally the two types of ultrasonic tests utilized today. Inspection is performed by an anlysis of the ultrasonic waves received either by the emitter transducer, as in pulse-echo testing, or from a second transducer, as in the through-transmission and pitch-and-catch techniques. The received mechanical ultrasonic wave, after conversion back into an electrical signal, is amplified and displayed on an oscilloscope. The amount of energy received may be directly related to the defect orientation and area with respect to the incident beam. The arrival time of the signal can usually be related to the depth of a defect. Three main modes of vibration are commonly used in ultrasonic inspection; longitudinal, shear and surface waves. For the types of cracks and weld defects under investigation, the ultrasonic shear-wave tests are generally employed.

Shear waves may be generated by special transducers which are cut to produce transverse vibrations. However, many problems arise when attempting to couple this wave into an object, since coupling liquids will not support shear vibrations. The usual procedure in shear-wave testing is to generate a longitudinal wave and couple it at an angle into the test specimen. This causes the original beam to refract into the material in various modes at different angles. Depending on the angle of incidence, both shear, longitudinal and surface waves may result from the probing beam. The relationship between the angle of incidence and the refracted wave angle is given by Snell's Law from Optics:

$$\frac{\text{Sim } \phi_1}{V_1} = \frac{\text{Sin } \phi_L}{V_L} = \frac{\text{Sin } \phi_S}{V_S}$$

ϕ_1 = Angle of incidence of longitudinal beam in medium 1 from normal to the interface between media,

ϕ_L = Angle of refraction from normal to the interface of the longitudinal beam in medium 2,

ϕ_s = Angle of refraction from normal to the interface of the shear beam in medium 2,

ϕ_1 = Velocity of sound wave in medium 1,

ϕ_L = Velocity of longitudinal wave in medium 2,

ϕ_s = Velocity of shear wave in medium 2.

In order to determine the shear and longitudinal wave velocities for the materials in this program, both modal velocities were measured in 10 specimens each of the two titanium and the two aluminum alloys. These data are shown in Table II. An analysis of the data, shows very little variation between either of the aluminum alloys or of the titanium alloys. This means that the parameters established ultrasonically for one alloy can be used for the other. Slight differences in density between alloys should not affect the wave transmission to any great extent in each alloy group, but will affect the amount of energy available between the aluminum and titanium materials.

From the velocity data in Table II, the incident angles in water to produce a 45 degree shear wave in the alloy were calculated to be:

Alloy	Incident Angle (Degrees)
2219 Al	19.55
2014 Al	19.60
6Al-4V Ti	18.30
5Al-2.5 Sn	18.90

After considering the uncertainties present in the velocity values, a fixed angle of incidence was used to produce the shear waves for all 4 alloys.

A review of the various methods for ultrasonic inspection indicates that articles first appeared in the literature in the early 1950's on the subject of weld inspection. The methods used for weld inspection and for surface crack detection are similiar as will be shown in the ensuing paragraphs. One of the leaders in the field of ultrasonic weld testing is the firm of Krautkramer in Cologne, Germany (16). Ultrasonic inspection of welds has been relied on in Europe to a greater extent than in the United States. Cracks, lack of fusion and incomplete penetration defects are extremely difficult to detect radiographically unless there is a sufficient gap to be resolved on the film.

TABLE II

ULTRASONIC LONGITUDINAL AND SHEAR WAVE VELOCITY MEASUREMENTS FOR TWO ALUMINUM AND TITANIUM ALLOYS

	Ultrasonic Wave Velocity x 10^5															
	2219-T87 Al				2014-T6 Al				6Al-4V Ti				5Al-2.5Sn Ti			
	L		S		L		S		L		S		L		S	
Specimen Number	cm/sec	in/sec	cm/sec	in/sec	cm/sec	in/sec	cm/sec	in/sec	cm/sec	in/sec	cm/sec	in/sec	cm/sec	in/sec	cm/sec	in/sec
1	6.319	2.488	3.179	1.252	6.292	2.477	3.150	1.240	6.207	2.444	3.227	1.270	6.122	2.410	3.257	1.282
2	6.357	2.503	3.179	1.252	6.409	2.523	3.147	1.239	6.455	2.541	3.383	1.332	6.205	2.443	3.250	1.279
3	6.345	2.498	3.175	1.250	6.370	2.508	3.165	1.246	6.466	2.546	3.423	1.347	6.253	2.462	3.292	1.296
4	6.570	2.587	3.190	1.256	6.385	2.514	3.181	1.252	6.305	2.482	3.501	1.378	6.305	2.482	3.274	1.289
5	6.283	2.474	3.142	1.237	6.371	2.508	3.171	1.248	6.330	2.492	3.489	1.374	6.295	2.478	3.261	1.284
6	6.286	2.475	3.149	1.240	6.379	2.511	3.152	1.241	6.185	2.435	3.101	1.221	6.262	2.465	3.291	1.296
7	6.405	2.522	3.152	1.241	6.381	2.512	3.169	1.248	6.299	2.480	3.543	1.395	6.226	2.451	3.232	1.273
8	6.342	2.497	3.158	1.243	6.424	2.529	3.144	1.238	6.179	2.433	3.184	1.254	6.261	2.465	3.274	1.289
9	6.378	2.511	3.179	1.252	6.268	2.468	3.158	1.243	6.194	2.438	3.192	1.257	6.267	2.467	3.277	1.290
10	6.263	2.466	3.132	1.233	6.218	2.448	3.155	1.242	-	-	-	-	6.270	2.468	3.266	1.286
Average	6.354	2.502	3.164	1.245	6.350	2.500	3.159	1.244	6.291	2.477	3.338	1.314	6.247	2.459	3.267	1.286
Standard Deviation ±	0.088	0.035	0.019	0.007	0.067	0.026	0.012	0.005	0.112	0.044	0.164	0.065	0.053	0.021	0.018	0.007
Expected Range of Variability ± 3S	6.354 ± .264	2.502 ±0.105	3.164 ±0.057	1.245 0.021	6.350 ±0.201	2.500 ±0.078	3.159 ±0.036	1.244 ±0.015	6.291 ±0.336	2.477 ±0.132	3.338 ±0.492	1.314 ±0.195	6.247 ±0.158	2.459 ±0.063	3.267 ±0.054	1.286 ±0.021

These defects can be extremely tight as will be seen in later illustrations.

Ultrasonic techniques to detect defects in welds have been developed primarily by Krautkramer, and include angle beam probes and a flaw locating ruler for determining the location and approximate depth of a flaw in a weld. The length of a defect can be determined from the longitudinal persistence of the defect as one scans along the axis of the weld. Other work on shear-wave weld inspection has been reported by Parker (17), Bobbin (18)(19), and DeSterke (20) which discuss the angle beam test technique and inspection results in the early stages of ultrasonic weld testing.

One of the latest papers of significant interest to this program is that by Socky (21) which discusses some experimental data for the response of the ultrasonic system to various hole diameters and notch depths. From his results, Socky concluded that the measured instrument response is not a linear function of reflection of the ultrasonic waves. He also discusses a further factor which is of importance, that is, the nature of the reflection and refraction of sound waves at a defect. Depending on how the shear waves strike the back surface of the plate and the defect itself, longitudinal and shear waves can be generated at the defect and at the bottom plate surface in the same manner as they are generated when the longitudinal beam enters the part. This makes the interpretation of ultrasonic signals from a crack extremely difficult. It can be anticipated, that the response to defects of equal size, one in the center of a weld and another at the surface, will be different and that these differences must be interpretable in order to adequately define the size and shape of an arbitrarily located defect.

Researchers at Automation Industries utilized this reradiated sound in combination with the reflected sound to make their measurements in what they have named the "delta technique". This technique has been successful in the inspection of steel welds for the Navy and for aluminum weldments for NASA (22,23).

b. Preliminary Evaluations

Based on this review of existing ultrasonic flaw detection techniques, the efforts for this program were concentrated on the shear-wave and the delta inspection methods. For these evaluations, TRW was assisted by Automation Industries research personnel in evaluating the application of the "delta technique" to the definition of defects. This inspection was carried out on simulated defective plate materials. At TRW, the evaluation of the shear wave inspection method was concentrated on defining defects by recording and analyzing the total available signal information.

To provide meaningful calibration standards that can be related to the types of defects anticipated, 1/8" titanium and aluminum alloy plates were constructed with known notch-type defects. The construction details of the plates are shown in Figure 4. The notch dimensions in these specimens are given in Table III. In the electrodischarge machining of these notches, it was difficult to obtain the exact desired dimensions which resulted in the actual measured dimensions being somewhat different from the design values. In general, the dimensions are within 10% of the required values with a few exceptions. The table shows that it was easier to hold the length dimension than the depth dimension. In making the specimens, holding one dimension constant to the value desired was not always possible. In most instances,

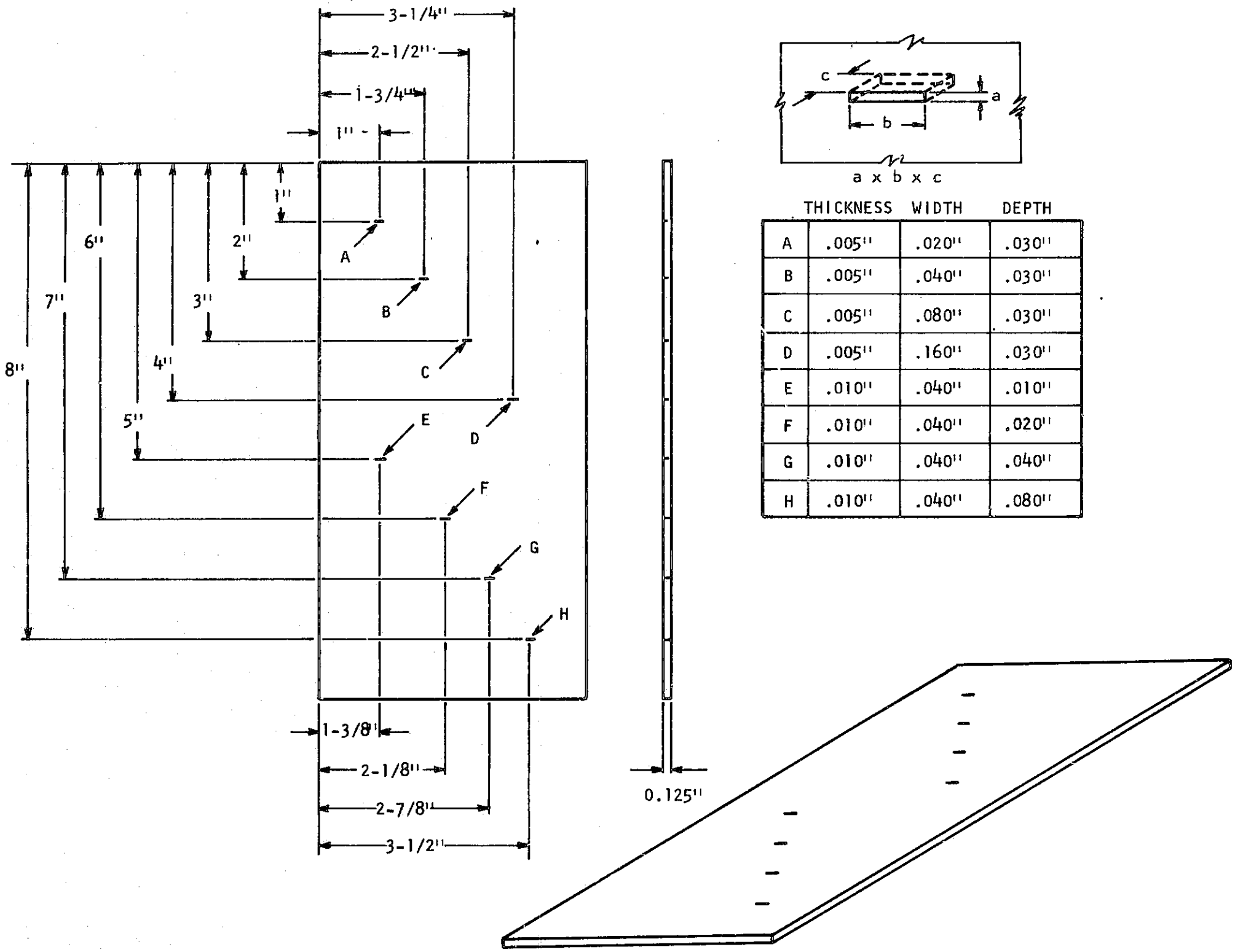

a x b x c

	THICKNESS	WIDTH	DEPTH
A	.005"	.020"	.030"
B	.005"	.040"	.030"
C	.005"	.080"	.030"
D	.005"	.160"	.030"
E	.010"	.040"	.010"
F	.010"	.040"	.020"
G	.010"	.040"	.040"
H	.010"	.040"	.080"

Figure 4. Calibration sample design for 0.125-inch titanium and aluminum.

TABLE III

NOTCH SIZES IN 0.125-INCH PLATES

Notch Identification	Notch Thkns.*	Notch Length*			Notch Depth*		
		Design	Actual		Design	Actual	
			Aluminum	Titanium		Aluminum	Titanium
A	0.005	0.020	0.029	0.029	0.030	0.033	0.030
B	0.005	0.040	0.044	0.046	0.030	0.030	0.026
C	0.005	0.080	0.082	0.082	0.030	0.025	0.032
D	0.005	0.160	0.161	0.158	0.030	0.025	0.030
E	0.010	0.030	0.027	0.022	0.010	0.015	0.013
F	0.010	0.030	0.025	0.024	0.020	0.019	0.018
G	0.010	0.030	0.027	0.022	0.040	0.034	0.034
H	0.010	0.030	0.027	0.025	0.080	0.078	0.079

* - all dimensions in inches.

however, the four dimensions held constant were within 10 percent of an average value for these dimensions. The variable dimension was measured and its actual value used in the analysis of data.

1) Shear-Wave inspection

The Krautkramer work showed that as the beam from a scanning transducer approaches a given defect, the received signal height increases to a maximum and then decreases as the beam passes beyond. The time interval over which the defect signal occurs can be related to the defect depth or to the distance the transducer and its beam moves past the defect. An experimental setup was assembled to fix the angle of incidence of an ultrasonic transducer at various angles, and at the same time allow the transducer to move laterally so that its position could be recorded as a function of the distance of lateral motion. This was accomplished (see Figure 5) by utilizing a cross-feed table having two calibrated directions of travel and with the screw for one direction of travel coupled to a ten turn potentiometer. By this method, a distance signal was fed to the X-axis of an X-Y recorder so that the signal intensity of the shear-wave beam could be plotted on the Y-axis as a function of the distance of travel of the transducer past the defect.

A focused transducer was used to concentrate the ultrasonic beam on a rather small area of the notch defect. The length of the crack was thought to be obtainable from the movement of the transducer parallel to the crack by determining over what distance the crack signal persisted.

In the initial trial, a Sperry UM-700 ultrasonic instrument was setup with a 3/16" diameter lithium sulfate 5 MHz focused transducer at a 20° incident angle in water. The instrument gain was adjusted for a suitable signal height on the largest width notch and the transducer was moved through the defect. Several scans were made through the crack at different points. The length and depth of the crack were obtained by determining at which translation of the crack the signal disappeared. With this apparatus, data were obtained and correlated with the depth and length of the crack.

In Figure 6, the ultrasonic chart reading is plotted as a function of the actually measured notch depth. This plotted chart reading is the scan length during which the ultrasonic indication was detectable at a particular UM-700 gain setting. From Figure 6, the ultrasonic response to depth, that is, the ultrasonic chart and recording distance obtained from the data, rises very quickly and then levels off at notch depths above 40 thousandths of an inch. A test such as this has little sensitivity to the depth of a notch or crack greater than 0.040-inch. This test was made using constant width notches in titanium plate so that depth was the only independent variable. These data were obtained with an incident angle of twenty degrees to normal which results in an approximate 50 degree shear beam in the titanium.

With the same settings on the ultrasonic system, measurements were made of the notch width on notches A through D and are shown in Figure 7. This relationship shows an almost linear response between the actual measured notch width and the ultrasonic chart recording distance. Figure 8 shows a reproduction of the chart recording data obtained with a 1/8-inch titanium plate on notch B for several scans at 0.010-inch spacing intervals. This is the same data which have been summarized and shown as point B in Figure 7. In Figure 8, the vertical scale from 0 to 160 represents 0 to 0.160-inch travel

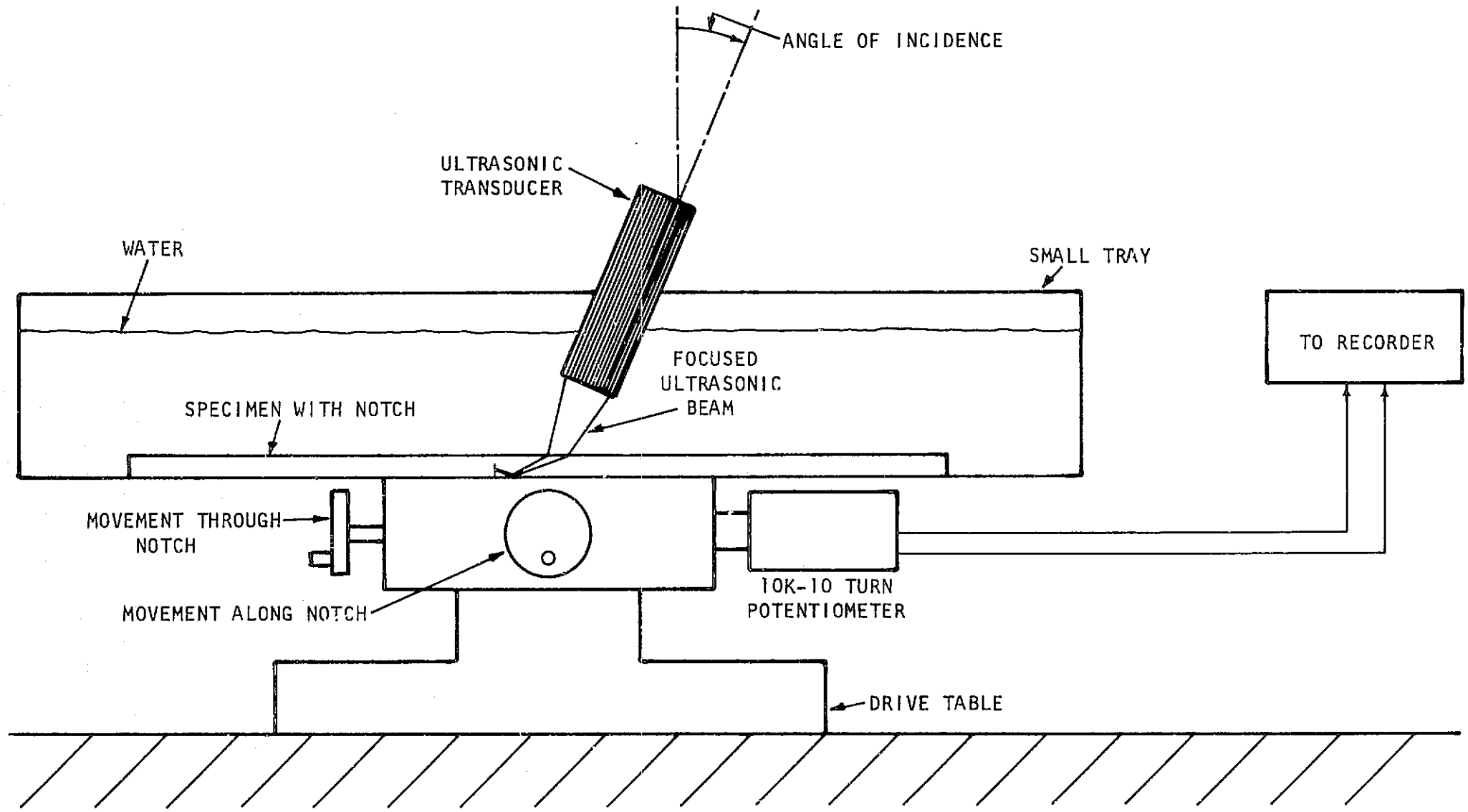

Figure 5. Illustration showing set-up for recording ultrasonic defect signal as a function of defect position relative to the transducer.

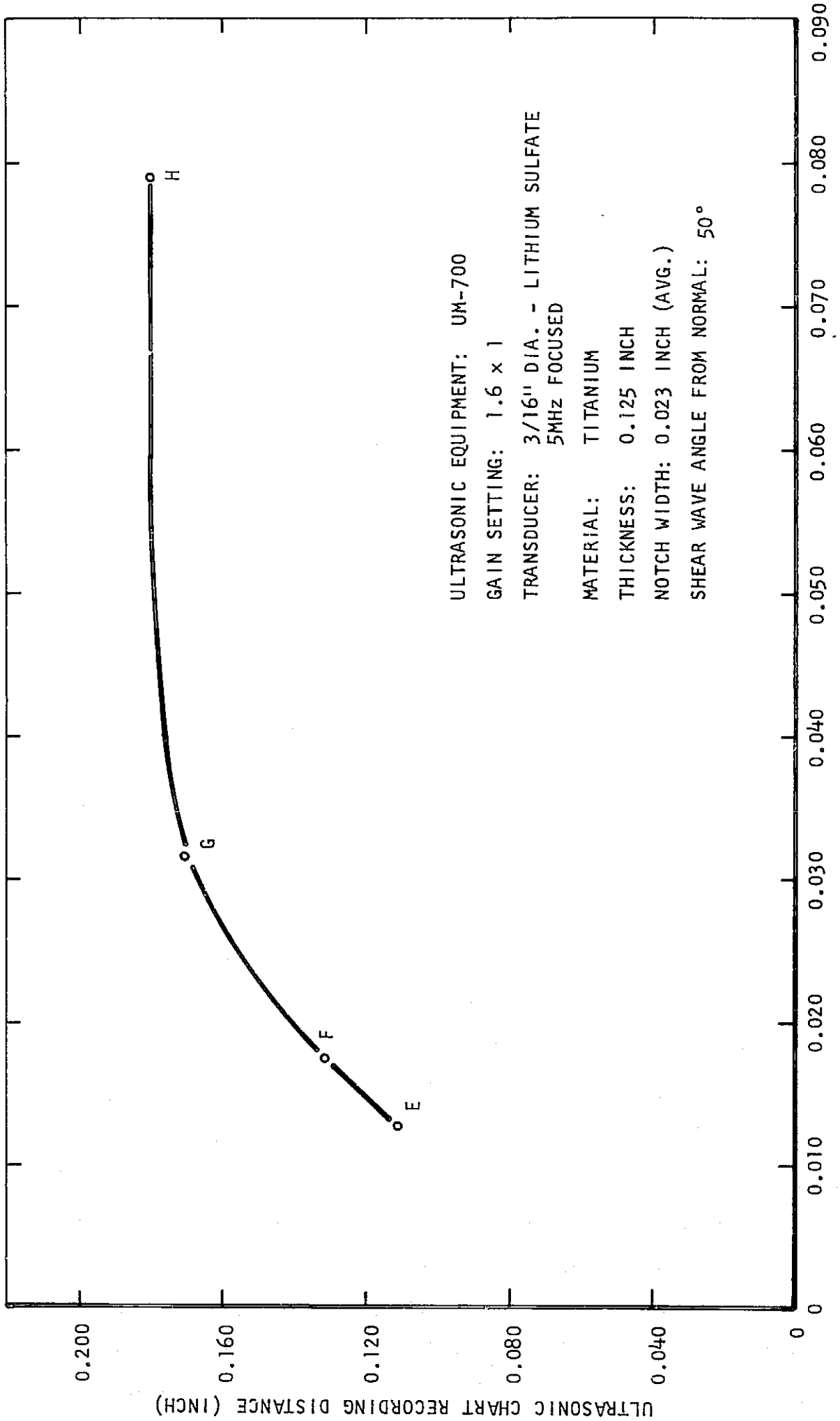

Figure 6. Actual measured notch depth as a function of ultrasonic chart recording distance for notches in 1/8-inch titanium plate, notch width constant, 50 degree shear beam.

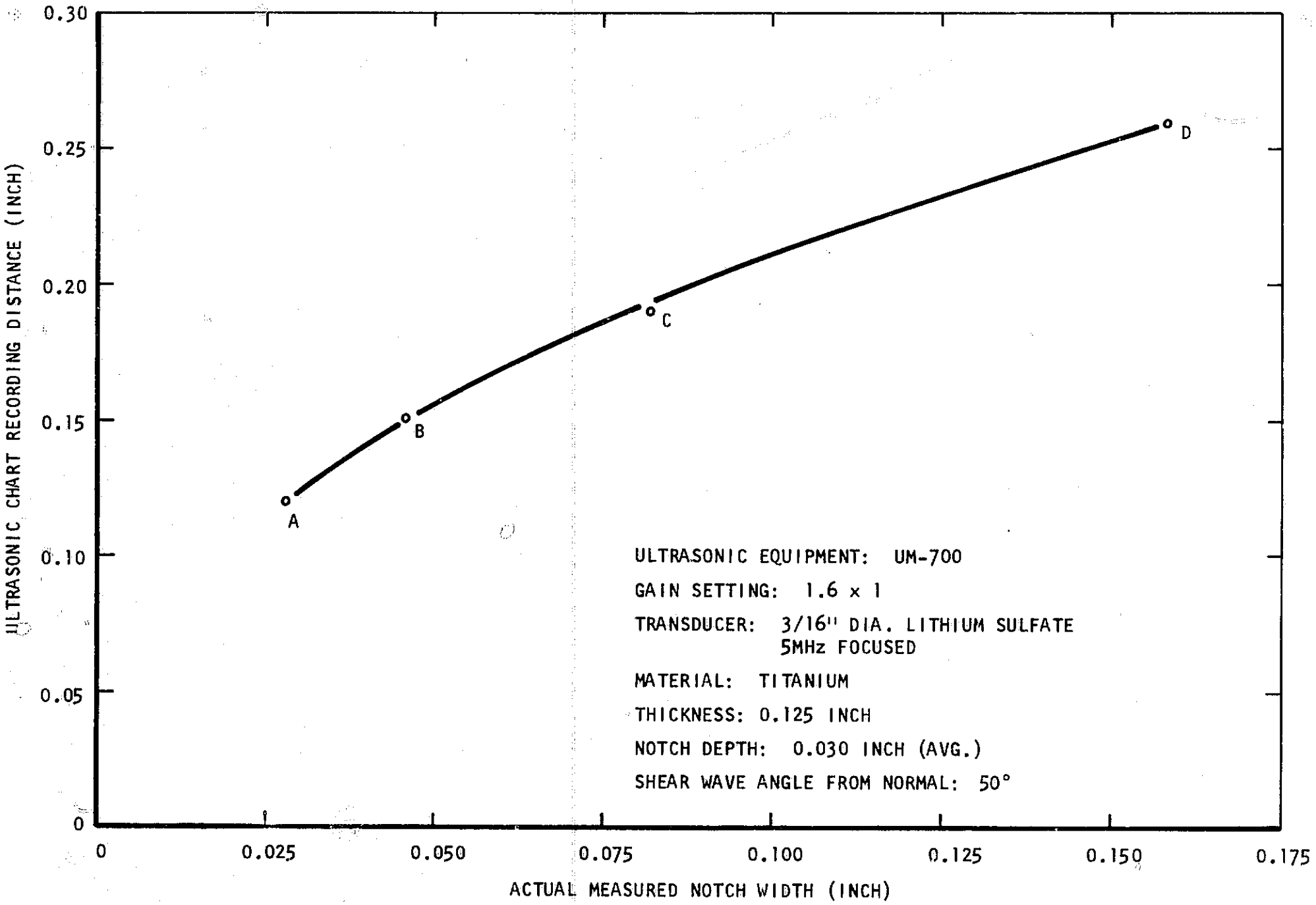

Figure 7. Actual measured notch width as a function of ultrasonic chart recording distance for notches in 1/8-inch titanium plate, notch depth constant, 50 degree shear beam.

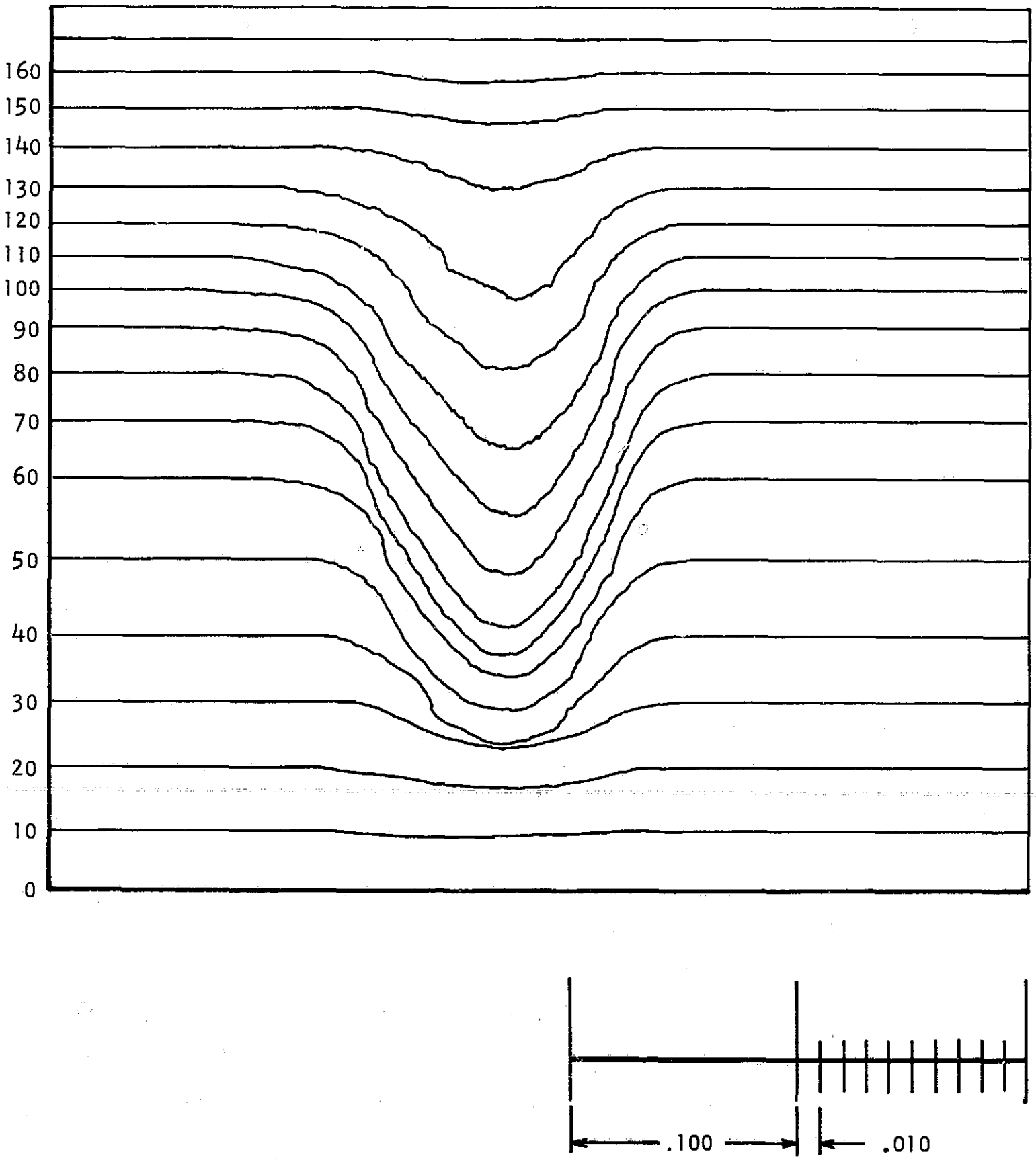

Figure 8. Reproduction of chart recording obtained on 1/8-inch titanium plate, notch B, for several scans at 0.010-inch intervals shown plotted in Figure 6.

5739 B

in 0.010-inch intervals parallel to the crack, while the horizontal scale with 0.100 and 0.010-inch markers representing travel across the crack. This type of data is only usable on a comparative basis and is only good for the conditions stated. At this angle of incidence, there appears to be a limitation in the response since the depth was not delineated very well at values greater than 0.040-inch.

Measurements were repeated at a 26 degree incident angle, an approximate 77 degree angle in the part. These data did not show any improvement; in fact since the incident angle approached the second critical angle where surface waves are generated, some confusion resulted in the interpretation of the received signal. The incident angle was reduced to 23 degrees giving an approximate 60 degree shear beam in the plate. The gain settings on the ultrasonic instrument were again changed, by necessity, from those used at 20 degrees and the data recorded as shown in Figures 9 and 10. The increase in incident angle causes the shear wave to approach the notch at a more normal angle. Comparison of Figures 6 and 9 shows that the notch depth function has changed. In particular, it is possible to delineate the notch depth from the ultrasonic chart readings above 0.040-inch. In Figure 10, however, the opposite has occurred and the notch length is not as distinguishable as it was at the 20 degree incident angle. It appears desirable to change the angle of the test in order to delineate the thickness or the depth of the defect.

With this type of ultrasonic signal recording, several traces were recorded across the defect. These were assembled into a three dimensional plot in which Z-axis height represents the signal amplitude as a function of the transducer position. Figure 11 is a photograph of the assembled data in three dimensions. Each of the individual scans across a given location on the crack were photographed, cut out, and mounted in a block. One can see the rise and the fall of the signal height as a function of distance along the crack and also across the crack. No attempt was made here to develop absolute numbers since the images were compared to known-notch-depth traces from the previously described specimens. Other work will be described which attempts to place absolute values on the scanning data so that cracks of various dimensions can be compared without reference to standard-notch-calibration curves.

2) Delta Inspection

In addition to the shear-wave study of flaw size and shape, Automation Industries Research Division performed an evaluation of their "delta technique". The four test samples sent to Automation Industries for this evaluation included two of the test samples previously described, the 1/8-inch aluminum and titanium calibration plates, and also two special 1/2-inch thick plates.

The test samples supplied for the 1/2-inch material are shown in Figure 12. Instead of the notch-type defects previously described for the 1/8-inch samples, calibration holes were drilled in the test plate in two directions. One set of test holes was drilled from the side of the plate and another set into the face of the plate. This provided identical holes at various depths in the material so that the ability of the delta test to distinguish the depth and length of these defects could be determined. The hole sizes and lengths are listed in Figure 12. Delta scan recordings were made of the four plate sections and the defect indications were then compared with the actual flaw shapes and positions known to exist in the material. From these tests, the correlation between flaw condition and delta scan recording was determined.

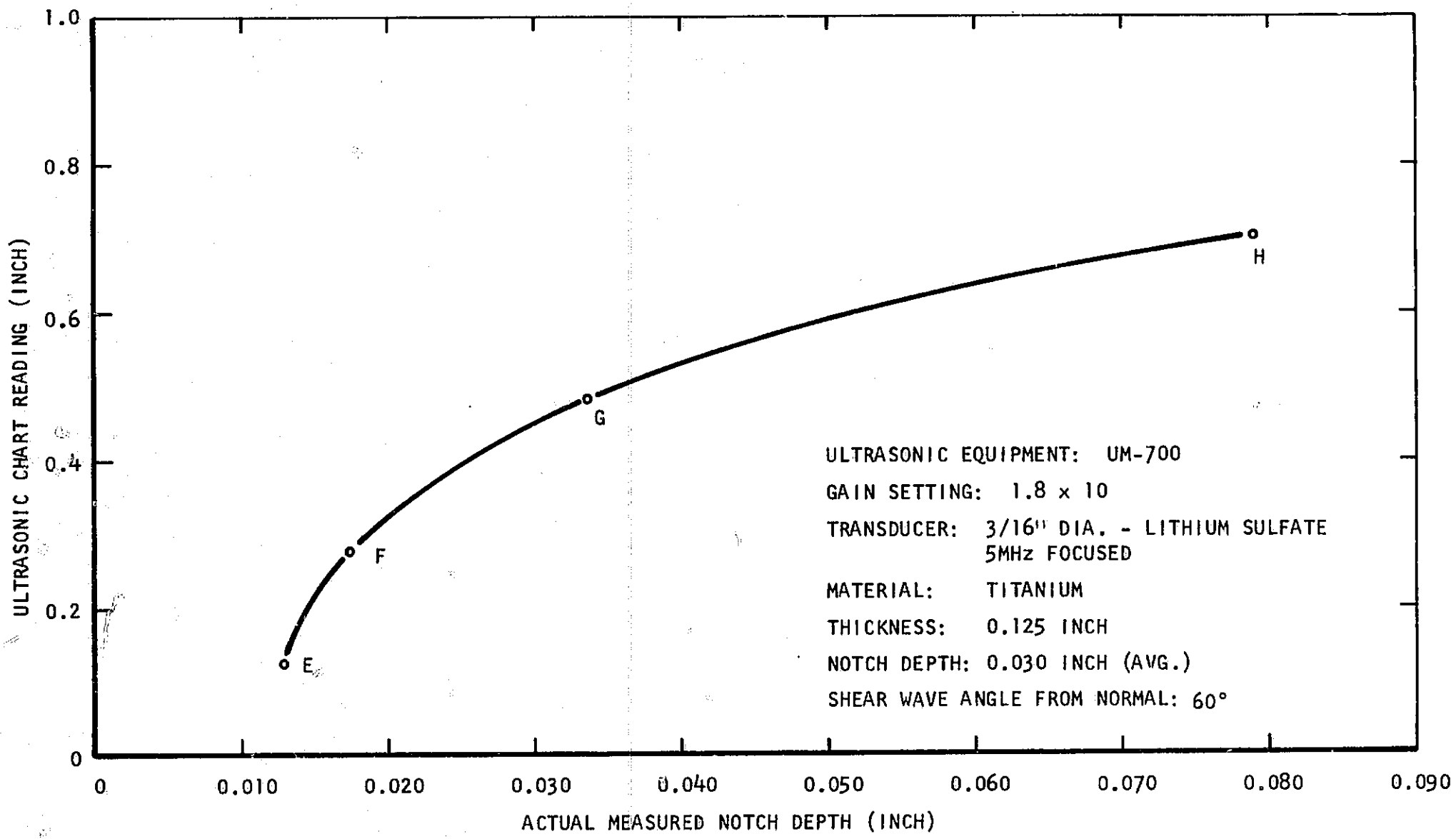

Figure 9. Actual measured notch depth as a function of ultrasonic chart recording distance for notches in 1/8-inch titanium plate, notch width constant, 60 degree shear beam.

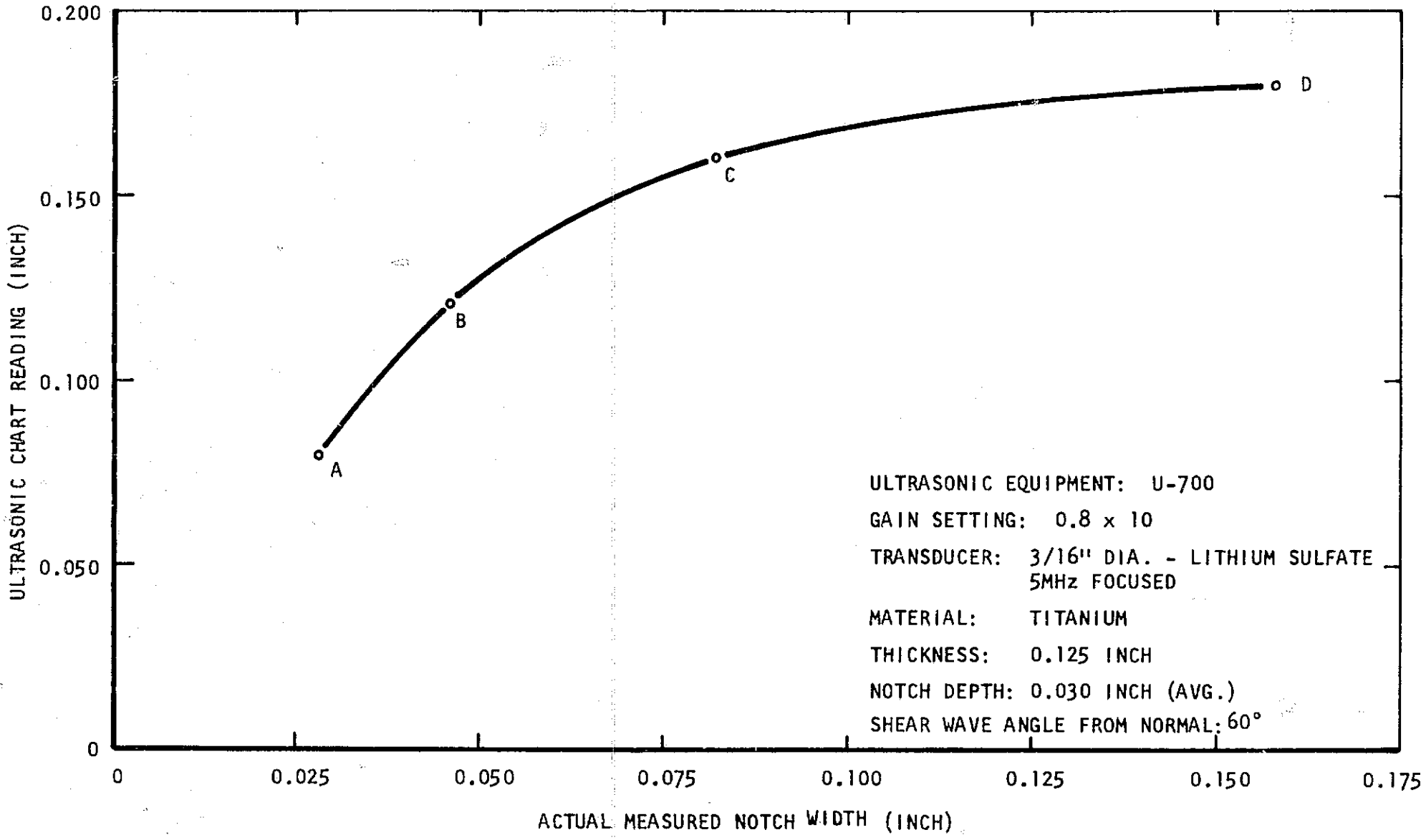

Figure 10. Actual measured notch width as a function of ultrasonic chart recording distance for notches in 1/8-inch titanium plate, notch depth constant, 60 degree shear beam.

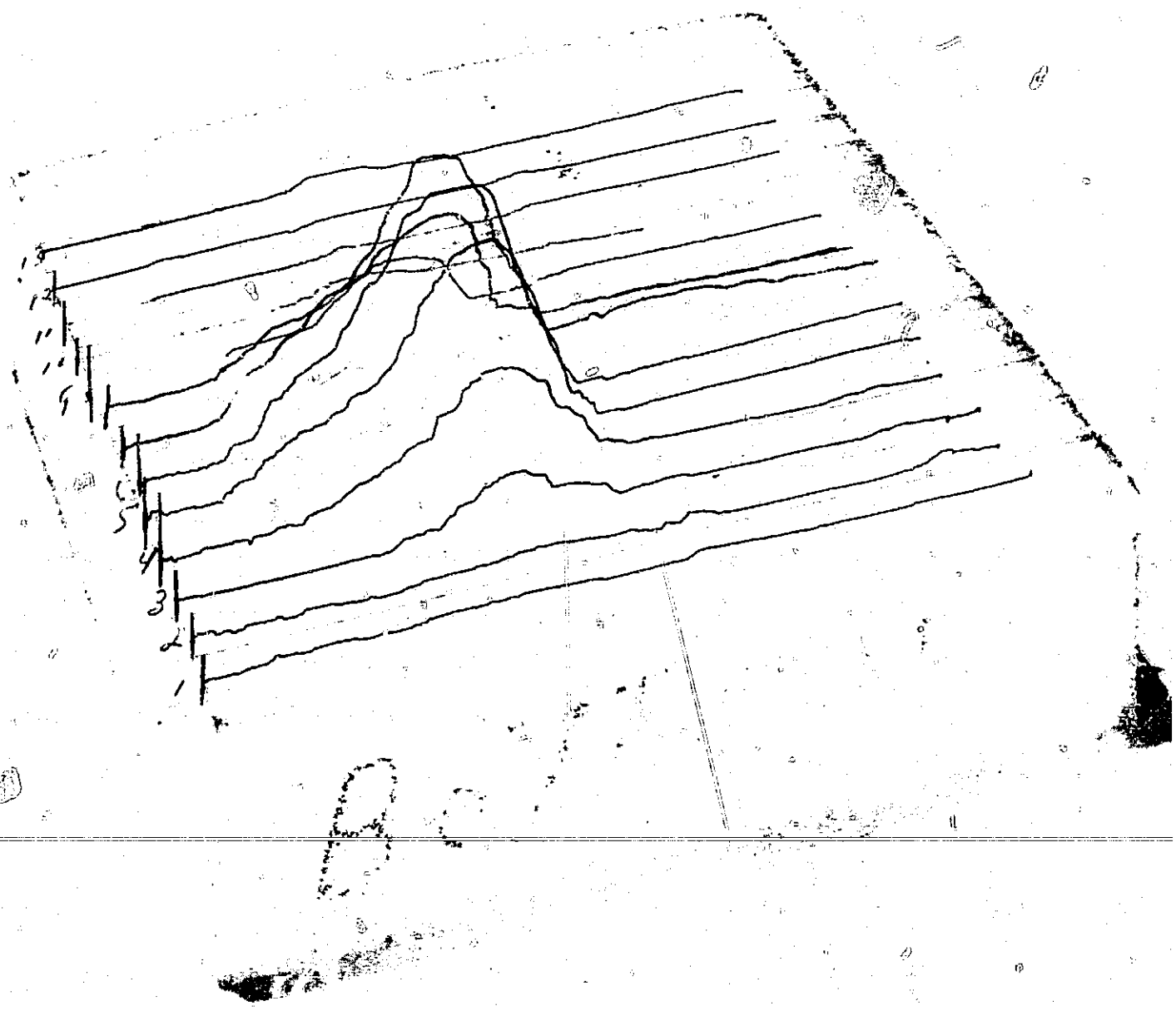

Figure 11. Composite photograph of assembled ultrasonic signal data in the two principle directions, both parallel and transverse to a crack. Measurements taken at 0.010-inch intervals parallel to the crack.

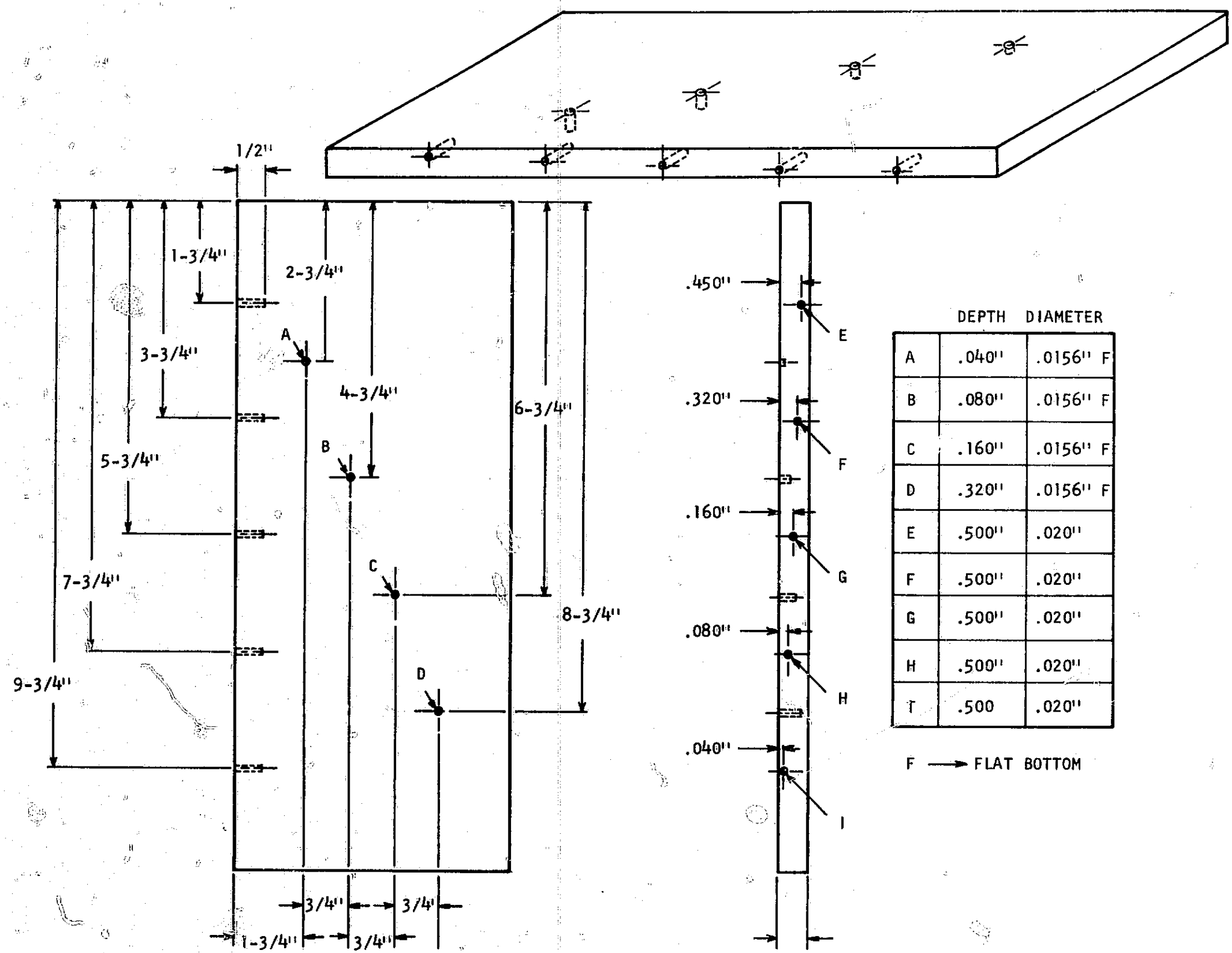

	DEPTH	DIAMETER
A	.040"	.0156" F
B	.080"	.0156" F
C	.160"	.0156" F
D	.320"	.0156" F
E	.500"	.020"
F	.500"	.020"
G	.500"	.020"
H	.500"	.020"
I	.500	.020"

F ⟶ FLAT BOTTOM

Figure 12. Calibration sample design for 0.500-inch material.

a) Inspection Methods

Separate inspections were performed using both the basic and shuttle delta configurations. Each of these variations required separate transmitter and receiver search units, and were performed in a small immersion tank at a 5.0 MHz frequency. Defect information was recorded with an Alden Facsimile Recorder.

The basic delta configuration is characterized by the fixed triangular position of two search units above the inspection surface. In this configuration, sound energy from the transmitter penetrates the test material and is refracted into the area below the receiver. Transmitted sound energy will propagate through the material unobstructed if no material imperfections are present. If defects are present, the transmitted sound energy strikes them causing a re-radiation of sound energy. Re-radiated sound propagates from the flaw and is detected by the receiver search unit. Excitation of internal defects by transmitted sound is an important characteristic of the delta effect. A basic delta configuration is shown in Figure 13.

The shuttle delta configuration is characterized by an oscillating motion of the transmitter search unit while the receiver remains stationary over the defect, and is illustrated in Figure 14. The depth of the material being inspected is determined by the distance separating the transmitter and receiver search unit. The depth increases as the distance separating the two search units increases. Bringing the search units close together permits flaws in the upper region of the plate materials to be detected.

b) Delta Test Results

0.500-inch Plates

Figures 15 and 16 are basic delta scan recordings of the 1/2-inch thick aluminum plate sample. A basic delta inspection using a fixed transmitter to receiver distance was made from the plate surface opposite the flat bottom holes. In this manner, all holes were detected as internal defects. Flat bottom holes A-D were recorded as round indications. Elongated indications were recorded for the side drilled holes E-I. Holes A and E were not recorded on the delta scan in Figure 15, but were recorded in a second delta scan, Figure 16. The second delta scan was made with an increased gain setting and a longer search unit separation distance.

Long band-like indications due to the support fixturing were recorded on a number of the delta scans. Two of these are found on the recording in Figure 16 near holes A & I. These indications appeared at high gain settings and should be disregarded since they represent the ends of a support plate used in the immersion tank. The sides of the drilled holes appear with an almost constant diameter regardless of depth in Figure 15, but become distorted at the higher gain setting in Figure 16.

Figures 17 and 18 are scan recordings of the 1/2-inch thick titanium plate sample obtained with the basic delta configuration. The hole diameters and positions in the 1/2-inch titanium plate were similar to those in the 1/2-inch thick aluminum samples. Holes A and E, not visible in Figure 17, were recorded using an increased separation distance between the fixed transmitter and receiver search units. Figure 18 shows the test results with holes A & E.

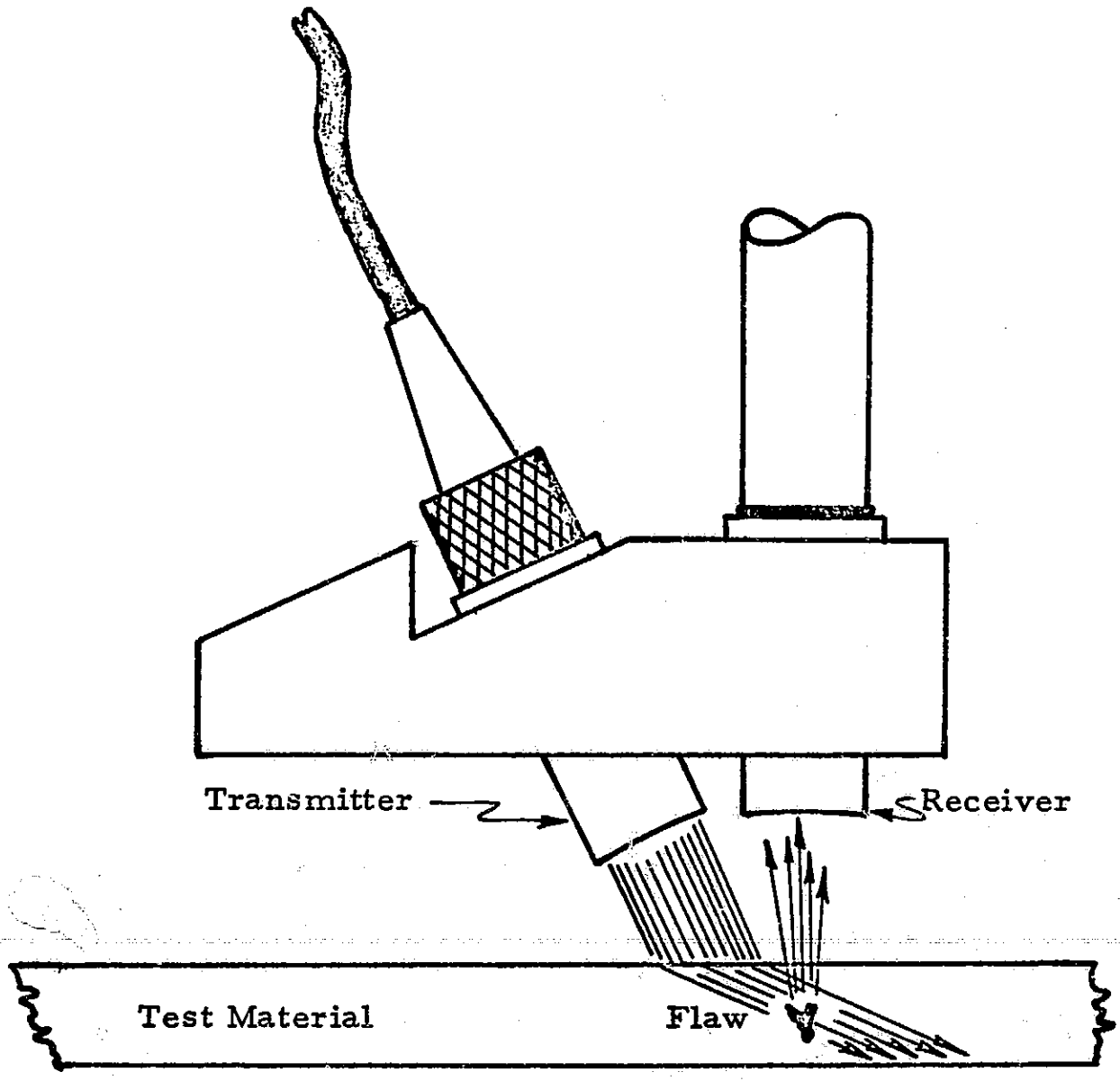

Figure 13. Basic delta ultrasonic inspection transmitter-receiver configuration.

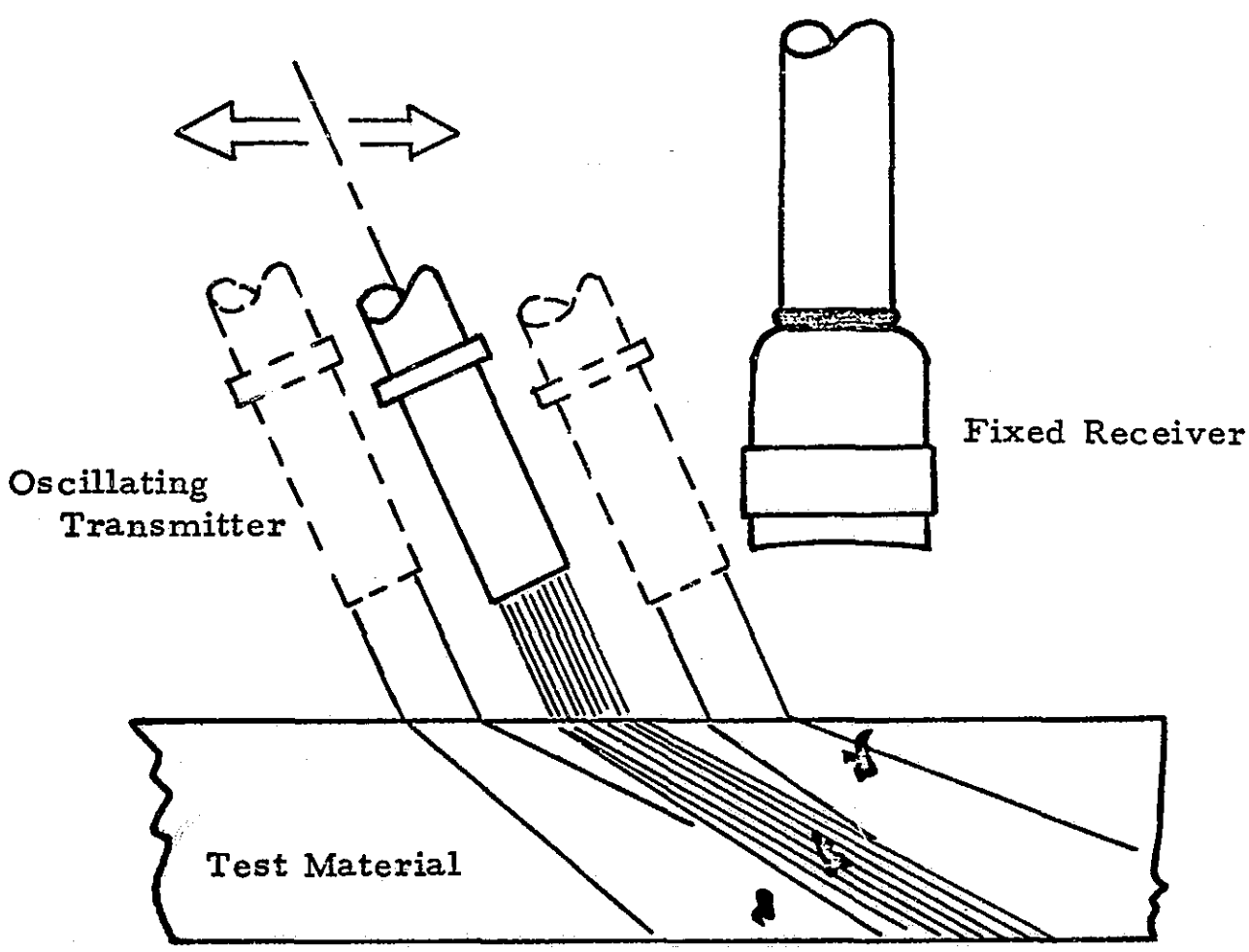

Figure 14. Shuttle delta ultrasonic inspection illustration showing stationary receiver and oscillating transmitter.

5743 B

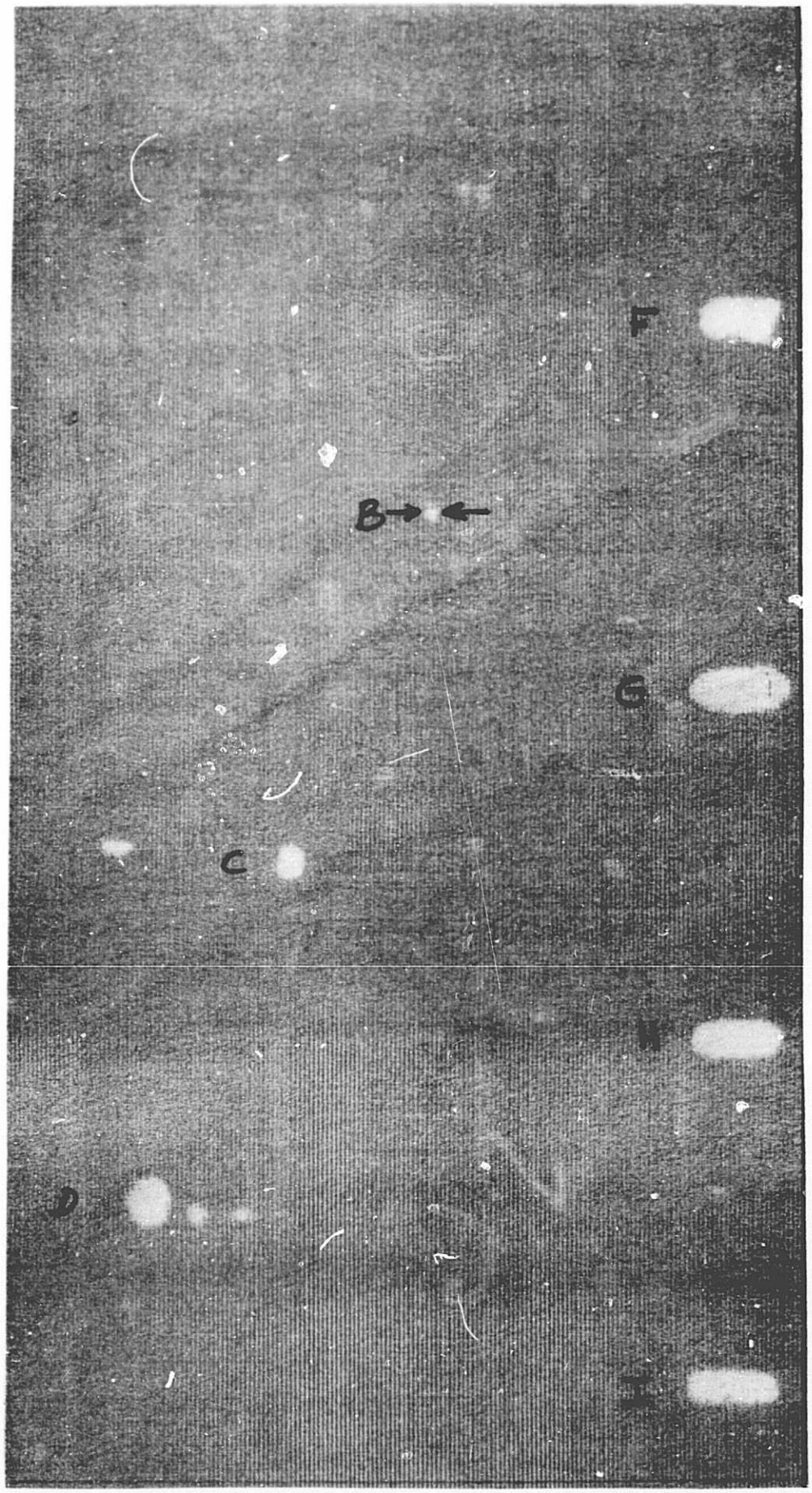

Figure 15. Delta ultrasonic scan recording showing test hole indications from 0.500-inch thick aluminum plate.

5807 B

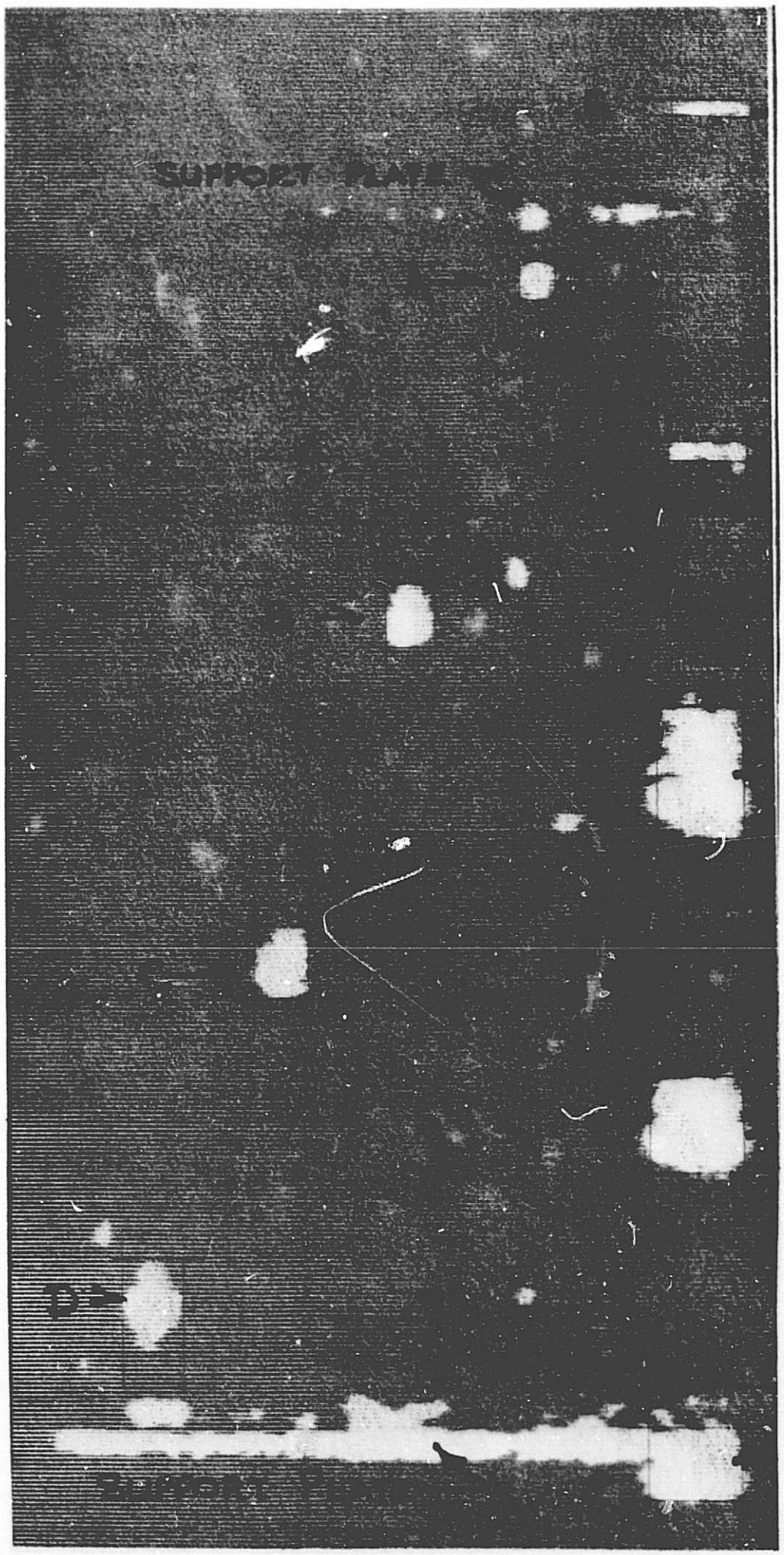

Figure 16. Delta ultrasonic scan recording showing test hole indications from 0.500-inch thick aluminum plate, higher gain setting and separation distance than Figure 13.

5808 B

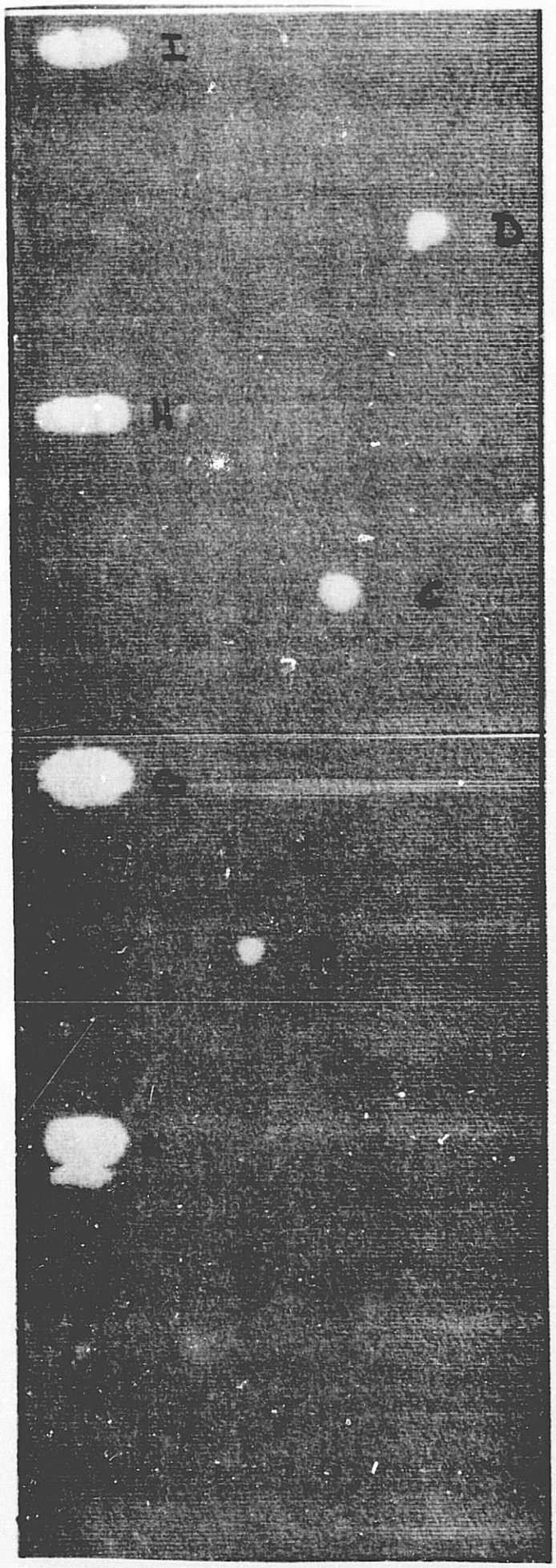

Figure 17. Delta ultrasonic scan recording showing test hole indications from 0.500-inch thick titanium plate.

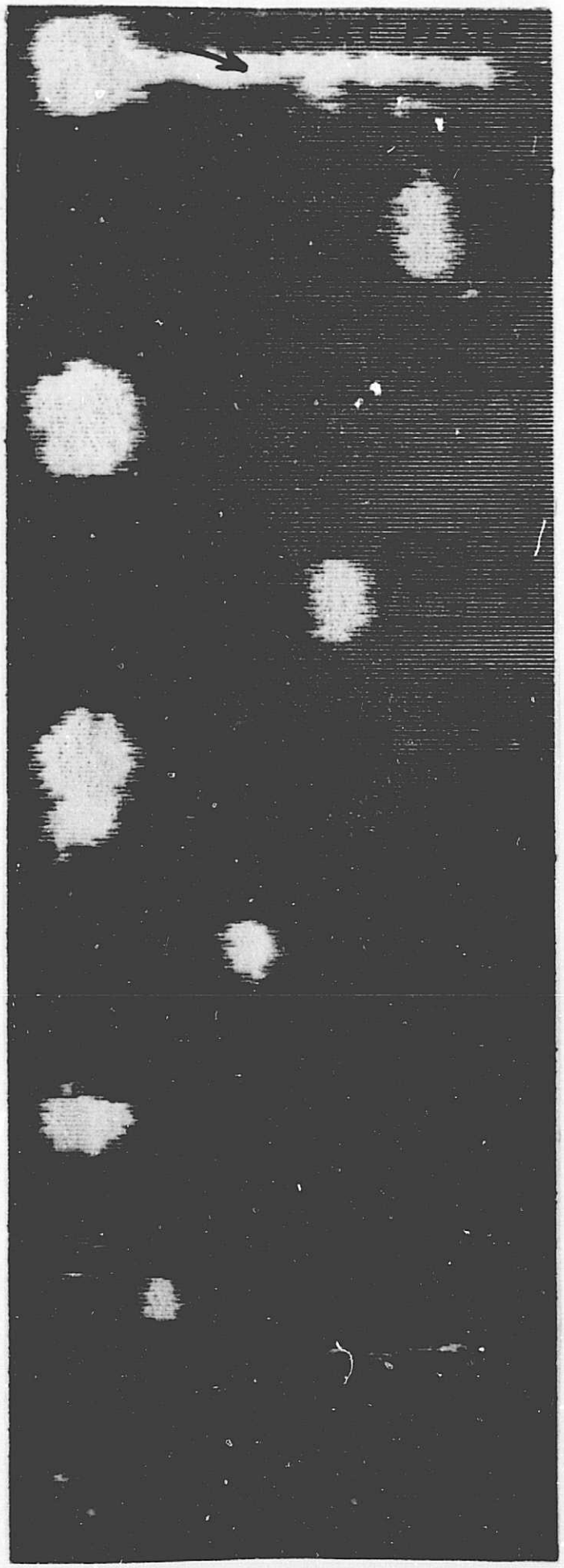

Figure 18. Delta ultrasonic scan recording showing test hole indications from 0.500-inch thick titanium plate, increased separation distance than in Figure 15.

Band-like indications from the support plate are also present on the Delta scan recording in Figure 18.

0.125-inch Plates

Figure 19 is a Delta scan of the 1/8-inch thick aluminum plate sample obtained with the basic configuration. The narrow rectangular notches in the back side of this plate are shown as round indications on the recording. Slot H has been outlined on the recording to separate it from the long band indication of the support fixture.

The delta scan recording of the 1/8-inch thick titanium plate is shown in Figure 20. For all practical purposes, the notch arrangement in the aluminum and titanium samples was identical. All notches, A-H, were detected and recorded as round indications. Notch E and F indications were very small but detectable.

0.500-inch Shuttle Delta Tests

A shuttle Delta recording of the 1/2-inch aluminum plate is shown in Figure 21. Flat bottom holes A-D are shown as elongated indications. For this inspection, the test plate was positioned with the ends of the flat bottom holes aligned directly below the receiver search unit. Therefore, these test holes appear in a straight line rather than staggered as in previous figures.

c) Discussion of Delta Test Results

Basic Delta Recordings, 1/2-Inch Aluminum

Flat bottom holes, B,C, and D shown in Figure 15 were detected by the basic Delta technique using a 5.0 MHz operating frequency. The diameters of the recorded indications increased on the Delta scan from 0.060-inch for hole B to 0.225-inch for hole D. Each flat bottom hole was the same diameter, 0.016-inch, but was drilled to various depths in the aluminum. Since the hole diameters were constant, the variation in recorded diameter was attributed to hole length. This variation should not be confused with hole depth from the inspection surface. Instead, hole size (area) rather than depth influences the basic delta scan indication for holes drilled perpendicular to the inspection surface. On the scan in Figure 15, the ratio of recorded diameter to hole length averaged about 0.75, the recorded diameter being smaller than the hole length.

Flat bottom hole A, 0.043-inch long, was not detected by the scan in Figure 15, while holes B, C, and D were quite visible. An increase in sensitivity permitted the recording of hole A as shown in Figure 16. Unfortunately, at this sensitivity, the indications from the larger holes were distorted by saturation of the signals. In Figure 16, hole A was recorded but the larger holes, C and D were distorted from their true perspective. Therefore, it is extremely important to know test sensitivity when considering defect size information on the recording.

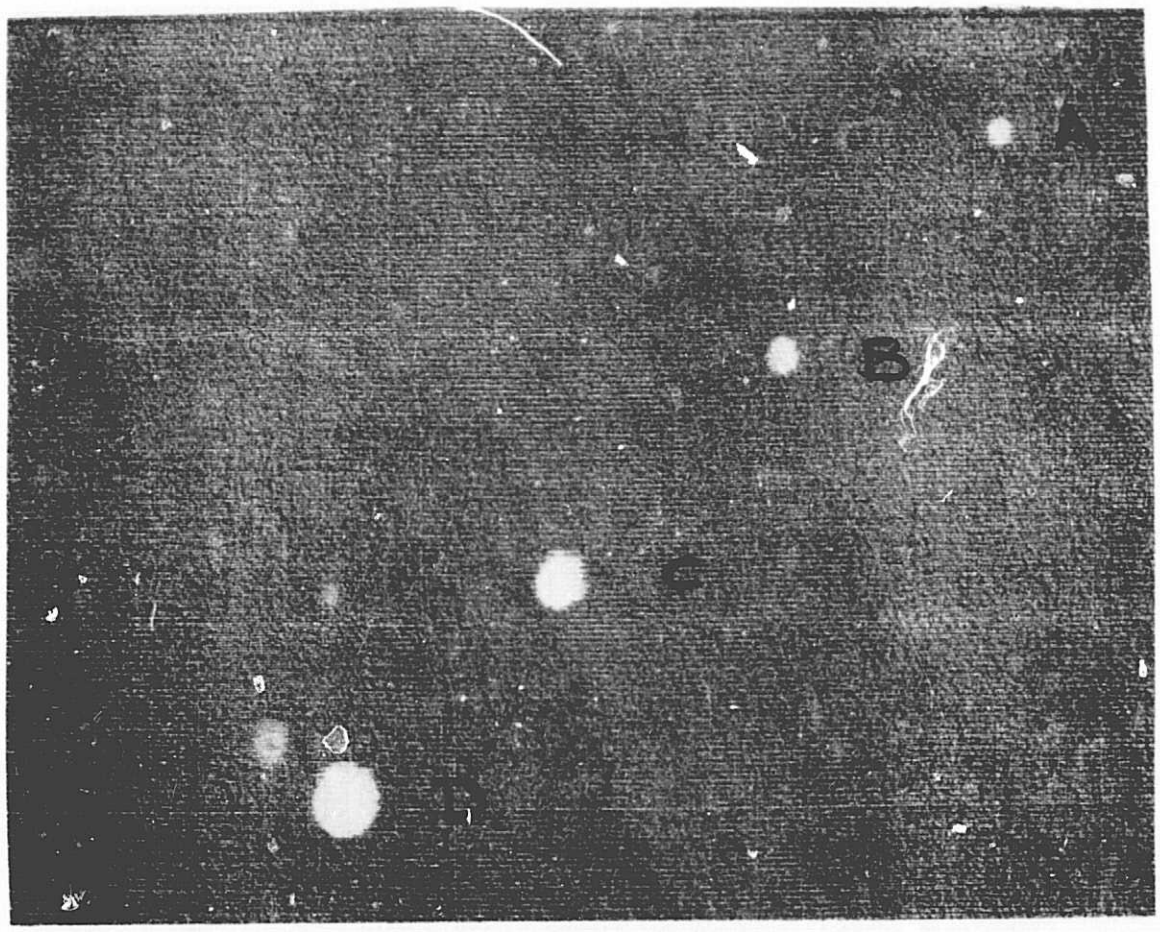

Figure 19. Delta ultrasonic scan recording showing test hole indications from 0.125-inch thick aluminum plate.

5811 B

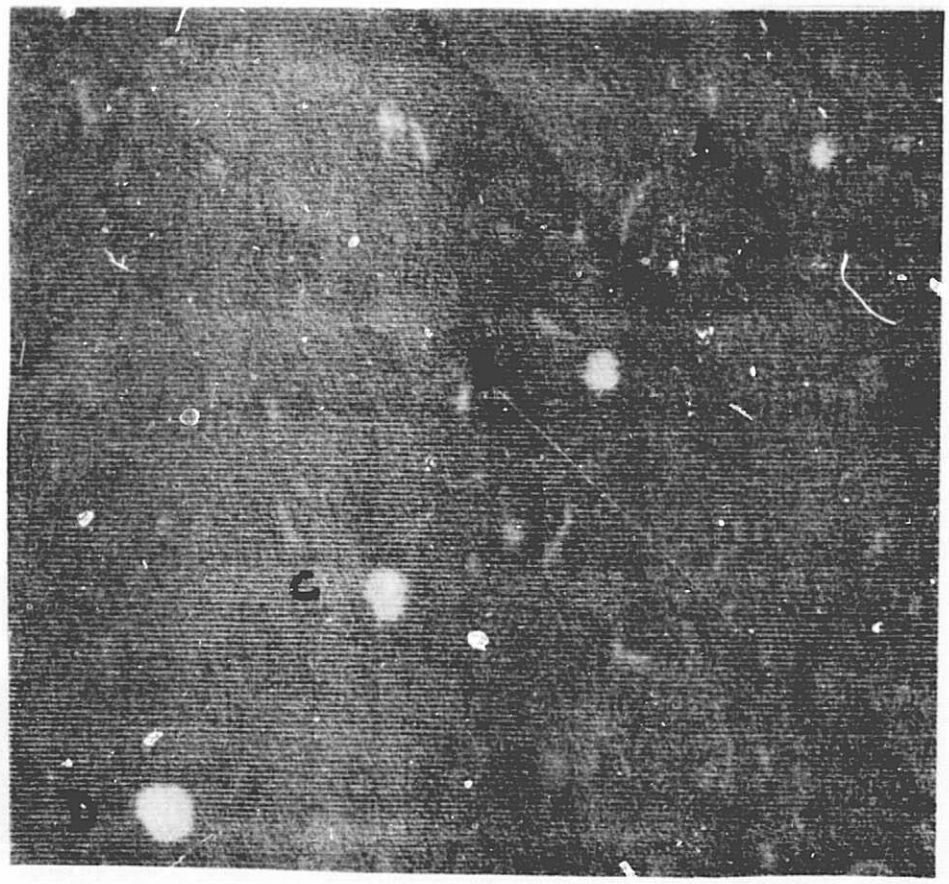

Figure 20. Delta ultrasonic scan recording showing test hole indications from the 0.125-inch titanium plate.

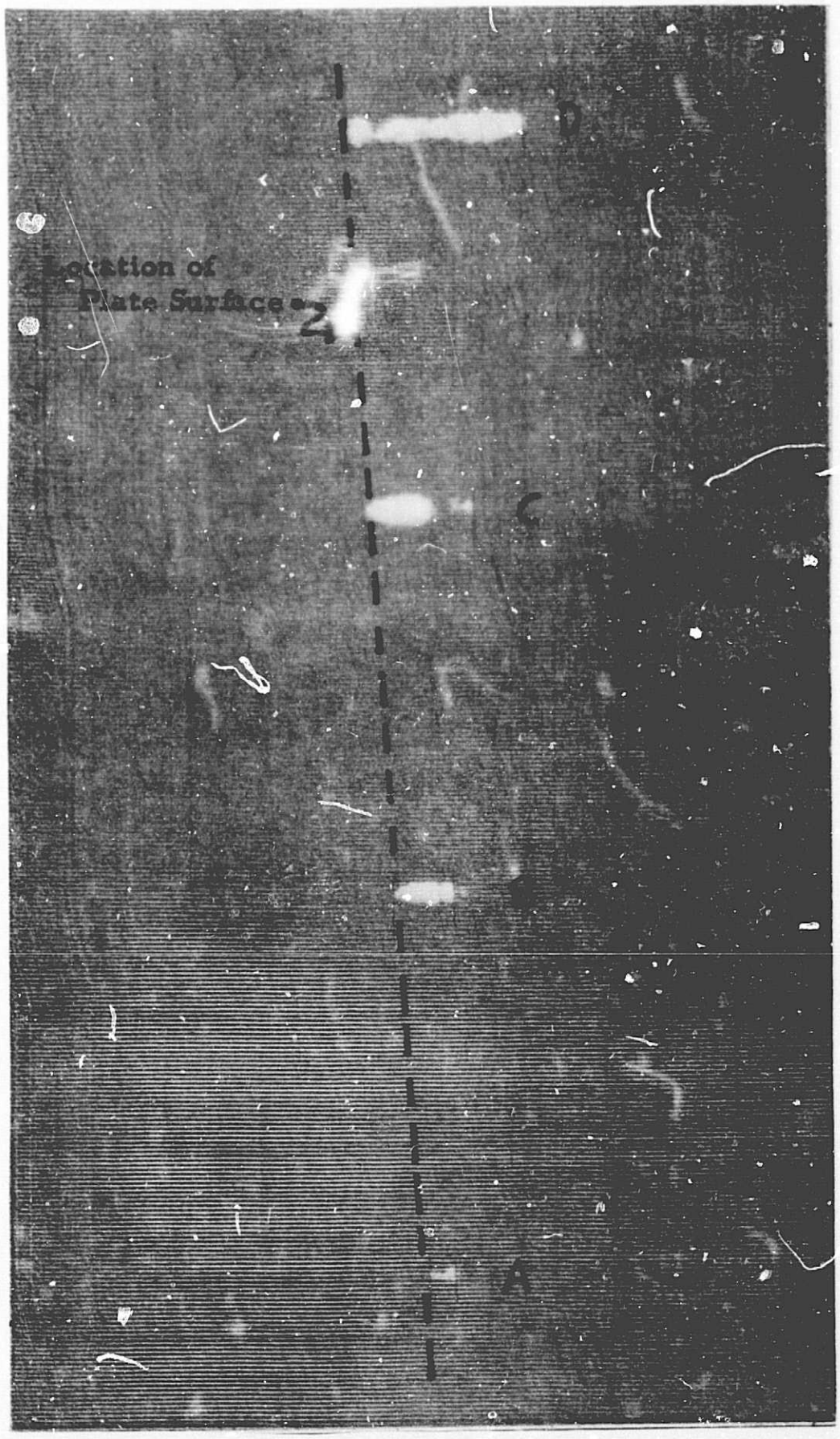

Figure 21. Shuttle delta ultrasonic scan recording showing test hole indications in the 0.500-inch thick aluminum plate.

Holes E-1, drilled parallel to the plate surface were detected in the basic Delta scan shown in Figures 15 and 16. The difference in appearance between Figures 15 and 16 resulted from a change in the search unit separation distances. In the first test, Figure 15, a short separation distance was fixed between the two search units so the transmitted sound energy passed through the inspection zone before striking the bottom surface of the plate. A longer search unit separation was used to obtain the results shown in Figure 16. By increasing the search unit separation, the transmitted sound reflects from the bottom surface of the test plate before entering the inspection zone. This approach was purposely used to detect hole E located 0.050-inch below the inspection surface. Hole E was visible in Figure 16.

Holes F-I, each 0.020-inch in diameter and 0.500-inch long appeared to be equal in size on the basic delta scan in Figure 15. The long rectangular appearance on the recording provides an indication of the hole length parallel to the inspection surface. All indications correlated to within 1/16-inch of the actual length. Depth information was not apparent in these indications although obvious changes were seen in Figure 16. The scan in Figure 16, as previously discussed, was made with a longer separation distance between search units. Sound striking round or spherical reflectors in the material was reflected in a fan-like pattern directly to the receiver search unit. The presence of re-radiated sound energy, characteristics of the "delta technique", may be masked by the presence of this high amplitude reflected energy. In this case, holes G, H, and I appear distorted while others appear normal, such as holes E and F.

Basic Delta Recordings, 1/2-Inch Titanium

In Figure 17, flat bottom holes B-D appeared round in the delta scan recording, similar to the flat bottom holes detected in aluminum plate. Again, all hole diameters were equal, 0.020-inch, slightly larger than the 0.016-inch diameter flat bottom holes in the aluminum. Since only the hole lengths varied, 0.043-inch to 0.318-inch for A through D, respectively, flaw indication variations on the recording were attributed to flaw length. As with the 1/2-inch thick aluminum plate, the indicated flaw variation was not related to flaw depth below the inspection surface.

Recorded indications of holes F through I were shown (Figure 17) as elongated or oval shaped. Hole lengths were recorded within 1/32-inch of their actual 0.5-inch length. Hole depth below the surface, in this case, did not alter the indication length; however, the indications for holes F and G were distorted. Apparently, indication width decreased as the hole depth increased; therefore, the recording does not give a true perspective of the hole diameter. Hence, indications of holes near the top surface were larger than indications of the deeper holes. Sound scattering and attenuation may account for flaw indication distortion.

A second test was made on the 1/2-inch thick titanium plate using an increased separation between the transmitter and receiver units. With this separation distance and increased sensitivity, holes A and E were detected and recorded as shown in Figure 18. Hole A at the bottom surface also could have been detected in the previous scan with an inc ease in test sensitivity, Detection of hole E requires an increase in search unit separation. The

remaining side-drilled holes F through I were distorted on the scan and bear little resemblance to the actual hole size. As with aluminum in Figure 16, the scattered and reflected energy from a round interface influences the flaw shape obtained on the delta scan recording.

Holes A, B, C, and D appear elongated in Figure 19 because the transmitted energy reflects upward from the side of the hole. Hole lengths could be estimated in practice if natural flaws always occurred with interfaces perpendicular to the inspection surface. Since flaw orientation can be a variable, use of reflected sound energy to evaluate flaw size must be used cautiously.

Basic Delta Recordings, 1/8-Inch Aluminum

In Figure 19, all notches in the 1/8-inch thick aluminum plate were detected except the smallest, E, at one sensitivity level. The absence of notch E from the recording was expected considering that notch D was 18 times larger than E. A second inspection at an increased sensitivity detected notch E. However, at this increased sensitivity level, the recording quality was reduced because surface scratches were also recorded.

The size of flaw indications on the Delta scan recordings was dependent on flaw size rather than depth. Flaw size in this case was a measure of the cross-sectional area intercepted by the transmitted sound beam. Notch F had the smallest cross-sectional area and notch D had the largest. On the recording (Figure 19), the indication of notch F was the smallest and the indication on notch D was the largest. If the flaw areas do not vary by a ratio greater than 5:1, then recorded indications can be used as a measure of flaw area. As an example, notches A, B, C, G, and H have cross-sectional areas within a 5:1 ratio (largest flaw to smallest flaw). The area of the flaw indications were multiplied by a constant and compared to the cross-sectional areas of the slots with good correlation. In practice, a reference standard must be used. This standard must be of the same material and thickness as the part being inspected and have holes or notches representing a 5:1 maximum and minimum reflector-area ratio. Practically speaking, two or more test sensitivities should be employed when the defects vary widely in size.

Basic Delta Recordings, 1/8-Inch Titanium

A discussion of flaw information in Figure 20 parallels the previous discussion concerning 1/8-inch thick aluminum material. Specifically, the flaw information recorded on the basic Delta scans was influenced more by flaw size than by depth. Yet, the variation in indicated flaw sizes on the recording of Figure 20 was not consistent with actual flaw size. For example, notch C is approximately twice the size of notch B but does not appear twice the size of B on the recording. In another instance, notch F was barely visible on the recording while the indication of notch E measured 0.030-inch in width; yet notch F is 50 percent greater in cross-sectional area. Such inconsistent results indicate a lack of ability to compensate for some unknown variable such as attenuation. Past experience with titanium reference standards has indicated that metallurgical variations cause substantial variation in the ultrasonic response. It is likely that metallurgical variations influence the ultrasonic response more than the size variation from small defects.

Shuttle Delta Technique, 1/2-Inch Aluminum

Figure 21 contains a shuttle Delta scan of the four flat bottom holes drilled into the 1/2-inch aluminum plate. The elongated appearance of holes B, C, and D is related to the hole length and can be thought of as a profile view normal to the top and bottom surfaces. Moving the transmitter search unit causes the refracted sound energy to scan through the inspection zone. As a result, the long hole D was shown at the upper end of the recording with its flat bottom on the right side. A straight line along the left edge of the indications represents the bottom surface of the test plate. Since the receiver moves in a straight line over the plate, only a narrow region below the receiver search unit is inspected. Therefore, the receiver search unit must be carefully positioned over the inspection area.

Measurement of hole length was made by comparing the recorded indications with those from known size artificial flaws in a reference standard. At a constant sensitivity level, flaws within a 5:1 ratio can be estimated from the recorded indication size.

d) Conclusions on Delta Evaluations

It can be concluded that both basic and shuttle Delta inspection techniques provide flaw size data to a degree in all but the 1/8-inch titanium plate. In addition, depth and length data might be interpreted using the shuttle variation for the 1/2-inch plates. Flaw measurements from recordings must be referenced to standards of the same material and thickness. Since the standards contain known size reflectors, their recorded size established a proportionality factor for determining actual flaw size.

In aluminum, reliable flaw size estimates were taken from the recordings when the flaw size variation was within a ratio of 5:1 (larger defect to smaller defect). In practice, two or more sensitivity levels may be required to obtain meaningful size information when a wide range of flaw sizes exist. A flaw size ratio was not established for titanium. The attenuation and sound scattering characteristics of titanium are two factors influencing this ratio.

3) Summary of the Ultrasonic Section

Both the conventional shear-wave technique, with the refinements in data recording and measurement, and the delta technique showed some potential for defining flaw dimension; these methods were then evaluated on actual defect specimens. The flaw detection and technique details which were developed to make the scan recordings on the defect specimens will be listed in the sections which describe this work.

4. Eddy-Current Tests

Eddy-current testing employs alternating current electrical signals in flat and donut shaped coils. The electrical current flow in the coil produces a magnetic field in-phase with the currents in a direction determined by the current flow. Currents at frequencies from near-DC, up to several megahertz have been employed to measure thickness, separate alloys and locate defects. The magnetic field generated by the current in the coil induces eddy currents within the material under test. These currents flow in a direction opposite to the flow of the current in the coil, and produce a reactive

magnetic field in opposition to the applied magnetic field. The phase shift and intensity of the reactive magnetic field are a function of the geometrical and electrical properties of the material. In eddy-current testing, the differences between the electrical conductivity and the apparent electrical conductivity due to defects or other disturbances in the eddy-current field are the most important factors which govern the inspection of the materials.

In order to develop sensitivity to the type of crack indications that are required for this program, extremely small coils would have to be used. Along with this, in the aluminum and titanium weldments, welding causes the electrical conductivity of the material to decrease.

Test were performed to determine the effects of welding on the electrical conductivity of titanium and aluminum alloys. 2014 aluminum and 5Al-2.5Sn titanium alloys were welded in a helium atmosphere to obtain a bead-on-plate weld with no filler metal. The resulting weld cross sections are shown in Figure 22. The electrical conductivity measured on the aluminum weldment was 29.9 percent of the International Annealed Copper Standard, and 32.2 percent IACS on the unwelded control samples. Similarly, the electrical conductivity of the unwelded titanium alloy was approximately 1.1l IACS, while the weld was slightly below this value. Both alloys were checked with Magnaflux ED-400 and ED-520 defect detection units. The welding induced change in electrical conductivity was in the same direction as fatigue-crack indications. In some instances the heat-affected zone effects were much stronger than the signals from the cracks. The specimens were surface ground to obtain minimum lift-off effects with the eddy current coils.

These experiments showed that it would be difficult to determine defect dimensions in weldments by eddy-current methods since changes would occur simultaneously from heat effects due to welding. The use of eddy-currents for the fatigue crack detection was not deemed worthwhile due to the availability of other more desirable test methods for crack detection.

5. Other Nondestructive Tests

There are several other nondestructive tests which might be used to determine the crack dimensions in some of the specimens. Such relatively new techniques as ultrasonic holography, optical holography, acoustic optical imaging of ultrasonic beams and ultrasonic imaging systems were not employed because of their present early state of development. These methods, when more refined, may ultimately provide the type of information that is wanted about the defects, since they will either produce a three-dimensional presentation of the defect or a three-dimensional view might be interpreted from the data, as in the case of the ultrasonic imaging systems. However, the present program was concerned with the present technology of nondestructive tests in determining defect dimensions. The explanation to follow in subsequent sections will describe the radiographic, penetrant and ultrasonic tests which were performed to interpret the defect dimensions in the prepared test specimens.

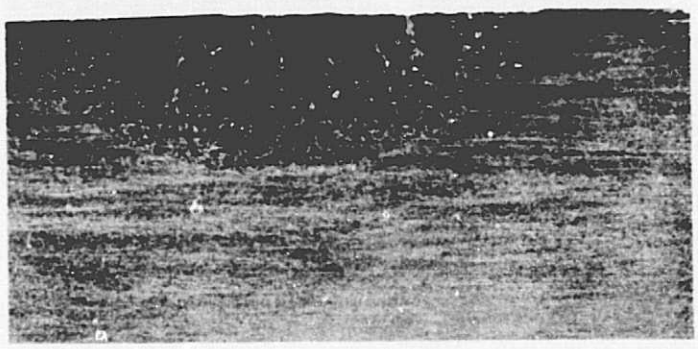

a

b

Figure 22. Macrostructures of bead on plate welds at 3X.

a) 5Al-2.5Sn titanium
b) 2014 aluminum

B. Preparation of Defect Specimens

The materials evaluated on this program were two titanium alloys, 6Al-4V ELI, 5Al-2.5 Sn ELI, and two aluminum alloys, 2014-T6 and 2219-T87. These materials are normally used in applications which involve liquid-hydrogen temperatures, -423°F. Fracture toughness values for these materials have been determined experimentally by various researchers and, hence, a considerable amount of data is available for various operating conditions.

1. Specimen Design

The surface-crack geometry selected for evaluation in this program represents a defect commonly observed in thin-walled pressure vessels. Relationships based on linear elastic fracture mechanics are available to allow a critical defect size calculated from the known fracture toughness and the operating stress to be compared with the crack size which can be defined by various NDT techniques. In generating specimens for evaluating the effectiveness of the nondestructive test techniques, the Irwin equation (24) was used to calculate the critical crack size at an applied stress equal to the yield strength of the material:

$$K_I = 1.1\pi^{1/2}\,\sigma(a/Q)^{1/2}$$

where K_I = opening mode stress intensity factor,

σ = uniform stress applied at infinity and perpendicular to the crack plane,

a = crack depth of the semi-ellipse

$Q = \phi^2 - 0.212\,(\sigma/\sigma_{ys})^2$

ϕ = complete elliptic integral of the second kind having modulus k defined as:

$$k = \frac{(c^2-a^2)^{1/2}}{c}$$

σ_{ys} = 0.2 percent offset yield strength

$2c$ = crack length

The results of these calculations are listed in Table IV and V. The critical crack depth for the 0.020-inch titanium and 0.020 and 0.125-inch aluminum samples is larger than the specimen thickness regardless of the aspect ratio (a/2c). These fracture toughness values are of little use here except to show that through cracks will probably not cause catastrophic failure. The defect length and depth values for titanium are much smaller than those that would be calculated for room temperature tests. For the aluminum alloys, the toughness of the material increases with decreasing temperature and room temperature values for defect depth and length will be smaller than those given in Table IV.

TABLE IV

CRITICAL CRACK SIZE AND MINIMUM SPECIMEN DIMENSIONS FOR SELECTED MATERIALS

Material	T °F	Yield Stress ksi	K_c ksi $\sqrt{in.}$	Appl. Stress ksi	a/2c	Critical Crack Depth, a (inch)	Critical Crack Length, 2c (inch)	B Thickness (inch)	W Minimum Width (inch)
2219 T87	-423	74	44	67	.1	0.117	1.172	1.000	3.52
					.1	"	"	0.500	"
					.1	"	"	0.125	"
					.1	"	"	0.020	"
					.3	0.167	0.555	1.000	1.67
					.3	"	"	0.500	"
					.3	"	"	0.125	"
					.3	"	"	0.020	"
					.5	0.260	0.520	1.000	1.56
					.5	"	"	0.500	"
					.5	"	"	0.125	"
					.5	"	"	0.020	"
2014 T6	-423	81	48	73	.1	0.117	1.177	1.000	3.53
					.1	"	"	0.500	"
					.1	"	"	0.125	"
					.1	"	"	0.020	"
					.3	0.167	0.5572	1.000	1.67
					.3	"	"	0.500	"
					.3	"	"	0.125	"
					.3	"	"	0.020	"
					.5	0.261	0.5221	1.000	1.57
					.5	"	"	0.500	"
					.5	"	"	0.125	"
					.5	"	"	0.200	"

TABLE V

CRITICAL CRACK SIZE AND MINIMUM SPECIMEN DIMENSIONS FOR SELECTED MATERIALS

Material	T °F	Yield Stress ksi	K_c ksi $\sqrt{in.}$	Appl. Stress ksi	a/2c	Critical Crack Depth, a (inch)	Critical Crack Length, 2c (inch)	B Thickness (inch)	W Minimum Width (inch)
5Al-2.5Sn-Ti	-423	210	54	189	.1	0.022	0.222	0.500	0.66
					.1	"	"	0.125	"
					.1	"	"	0.020	
					.3	0.031	0.105	0.500	0.31
					.3	"	"	0.125	"
					.3	"	"	0.020	"
					.5	0.049	0.098	0.500	0.29
					.5	"	"	0.125	"
					.5	"	"	0.020	"
6Al-4V-Ti	-423	220	54	189	.1	.017	0.173	0.500	0.52
					.1	"	"	0.125	"
					.1	"	"	0.020	"
					.3	.024	.0822	0.500	0.24
					.3	"	"	0.125	"
					.3	"	"	0.020	"
					.5	.038	.0770	0.500	0.23
					.5	"	"	0.125	"
					.5	"	"	0.020	"

In the test specimens, defects were generated either by electrodischarge machining an appropriate slot and fatigue cracking, or by incorporating a selected type of weld defect. In some cases, a range of defect sizes was desired in order to determine the ability of the test methods to distinguish differences in the crack sizes. Some cracks were equal to the critical size while others were either twice or one-half the critical size. In this manner, the ability of the NDT method to detect defects would be defined over a range of crack sizes which were meaningful with respect to the actual material performance characteristics. When the calculated critical defect size was relatively large and represented no detection problem for the NDT method as in the case with the 0.020-inch material, the crack size was arbitrarily selected to be in the range where the sensitivity of the NDT method would be challenged.

The test sequence involved: 1) calculating the defect sizes which would be critical at -423°F; 2) generating the defect either by fatigue precracking or welding; 3) determining the defect size and position by selected nondestructive methods; 4) pulling the specimen to failure to allow direct measurement of the defect; and, 5) comparing the actual defect size with that determined by NDT methods.

2. Specimen Fabrication

The test specimens selected for the program are listed in Table VI. A representative sample of both fatigue cracks and weld defects were fabricated. The actual specimen designs are illustrated in Figure 23 with the tabulated final specimen dimensions. A typical sample of various specimens is illustrated in Figure 24. The width of the gage section in the specimens was at least three times the critical crack length and larger in most instances. The overall length of the specimens was at least 18 times the critical defect length, or at least 6 times the test section width. Of the 99 specimens for the program, 81 were fatigue cracked while 18 contained weld defects.

a. Fatigue Precracking

The precracking was achieved by flexure for the 0.125, 0.500 and 1.000-inch samples and by tension-tension procedures for the 0.020-inch material. Starter notches were electrodischarge machined into the specimens. Because tight defects were desired, the starter notches were machined with an approximate 0.004-inch thickness. The length and depth of the starters were determined on the basis that the cross-sectional area of the starter notch would be approximately one-ninth of the defect's final cross-sectional area.

b. Weld Specimens

The weld specimen samples were designed to provide defects which are typically encountered in processing. Of particular interest was incomplete penetration in the aluminum alloys. The high temperature in the welding process causes the base plates to expand during welding and results in a weld joint with virtually no gap. The opposing faces of the weld preparation come together in intimate contact producing a defect condition which is difficult to detect by nondestructive tests. To reproduce these conditions, the weld preparation was designed to have larger section thicknesses in the lands of double butt joints. Figure 25 illustrates test plate dimensions to produce different amounts of incomplete penetration. Figure 26 shows macrographs of the three different land thicknesses after welding. From the macrographs, the

TABLE VI

DEFECT SPECIMENS FOR PROGRAM

Material	Thickness (inch)	a/2c	Defect Type *	Initial Specimen Width (inches)	Specimen Length (inches)	Number of Specimens
Aluminum 2219-T7	1.0	0.1	I.P	5.675	22.0	2
	0.5	0.1	I.P	"	22.0	2
	1.0	0.3,0.5	4FC,2I.P	3.375	11.0	6
	0.5	0.3,0.5	FC	"	11.0	9
	0.5	0.5	FC	6.675	22.0	2
	0.125	-	FC	3.0	8.0	6
	0.020	-	FC	3.0	8.0	4
Aluminum 2014-T6	1.0	0.1	I.P	5.675	22.0	2
	1.0	0.3,0.5	2FC,2I 2FC,2I.P	3.375	11.0	6
	0.5	0.3,0.5	FC	"	11.0	2
	0.125	-	FC	3.0	8.0	6
	0.020	-	FC	3.0	8.0	3
Titanium 6Al-4V	0.5	0.1,0.3,0.5	FC	3.0	8.0	3
	0.125	0.1,0.3,0.5	FC	"	"	6
	0.020	-	10FC,2I.P	"	"	12
Titanium 5Al-2.5Sn	0.5	0.1,0.3,0.5	2I.P,9FC	3.0	8.0	11
	0.125	0.1,0.3,0.5	FC	"	"	6
	0.020	-	2I.P,9FC	"	"	11

* - FC - Fatigue Crack
I.P - Weld Incomplete Penetration
I - Weld Inclusion

MAX. TAPER .010 OVER GAUGE LENGTH "E" FOR DETAILS 1 & 6; .005 FOR DETAILS 2, 3, 4, & 5

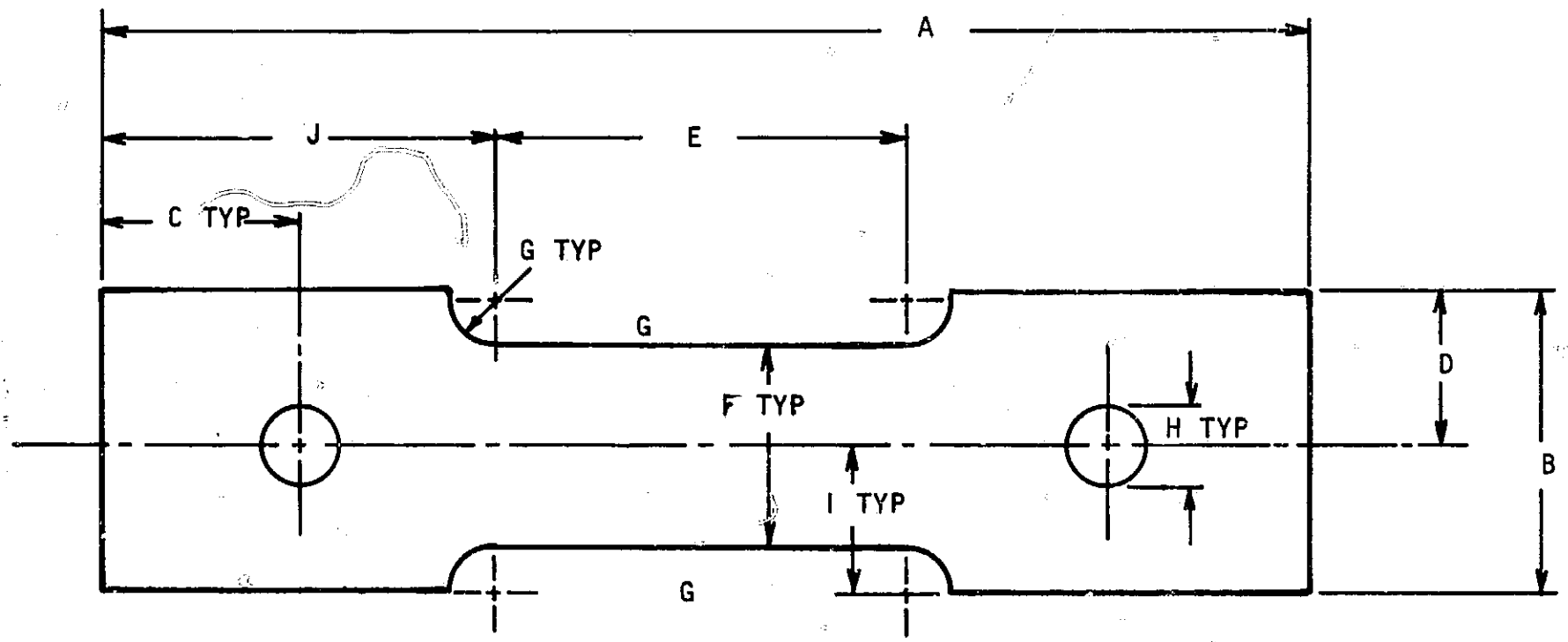

DET.	A	B	C	D	E	F	G	H	I	J
-1	22.00	5.67	3.25	2.837	7.00	3.250	1.250	1.250	2.875	7.50
-2	11.00	3.37	1.75	1.687	3.38	1.560	0.875	0.875	1.655	3.81
-3	8.00	3.00	1.50	1.500	2.00	1.000	0.750	0.500	1.250	3.00
-4	8.00	3.00	1.50	1.500	2.00	0.675	0.750	0.500	1.088	3.00
-5	8.00	3.00	1.50	1.500	2.00	0.375	0.750	0.500	0.938	3.00
-6	22.00	6.67	3.25	3.387	7.00	3.250	1.250	1.250	2.875	7.50
	±.05	±.02	±.03	±.010	±.02	±.005	±.010	+.005 -.000	±.010	±.02

Figure 27. Illustration showing designed defect specimen dimensions.

5744 B

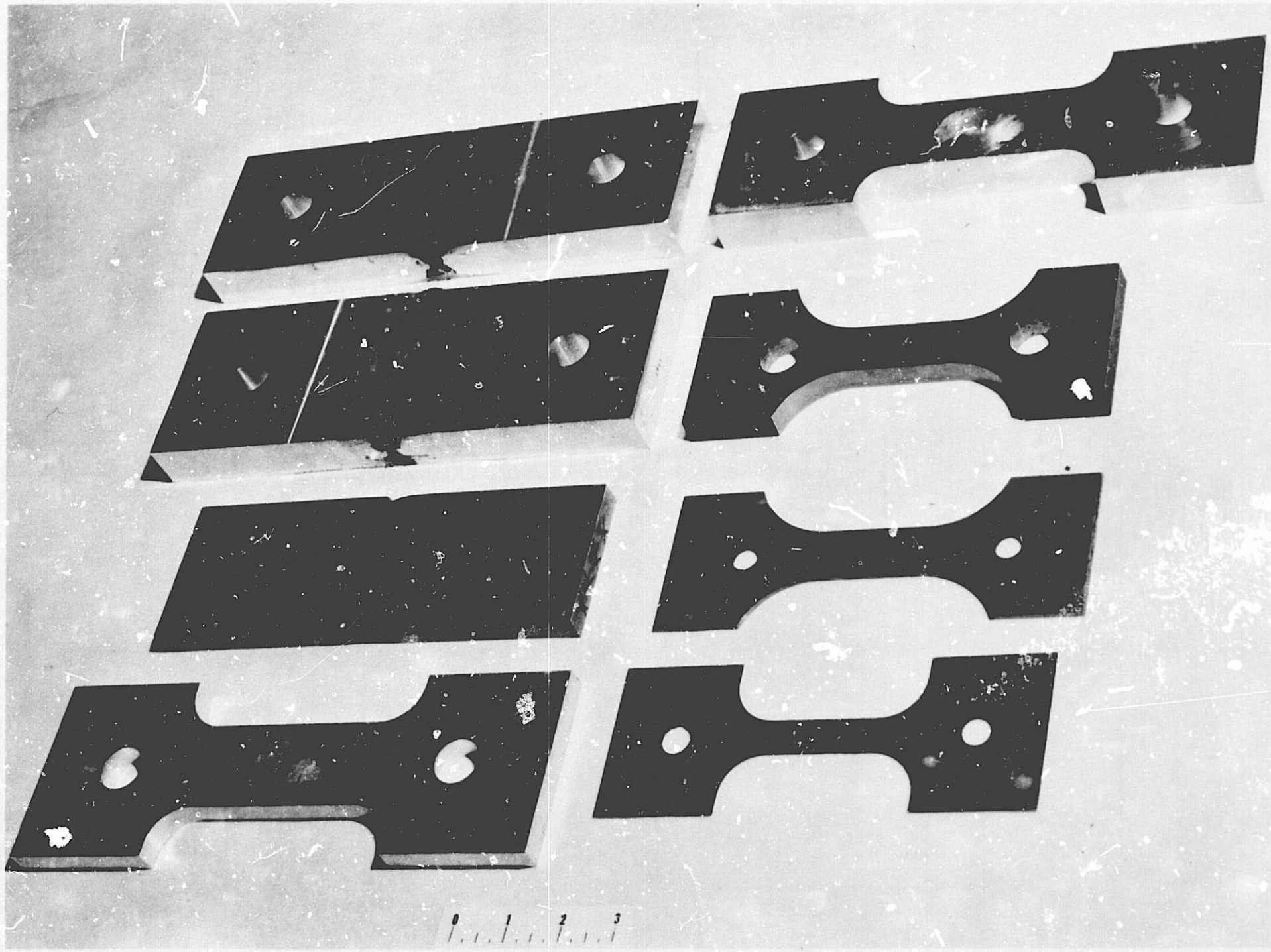

Figure 24. Several defect specimens in various stages of preparation.

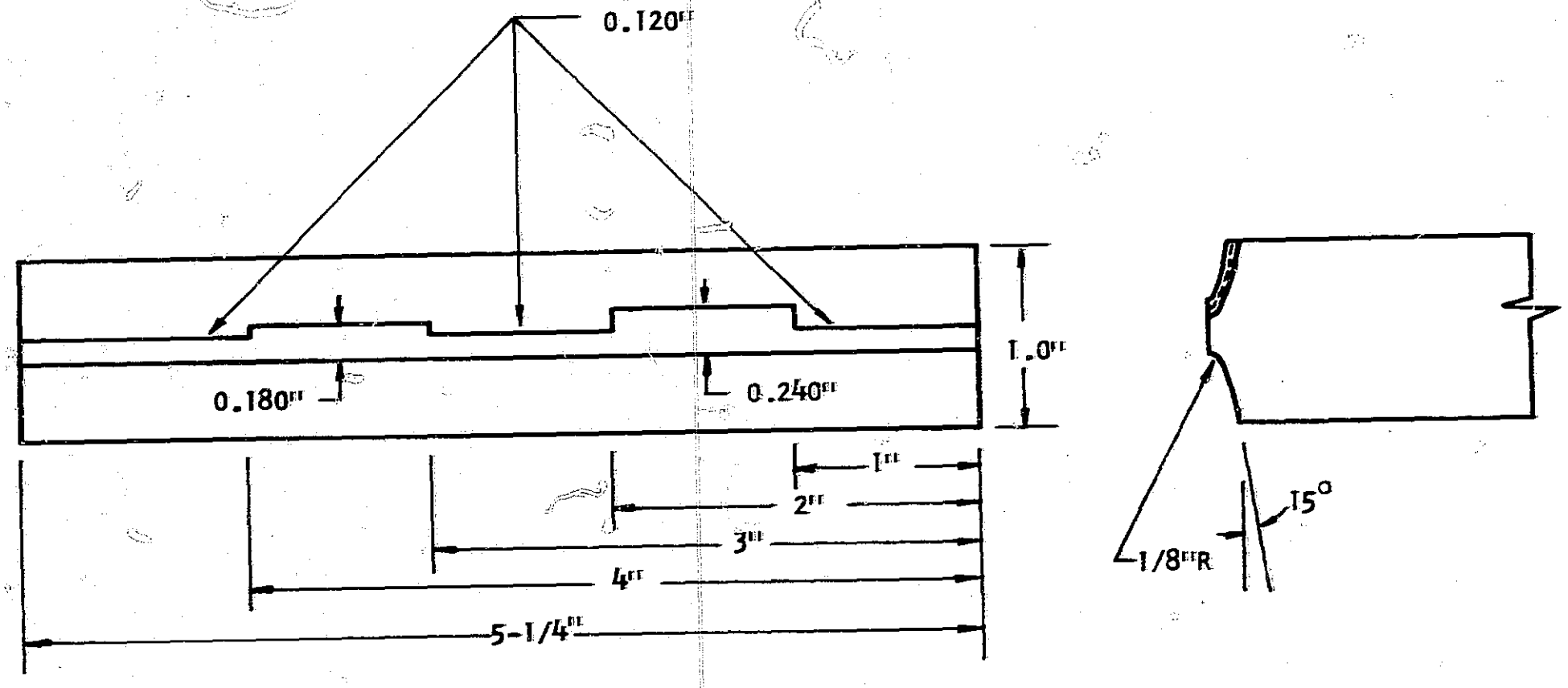

Figure 25. Weld groove preparation for defect test specimens in 1.0-inch aluminum.

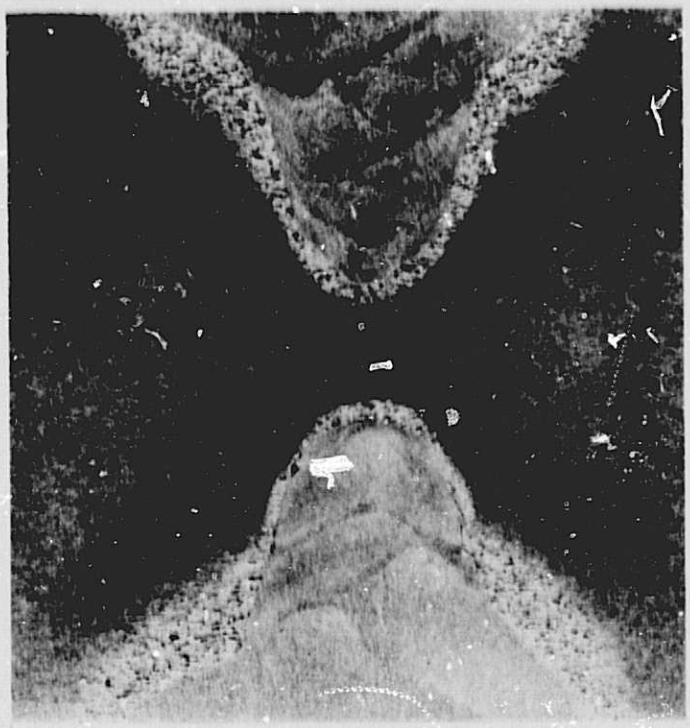

a

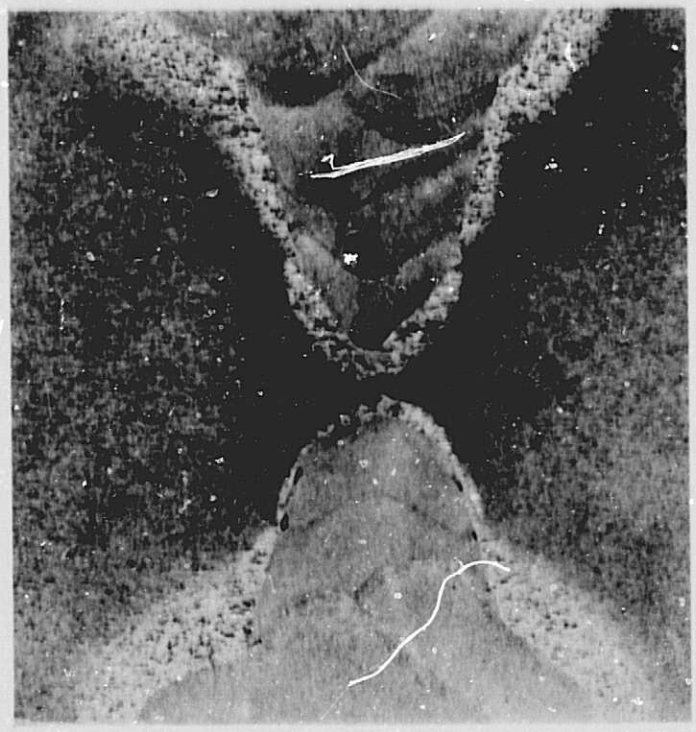

b

c

Figure 26. Macrographs of aluminum weld cross sections from weld preparations illustrated in Figure 25 at 3X.

characteristic gap is not visible at the tip of the weld but can be seen at higher magnifications.

Welding parameters were established for each of the materials and thicknesses that were welded to give approximately 55 percent penetration of the cross-section from each side of the joint with the normal joint preparation. Inclusion specimens were produced by seeding a piece of tungsten electrode in the joint prior to welding. For the 0.020-inch material, incomplete penetration defects were obtained by welding over thin strips placed across the weld joint. The welding parameters for the weld specimens are summarized in Table VII.

TABLE VII

SUMMARY OF WELD PARAMETERS FOR DEFECT SPECIMENS

Material	Thick (inch)	Weld Method	Filler Wire	Travel Speed (in/min.)	Pass Number	Shielding Gas (Cubic Feet/Hour)	Voltage (Volts)	Current (Amps.)	Backup Gas (CFH)	Trailer Shield (CFH)
2014-2219 Al	1.0	MIG	3/64"D-4043	19	1 thru 2	50 Ar	20.5	160	-	-
		MIG	3/64"D-4043	15	3 thru 12	50 Ar	20.5	160	-	-
2219 Al	0.500	MIG	3/64"D-4043	20	1 thru 8	50 Ar	20	160	-	-
5Al-2.5Sn Ti	0.500	TIG	-	10	1	50 He	14	110	10 Ar	65 Ar
		"	1/16"D-6Al-4V Ti	10	2 thru 5	50 He	16	110	10 Ar	65 Ar
		"	1/16"D-6Al-4V Ti	10	6 thru 17	50 He	16	130	10 Ar	65 Ar
6Al-4V Ti	0.020	TIG	-	13.5	1	30 He + 5 Ar	15	10	5 Ar	30 Ar

III - EXPERIMENTAL PROGRAM AND RESULTS

With the previously described specimens, four types of nondestructive tests were performed on each sample, where applicable, to reveal the critical defect dimensions. As a part of the investigations, the effects of stress states were determined on detectability of some defects by the ultrasonic shear-wave technique. Tensile tests were then performed on the various specimens to develop fracture toughness values where possible, and to reveal the actual defect shapes and dimensions.

A. Nondestructive Testing

The nondestructive tests selected from the review of applicable test methods for surface and subsurface defects were radiographic, penetrant and two ultrasonic inspections. The techniques applied will be described and the defect dimensions or signal strengths revealed by the test method will be listed with the actual defect length and/or depth.

1. Radiographic Tests

The radiographic tests performed on the specimens were determined on an empirical basis since there are no analytical techniques of analysis widely accepted. Standard radiographic penetrameters (Military Specifications 453 and 271) were used on the 1/2 and 1-inch thick materials to reveal the 1T holes. Two types of X-ray generators were selected for radiography, both having be- - llium windows. A modified Picker X-ray Minishot II having a 0.5 millimeter focal spot and a 10 to 110 kev energy range was utilized for the majority of tests. The Picker unit is shown in Figure 27. On the larger specimens where the length was too long for the cabinet unit, the specimens were radiographed at equivalent energies on a Norelco 150 kev constant-potential unit. A summary of the radiographic techniques utilized for the specimens is listed in Table VIII. Variations in technique were made to compensate for lower physical densities in the weld or longer exposures for weld buildup. In most instances, two films were exposed for automatic and manual processing. The film quality from automatic processing varied because of artifacts that at times were in the primary area of interest.

a. Fatigue-Crack Specimens

Crack measurements on the radiographs were made with an optical comparator. The indicated crack lengths on the 0.020-inch aluminum and titanium fatigue-crack specimens are compared in Table IX with the actual crack length as measured on the broken specimens. In general, the cracks at this thickness were all detected except for one specimen that had the smallest crack length generated in any of the 0.020-inch specimens. The indicated lengths are less than the actual length in almost all cases. Some of the measurement discrepancies are caused by the difficulty in accurately measuring the actual crack length. Some of the dimensions of the fatigue cracks were not clearly distinguishable due to the texture of the fracture surfaces.

Crack-length data for the 0.125-inch specimens are listed in Table X. None of the cracks in aluminum alloys were detectable, and only seven of the twelve cracks in the titanium alloys were detected. This can be expected since

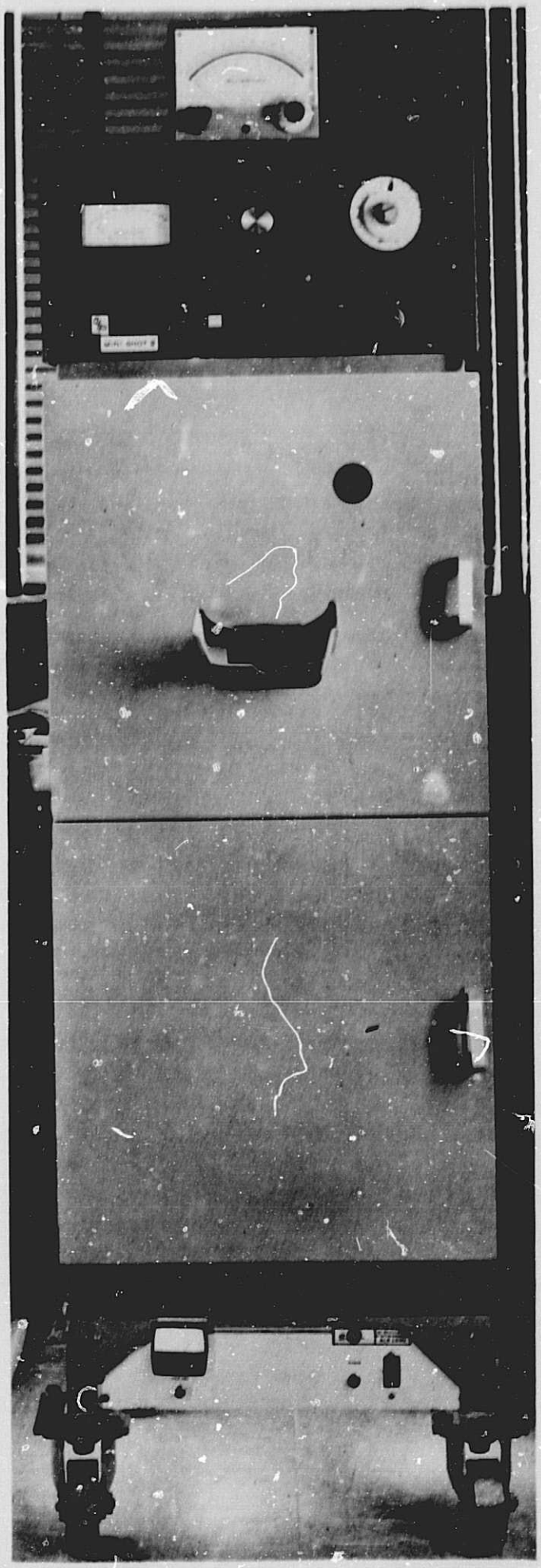

Figure 27. Modified Picker Minishot II X-ray generator.

TABLE VIII

RADIOGRAPHIC TECHNIQUES FOR PICKER MINISHOT II
110 KV X-RAY GENERATOR ON VARIOUS ALLOYS AND THICKNESSES
AT 24-INCH TARGET-FILM-DISTANCE, 2.0 FILM DENSITY ON EASTMAN KODAK
TYPE R FILM

Alloy	Thickness (inch)	Energy (kilovolts peak)	Exposure (milliampere-seconds)
2219 Al	0.020	25	600
	0.125	40	1230
	0.500	65	1670
	1.000	90	1680
2014 Al	0.020	25	540
	0.125	40	1090
	0.500	65	1620
	1.000	90	1600
6Al-4V Ti	0.020	45	480
	0.125	70	840
	0.500	110	1800
5Al-2.5Sn Ti	0.020	45	530
	0.125	70	1200
	0.500	110	2700

X - Omat Processing

TABLE IX

COMPARISON OF RADIOGRAPHIC TEST RESULTS ON 0.020-INCH FATIGUE-CRACK SPECIMENS WITH ACTUAL MEASURED CRACK-LENGTHS

Specimen Identification	Actual Crack Length (inch)	Indicated Crack Length (inch)
2014-1	0.088	0.085
2014-1A	0.094	0.073
2014-2	0.087	0.085
2219-1	0.189	0.080
2219-2	0.190	0.085
2219-3	0.138	0.130
2219-4	0.125	0.115
5-2.5-1	0.116	*
5-2.5-3	0.140	*
5-2.5-4	0.121	*
5-2.5-6	0.121	0.120
5-2.5-7	0.112	0.075
5-2.5-8	0.062	0
5-2.5-9	0.087	0.080
5-2.5-10	0.075	0.080
5-2.5-12	0.116	0.115
6-4-1	0.261	*
6-4-2	0.118	*
6-4-3	0.067	*
6-4-11	0.172	0.150
6-4-13	0.137	0.130
6-4-15	0.130	0.135
6-4-16	0.092	0.085
6-4-17	0.085	0.090
6-4-18	0.112	0.105
6-4-19	0.082	0.080

* - No data available.

TABLE X

COMPARISON OF RADIOGRAPHIC TEST RESULTS ON 0.125-INCH FATIGUE-CRACK SPECIMENS WITH ACTUAL MEASURED CRACK-LENGTHS

Specimen Identification	Actual Crack Length (inch)	Indicated Crack Length (inch)
2014 2219	Various	*
5-2.5-1A	0.098	0*
5-2.5-2	0.058	0*
5-2.5-3	0.054	0*
5-2.5-4	0.222	0.200
5-2.5-7	0.200	0.170
5-2.5-8	0.075	0*
6-4-1	0.077	0.060
6-4-1B	0.054	0*
6-4-3	0.062	0.050
6-4-4	0.158	0.160
6-4-5	0.065	0.085
6-4-6	0.158	0.110

* - No crack length detectable radiographically.

the crack alignment in the radiographic beam is very critical. Almost the reverse occurred for the 0.500-inch test specimens listed in Table XI. None of the radiographs for the titanium specimens revealed any fatigue cracks, while the radiographs of the aluminum specimens revealed the cracks in most cases. The reasons for the differences are probably traceable to operator variables during the radiographic tests and the alignment of the X-ray beam with the crack. The six cracks in the 1.0-inch aluminum alloy specimens were all detectable, but the full lengths of the cracks were not revealed, as shown in Table XI. The physical size of the cracks in the 1/2-inch specimens are generally larger than those for the titanium alloys, providing an easier defect for detection radiographically.

b. Weld Defect Specimens

The weld defect specimens were fabricated with different amounts of incomplete penetration and inclusions as previously listed. The results of the radiographic tests on these specimens are detailed in the following sections.

1) 0.020-Inch Titanium Welds

The radiographic techniques for the 0.020-inch welds easily revealed the four incomplete penetration conditions and their extent in the welds. The defects extended across the thickness and represented a through defect condition.

2) 0.500-Inch Titanium Welds

No defects were visible in the radiographs of these two welds and the absence of defects was confirmed after fracture of the welds. The welding technique provided deeper penetration than expected.

3) 0.500-Inch Aluminum Welds

Two incomplete penetration samples were prepared in the 2219 alloy, with the defects of different depths. The lack of penetration was revealed in the radiographs of specimens 5A and 5B by an unconventional technique. Since the filler metal-base metal interaction in the weld zone produced welds with a lower physical density than the base metal, incompletely penetrated welds result in a lower film density than completely penetrated welds. Figures 28 and 29 show the radiographs for these two welds and the fracture surfaces of the welds. The incomplete penetration is approximately 0.070-inches in depth and 1.217-inches long in specimen 5A. The radiographic length is not adequately defined since the defect tapers off to zero thickness at the ends, but is between 1.0 and 1.3 inches. For specimen 5B, the depth of incomplete penetration is approximately 0.048 inch, while the length is 0.951 inch. Again the density transition is not sharp and the radiographic length is approximately 1 inch. The radiograph also reveals two large and several small pores. However, no dark lines can be seen in the radiographs to indicate incomplete penetration, as one would normally find in welds. Radiographic techniques will not reveal the defect without the use of filler metals having lower densities than the base metals.

4) 1.0-Inch Aluminum Welds

All of the 1.0-inch weld specimen radiographs indicated a large number of defects with the incomplete penetration defects being revealed only by the film density transitions. Even the inclusion specimens containing the inserted

TABLE XI

COMPARISON OF RADIOGRAPHIC TEST RESULTS ON 0.500 and 1.0-INCH FATIGUE-CRACK SPECIMENS WITH ACTUAL MEASURED CRACK-LENGTHS

Specimen Identification	Actual Crack Length (inch)	Indicated Crack Length (inch)
2014-1	0.589	0.535
2014-2	0.554	0.500
2219-1	0.386	0*
2219-2	0.313	0*
2219-3	0.323	0.310
2219-4	0.334	0.230
2219-5	0.299	0*
2219-6	0.354	0.230
2219-7	0.340	0.235
2219-8	0.612	0.415
2219-9	0.600	0.510
2219-1A	0.482	0.310
2219-1E	0.486	0.425
5-2.5 6-4 Titanium	Various	0*
2014-1.0-1	0.567	0.425
2014-1.0-2	0.550	0.415
2219-1.0-1	0.543	0.325
2219-1.0-2	0.617	0.365
2219-1.0-3	0.530	0.335
2219-1.0-4	0.473	0.285

* - No indicated defect.

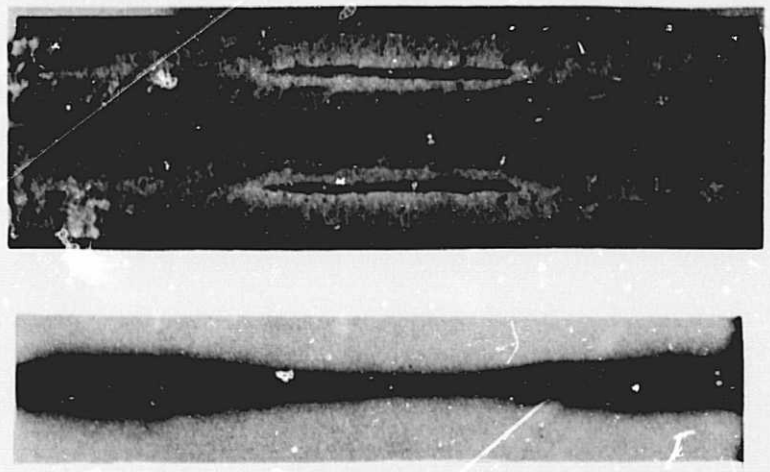

Figure 28. Radiograph and fracture surface macrograph of weld 2219-0.5-5B at IX.

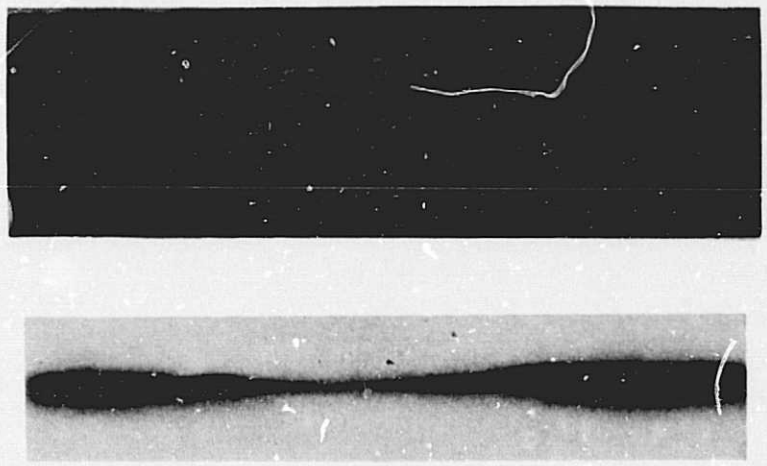

Figure 29. Radiograph and fracture surface macrograph of weld 2219-0.5-5B at IX.

tungsten electrodes contained unwanted incomplete penetration, many indications of porosity, and lack of fusion. Two macrographs of the fracture surfaces of welds in the 2014 alloy are shown with the corresponding radiographs in Figures 30 and 31. Besides the large amounts of porosity in the radiograph, no outstanding evidence of either lack of fusion or incomplete penetration is evident in the radiographs, though they exist in the specimens as revealed on the fracture surfaces. In Figure 32, the fracture surface and radiograph of specimen 2014-1.0-3C is shown. The tungsten inclusion is evident along with varying amounts of porosity and lack of fusion with incomplete penetration extending across the specimen width. Again however, the incomplete penetration is not detectable and the lack of fusion is marginal in the radiographs.

Weld 2219-1.0-3A shown in Figure 33 also had large amounts of porosity and a 3/4 inch long incomplete penetration. In addition, a rather large area on the fracture surface was not fused and was not detected in the radiograph. The following list summarizes the defects in each of the aluminum 0.5 and 1.0-inch specimens with defects detectable in the radiographs:

Specimen ID	Defects*	Defects Radiographically Detectable*
2219-0.5-5A	LP, P, I	P, I
2219-0.5-5B	IP, P	P
2219-1.0-3A	IP, P, LF	P
2219-1.0-3B	IP, P, LF	P, LF
2219-1.0-4A	IP, LF, P	P
2219-1.0-4B	IP, LF, P	P
2014-1.0-2A	IP, LF, P	P
2014-1.0-2B	IP, LF, P	P
2014-1.0-3A	LF, IP, P, I	I, P
2014-1.0-3B	LF, IP, P	LF, P
2014-1.0-3C	I, LF, IP, P	I, LF, P
2014-1.0-3D	I, LP, LF, P	I, LF, P

* I - Tungsten Inclusions
IP - Incomplete Penetration
LF - Lack of Fusion
P - Porosity

In general, none of the radiographs revealed incomplete penetration without the use of the change in radiographic density as an indicator. Lack of fusion was only revealed in the most severe cases, while porosity and inclusions were readily detectable.

2. Penetrant Tests

The penetrant tests were performed on all external defect specimens. Tracer Tech P-151 initially was used as the penetrant, but subsequent studies included Magnaflux ZL-30A. These high resolution penetrants did not perform well on the 0.5 and 1.0-inch aluminum fatigue crack specimens even though excessive penetration times were tried. One of the problems encountered resulted from the use of fluorescent penetrants in the precracking operation in order to follow crack growth. The penetrant trapped in the cracks during precracking could be washed out in the 0.020-and 0.125-inch samples, but great difficulty was

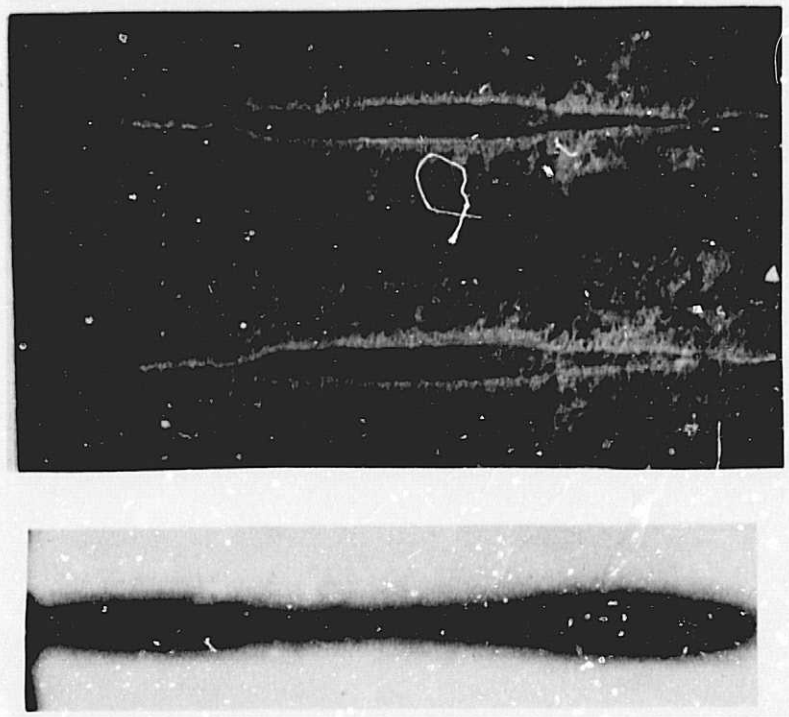

Figure 30. Radiograph and fracture surface macrograph of weld 2014-1.0-2A at 1X

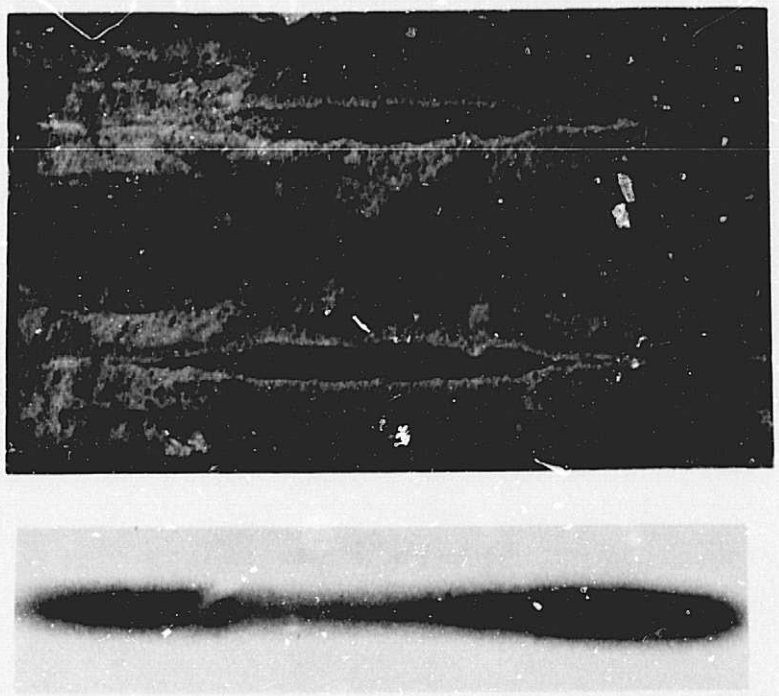

Figure 31. Radiograph and fracture surface macrograph of weld 2014-1.0-2B at IX.

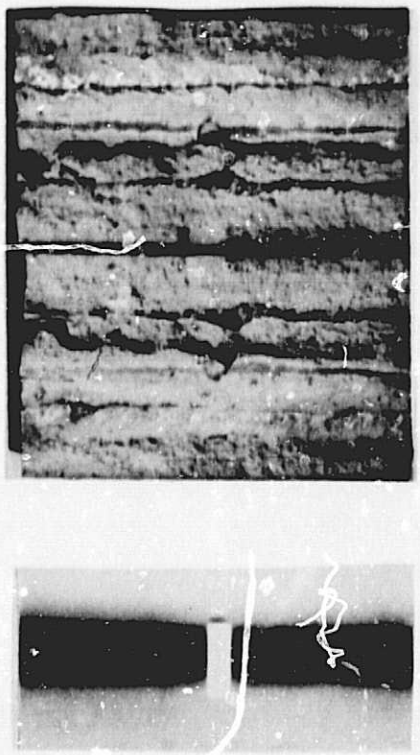

Figure 32. Radiograph and fracture surface macrograph of weld 2014-1.0-3C at IX.

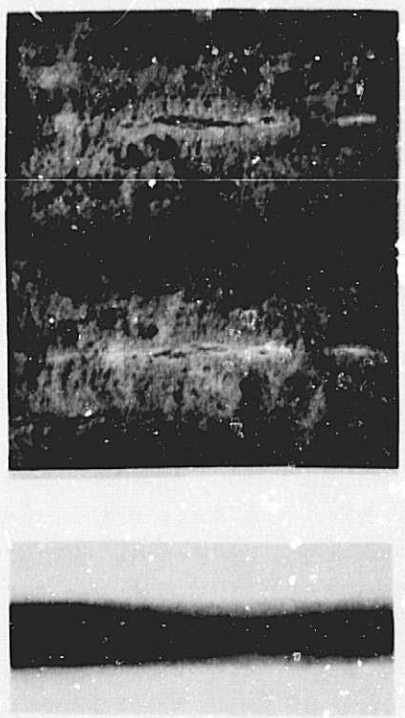

Figure 33. Radiograph and fracture surface macrograph of weld 2219-1.0-3A at IX.

5815 B

encountered with the larger thicknesses. Consequently, either because the cracks were extremely tight or because precracking penetrant blocked the crack, various degrees of success were achieved in determining crack length. The tight and deep nature of the cracks was thought to be the most hinderance since the defect indications obtained in the 0.125-inch material and the 0.500-inch titanium did not always resolve the full length of the crack.

In order to illustrate the differences in crack detectability, a titanium specimen, 5-2.5-0.125-4, was processed with ZL-30A penetrant as fatigue cracked after precrack penetrant removal. Under a tensile bending stress, the penetrant was applied and the difference in detectability of the crack observed as shown in Figure 34a and b. The crack length in Figure 34a at zero stress is somewhat less than 0.110-inch while the true crack length revealed in Figure 34b under tensile stress is approximately 0.225-inch. An estimate of the effect of this crack on the performance of the specimen would be much impaired by the zero-stress measurement.

The penetrant penetration times for the various specimens varied widely. Five-minute penetration times with ten-second emulsification times were adequate for the 0.020-inch specimens which contained through cracks. The penetration time was increased as the crack detectability became more difficult. Typically, penetration times of 2.5 hours were used for the titanium alloys with up to 30 second emulsification times. The aluminum alloys proved to be extremely difficult to detect crack lengths, even with penetration times up to 95 hours.

The data from the penetrant tests are compared in Table XII, for the 0.020-inch specimens, to the actual measured crack lengths after destructive tests. Developer was not used in any of the tests because it caused rapid pull-out of the penetrant and exaggerated crack dimensions. The photograph in Figure 35a shows the penetrant indication for specimen 5-2.5-0.020-9, and the fracture surface in Figure 35b. The penetrant indication is only slightly different from the actual value. Another difficulty encountered in obtaining accurate crack lengths was noticeable for one specimen in particular. The penetrant indication measured 0.073-inch for specimen 6-4-0.020-16 which is slightly below the actual surface length of 0.077-inch. However, the actual maximum crack length below the surface is 0.092-inch and is not fully revealed by the penetrant test. All the cracks were detectable with the penetrant for the 0.020-inch specimens.

For the 0.125-inch fatigue crack specimens, the test results are listed in Table XIII. The data show that all cracks were detected and the results agree well with the actual crack lengths for all but the last titanium specimen, 6-4-0.125-6. Here the indicated crack length is approximately half the actual value. The penetrant indication for this crack is shown in Figure 36 along with the fracture surface macrograph. Two small dots are visible in the photograph of the penetrant indications at the extremes of the crack, but were not initially interpreted as part of the crack. As a result, approximately 0.040-inch on each end of the crack was not measured.

The test results listed in Table XIV reveal a large variation in the detectability of crack length in the 0.500-inch specimens. Good results were obtained on the titanium specimens, while no crack length indications were obtained on the aluminum specimens. In addition, none of the cracks were detected in the 1.0-inch specimens with either of the penetrants. Cracks are generally deeper in the 0.500-inch aluminum alloys than in the titanium alloys, which may account for some of the differences in crack detectability.

a

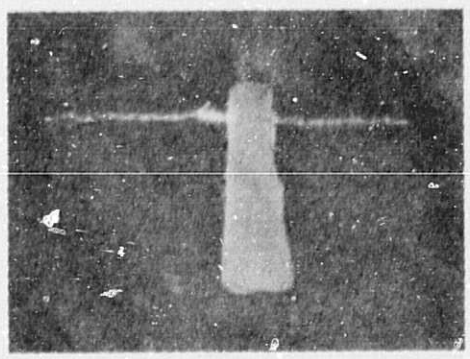

b

Figure 34. Fluroescent penetrant indications of a fatigue crack in specimen 5-2.5-0.125-4 at 10X.

a) unstressed
b) tension bending stress on crack

TABLE XII

PENETRANT AND DESTRUCTIVE TEST CRACK-LENGTH MEASUREMENTS FOR 0.020-INCH SPECIMENS

Specimen Identification	Penetrant Crack Length (inch)	Actual Crack Length (inch)
2014-0.020-1	0.089	0.088
2014-0.020-2	0.088	0.087
2014-0.020-1A	0.092	0.094
2219-0.020-1	0.175	0.189
2219-0.020-2	0.220	0.190
2219-0.020-3	0.142	0.138
2219-0.020-7	0.143	0.125
5-2.5-0.020-1	0.103	0.116
5-2.5-0.020-3	0.111	0.140
5-2.5-0.020-4	0.112	0.121
5-2.5-0.020-6	0.128	0.121
5-2.5-0.020-7	0.080	0.112
5-2.5-0.020-8	0.054	0.062
5-2.5-0.020-9	0.084	0.087 **
5-2.5-0.020-10	0.072	0.075
5-2.5-0.020-12	0.110	0.116
6-4-0.020-1	0.252	0.261
6-4-0.020-2	0.102	0.118
6-4-0.020-3	0.061	0.067
6-4-0.020-11	0.165	0.172
6-4-0.020-13	0.132	0.137
6-4-0.020-15	0.126	0.130
6-4-0.020-16	0.073	0.077
6-4-0.020-17	0.083	0.085
6-4-0.020-18	0.105	0.112
6-4-0.020-19	0.076	0.082

** - Did not break at crack.

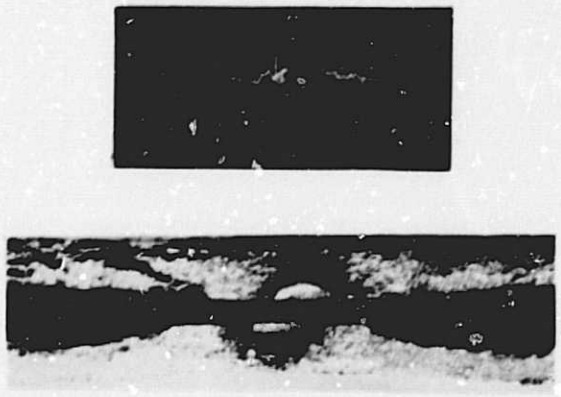

Figure 35. Fluorescent penetrant indications of a fatigue crack and macrograph of the fracture surface of specimen 5-2.5-0.020-9 at 10X.

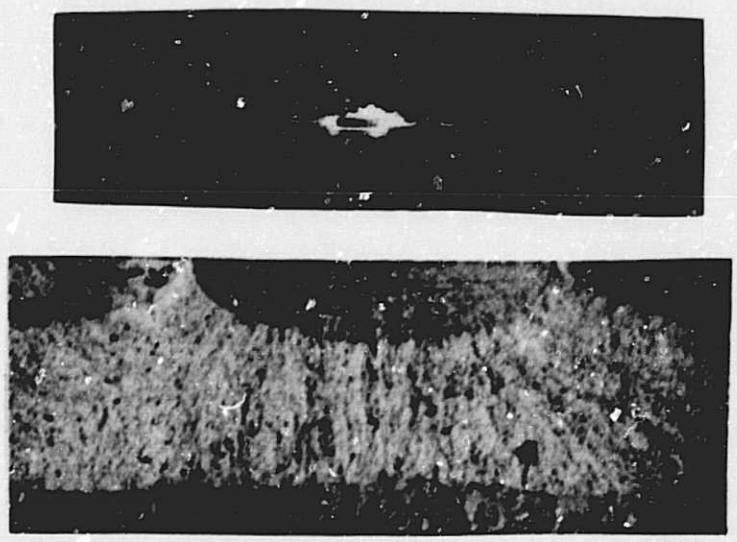

Figure 36. Fluorescent penetrant indication of a fatigue crack and macrograph of the fracture surface of specimen 6-4-0.125-6 at 10X.

5816 B

TABLE XIII

PENETRANT AND DESTRUCTIVE TEST CRACK-LENGTH MEASUREMENTS FOR 0.125-INCH SPECIMENS

Specimen Identification	Penetrant Crack Length (inch)	Actual Crack Length (inch)
2014-0.125-1	0.054	0.062
2014-0.125-2	0.083	0.075
2014-0.125-3A	0.038	0.046
2014-0.125-3B	0.042	0.064
2014-0.125-4A	0.086	0.091
2014-0.125-4B	0.047	0.063
2219-0.125-1	0.075	0.075
2219-0.125-2	0.073	0.082
2219-0.125-3	0.078	0.064
2219-0.125-4	0.075	0.077
2219-0.125-5	0.040	0.040 *
2219-0.125-6	0.043	0.035 *
5-2.5-0.125-1A	0.096	0.098 **
5-2.5-0.125-2	0.060	0.058
5-2.5-0.125-3	0.051	0.054
5-2.5-0.125-4	0.200	0.222
5-2.5-0.125-7	0.176	0.200
5-2.5-0.125-8	0.074	0.075
6-4-0.125-1	0.075	0.077
6-4-0.125-1B	0.052	0.054
6-4-0.125-3	0.062	0.062
6-4-0.125-4	0.135	0.158
6-4-0.125-5	0.067	0.065
6-4-0.125-6	0.080	0.158

* - Possibly no crack - notch only.
** - Did not break at notch.

TABLE XIV

PENETRANT AND DESTRUCTIVE TEST CRACK-LENGTH MEASUREMENTS FOR 0.500-INCH SPECIMENS

Specimen Identification	Penetrant Crack Length (inch)	Actual Crack Length (inch)
2014-0.500-1	Not Obtainable	0.589
2014-0.500-2	"	0.554
2219-0.500-1	"	0.386
2219-0.500-2	"	0.313
2219-0.500-3	"	0.323
2219-0.500-4	"	0.334
2219-0.500-5	"	0.299
2219-0.500-6	"	0.354
2219-0.500-7	"	0.340
2219-0.500-8	"	0.612
2219-0.500-9	"	0.600
2219-0.500-1A	"	0.482
2219-0.500-1E	"	0.486
5-2.5-0.500-2	0.163	0.188
5-2.5-0.500-4	0.216	0.243
5-2.5-0.500-5	0.218	0.246
5-2.5-0.500-6	0.095	0.121
5-2.5-0.500-7	0.114	0.140
5-2.5-0.500-8	0.130	0.155
5-2.5-0.500-9	0.086	0.103
5-2.5-0.500-10	0.057	0.062
5-2.5-0.500-11	0.058	*
6-4-0.500-1	0.092	0.095
6-4-0.500-3	0.110	0.121
6-4-0.500-12	0.120	0.147

* - Broke away from crack

3. Ultrasonic Tests

Two types of water-immersion ultrasonic tests were performed on the test specimens. These were the shear-wave technique and the Automation Industries developed delta-scan technique using reradiated ultrasonic energy. A method of analysis of the shear-wave data was developed so that three measurable quantities were obtained from the tests that could be correlated with defect data. The following sections describe the ultrasonic tests and the data generated.

a. Shear-Wave Inspection

Shear-wave inspection techniques were developed for fatigue crack and weld defect detection which utilized both single and double transducer systems. The basic system has been previously described and illustrated in Figure 4. The strength of reflections from the defect were measured by gating on the signal from the defect and measuring the analog output voltage produced by this signal. The analog voltage was measured at specific intervals by a digital voltmeter and recorded on a printer, and continuously on an X-Y recorder.

1) Inspection Technique

The ultrasonic signal strength which results from a given defect is a function of the area of the defect. The reflected energy from the defect will cause a definite voltage to be generated by the transducer. This signal is amplified in the ultrasonic unit and displayed on its oscilloscope screen. The amplifiers in the ultrasonic unit are nonlinear so that a defect which reflects twice as much energy does not appear twice as large. In order to allow for this nonlinearity, the ultrasonic unit must be calibrated so that the response to a given input signal is known. Performing this calibration permits the application of measurable units to the defect signal so that signals from a large range of defects can be compared.

The ultrasonic unit used for the shear-wave tests on the 0.125, 0.500 and 1.000-inch specimens was a Sperry Products UM-700 shown in Figure 37. This unit was calibrated with a Hewlett Packard Model 606A Signal Generator so that the input signal to produce an 80 percent signal height on the unit's oscilloscope screen was a known function of the gain or sensitivity switch settings. The resulting calibration curve is shown in Figure 38. These curves were obtained by providing fixed 5MHz voltage inputs to the receiver and then adjusting and recording the sensitivity switch positions for the 5N Pulser-Receiver. In order to use these curves to compare defects, the maximum signal from a defect is adjusted to obtain an 80 percent screen height and then the input voltage is determined from the dial readings on the fine sensitivity control and coarse sensitivity range switch settings. As an example, a fine sensitivity setting of 4 with the times 1 coarse sensitivity produces an 80 percent signal from a 1 millivolt input signal for the 5MHz setting of the 5N pulser-receiver amplifiers. In this way, a signal can be related to the original signal intensity that the returning pulse generates in the transducer.

From the preliminary work, a relationship was established showing that depth and length data could be obtained from the ultrasonic scans on smooth surface calibration notches. This work was performed with fixed gain settings on the instrument so that all measurements were relative and a function of the setting. The basic recording of a scan across a defect is illustrated in Figure 39a. As the ultrasonic beam reflected from different portions of the defect, the signal response varied. Although the defect signal shifted in

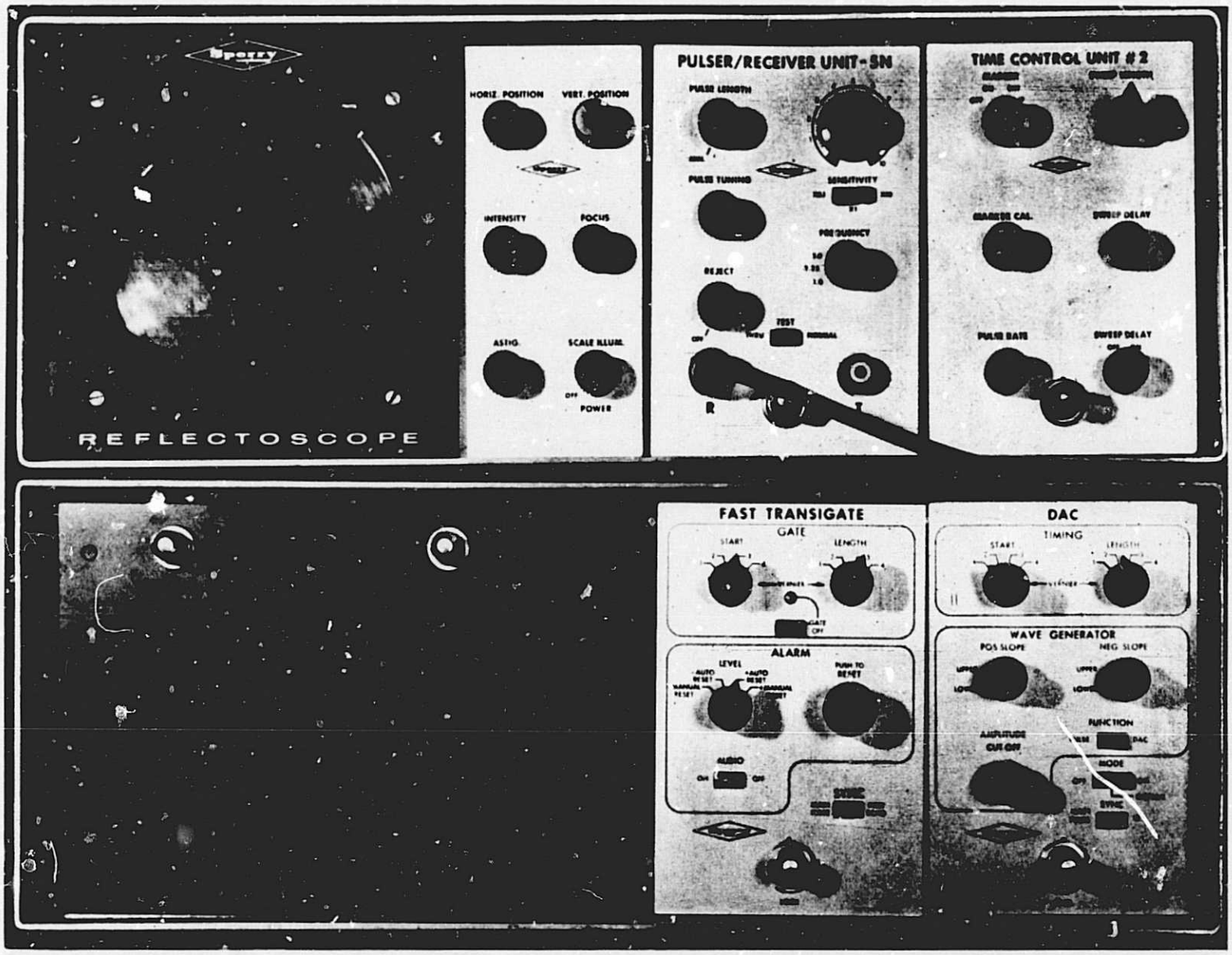

Figure 37. Sperry Products UM-700 Ultrasonic Unit.

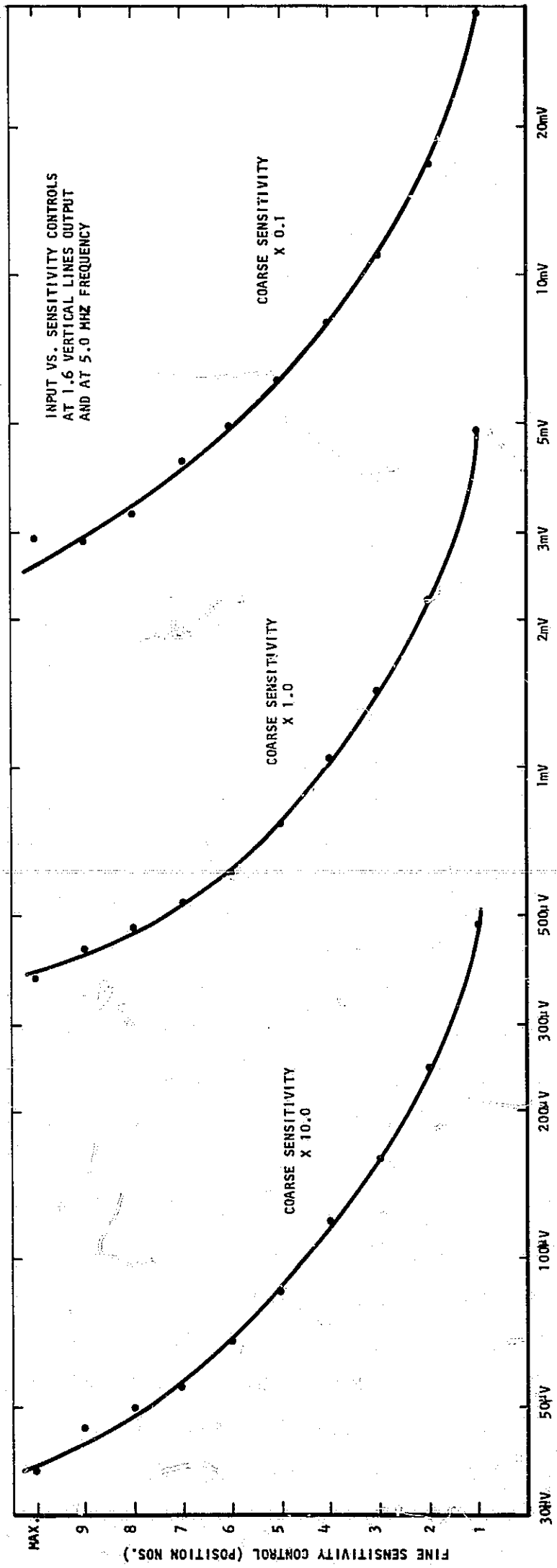

Figure 38. Input voltage to achieve 80 percent screen height on the Sperry UM-700 unit as a function of gain settings for the 5N Pulser-Receiver at 5 MHz.

5748 B

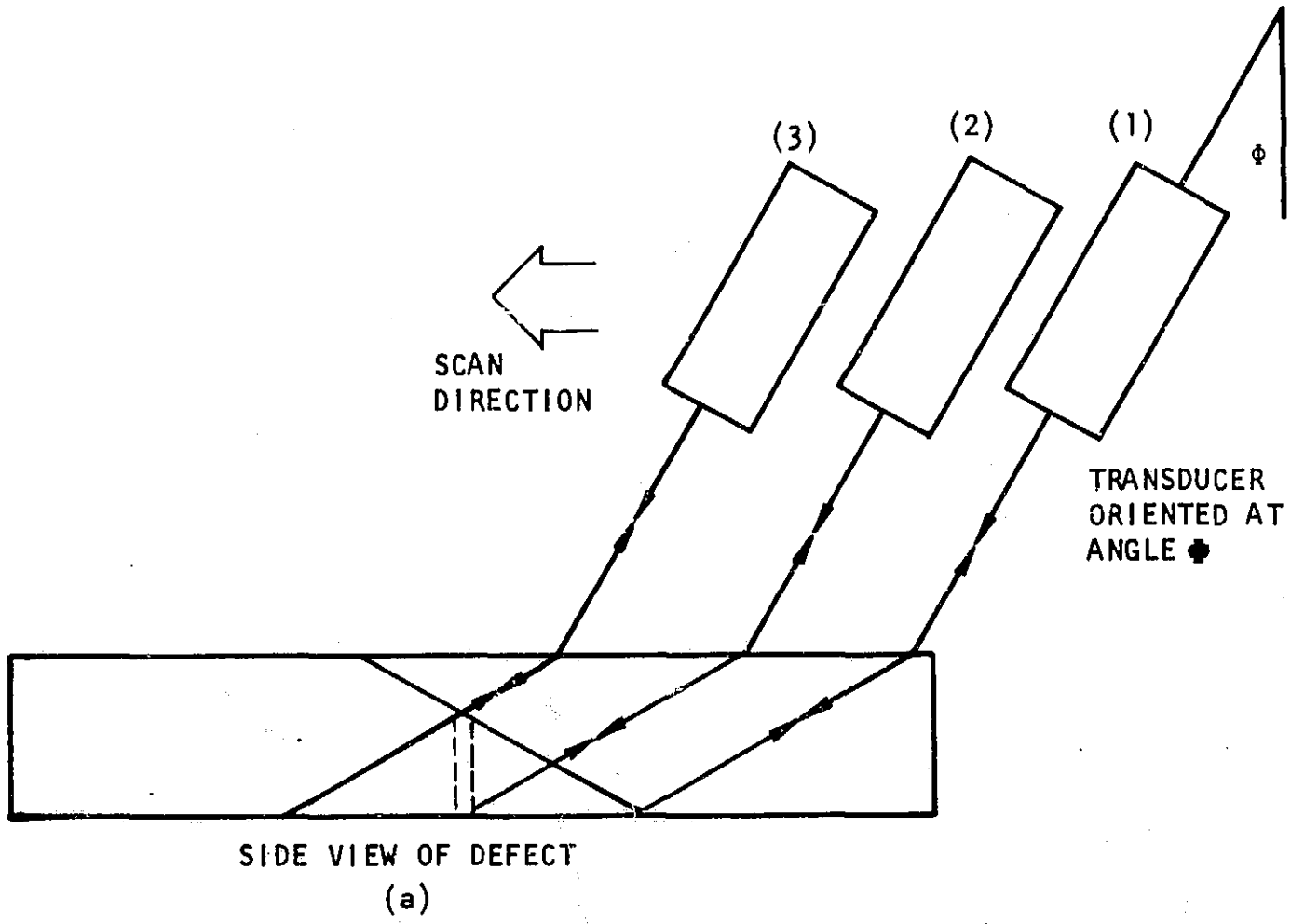

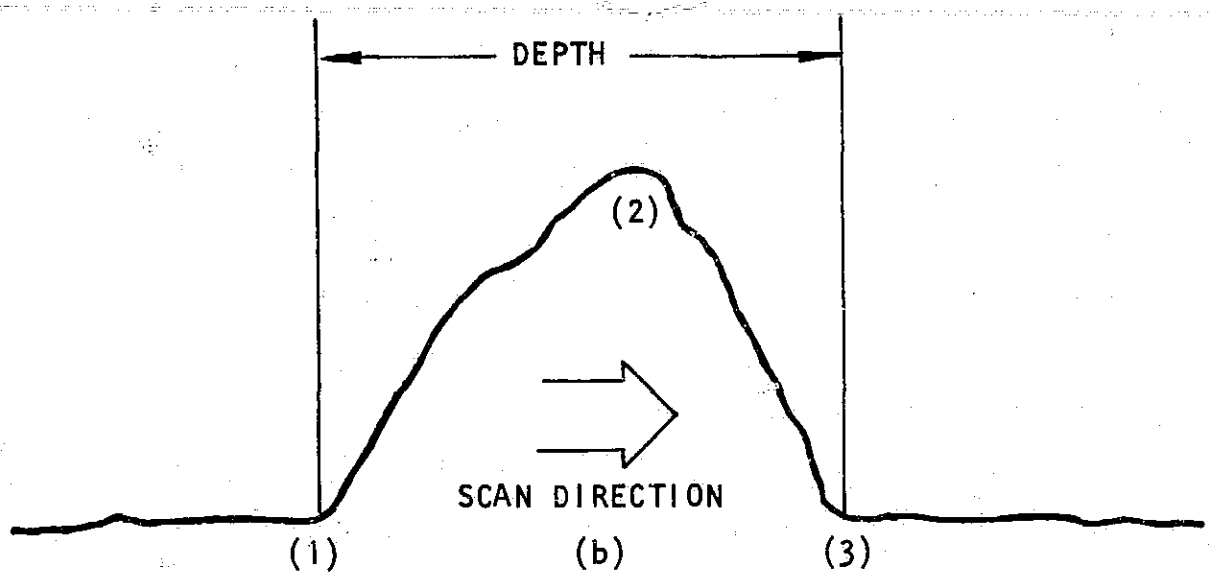

Figure 39. Illustration showing the relationships between ultrasonic beam and defect for various positions of the transducer (a) and a typical trace recorded across the defect (b).

5750 B

its relative time position on the oscilloscope, the transigate on the ultrasonic instrument was adjusted so that the complete time interval of the defect was within the gate. The analog output voltage from the gate, which corresponds to the highest signal in the gated time interval, was recorded on an X-Y recorder. The X-axis of the recorder was controlled by a 20K ohm potentiometer coupled to the specimen translation device, and hence the signal intensity and the relative position of the ultrasonic beam in relation to the crack can be determined. A typical trace obtained as the ultrasonic beam scans the defect is shown in Figure 39b.

The analog output voltage from the gate is a linear function of the signal height within the gate. Measurements were made of the signal height on the oscilloscope screen and the corresponding analog output voltage from the gate and the data are shown graphically in Figure 40. This voltage is a nonlinear function of the defect signal voltage and is negative for this particular unit.

The complete system for measuring and recording the signal intensity as a function of position is shown in Figure 41. The analog output voltage was recorded on the X-Y recorder and at fixed intervals of 0.010-inch movement on the printer. The data were then integrated as a function of distance and divided by the gain of the amplifiers, resulting in voltage-distance units. The scan distance for which measurable data were recorded was determined, for defect depth, by a scan across the defect at the location of maximum signal strength. This distance was measured by noting the location at which a signal above the base-line analog gate voltage was first generated and at that location where the voltage returned to the base-line value. The increment value for depth was the distance between these two locations. Subsequent scans were made along the defect at fixed intervals on both sides of the position where the maximum signal occurred. These scans were made as long as any measurable signal was generated by the defect. Defect length was determined by the number of scans between the positions where the signals were first detectable at the opposite ends of the defect. Since all three of these measurements were made for various defects at different gain settings on the ultrasonic instrument, the measurements were normalized by dividing by the gain of the ultrasonic instrument so that each defect was judged on the same basis. These three measurements, the area value and the two distance increments, were correlated with the critical defect parameters.

The integrated measurement was an area obtained by summing the voltage times the distance increment (0.010-inch), using the following equation:

$$A = \Delta x \left(nE_o - \sum_{i=1}^{n} e_i \right)$$

where A = area in voltage-distance units (volts-inch)
Δx = inches of increment
n = number of increments
E_o = no defect signal (volts)
e_i = defect signal (volts)

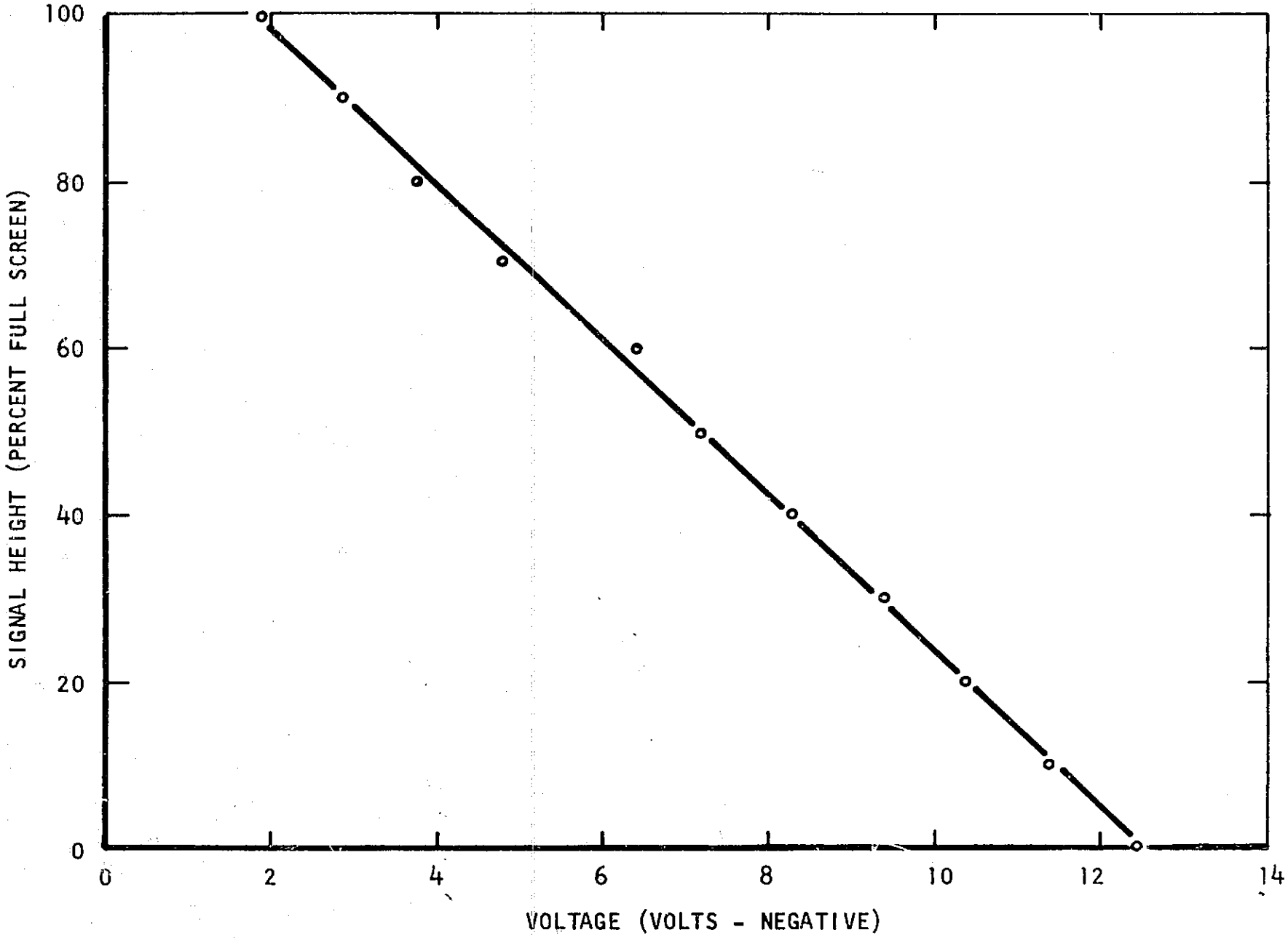

Figure 40. Signal height on the UM-700 oscilloscope screen as a function of the analog gate output voltage.

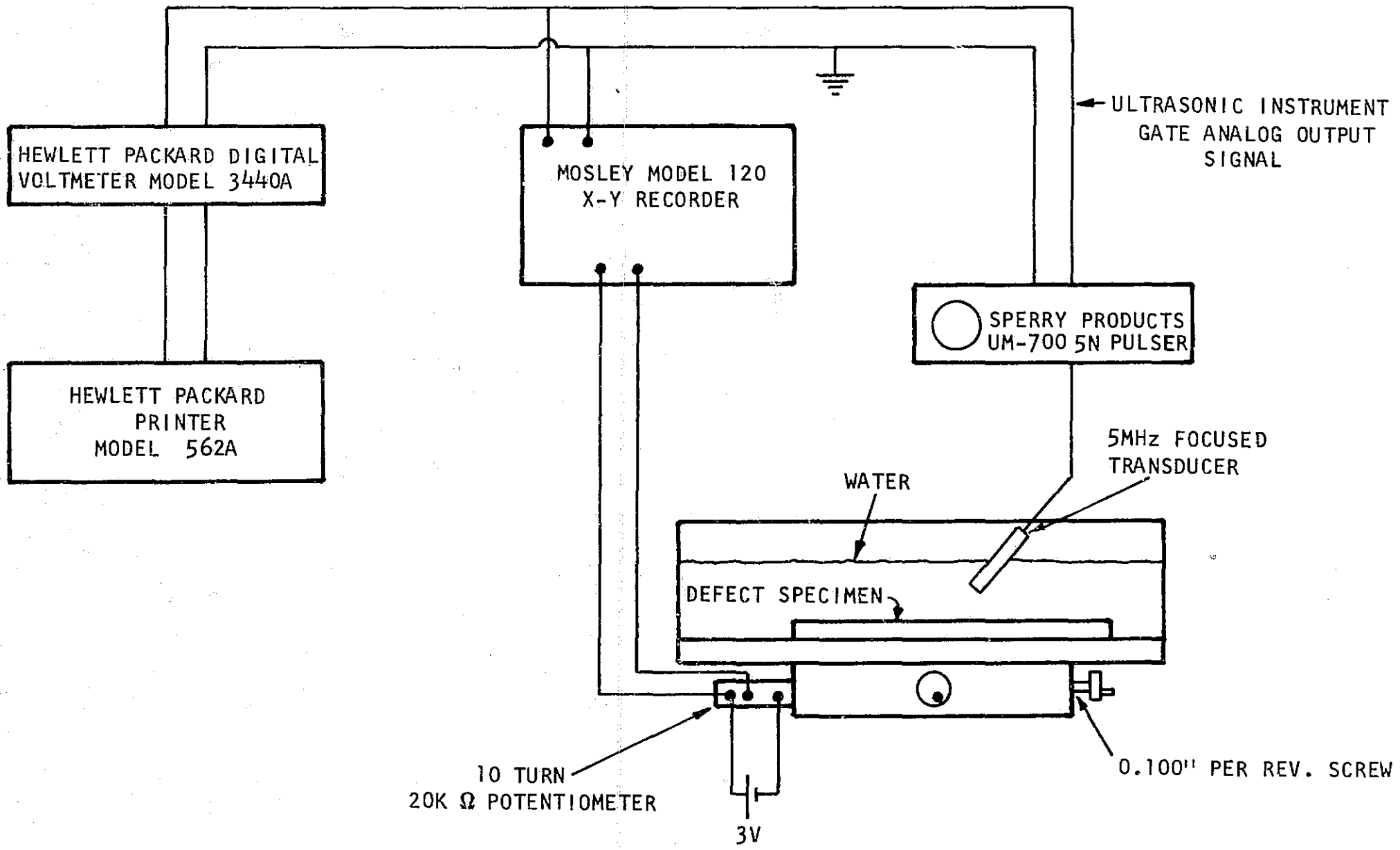

Figure 41. Apparatus for performing measurement and recording of defect information.

The area value obtained in voltage-distance units then was normalized by multiplying by the input voltage from Figure 38 and by dividing by the net gate output voltage (8 net volts from Figure 40 for an 80 percent screen height). This value is the sum of the voltage received by the transducer as a function of the position of the ultrasonic beam relative to the defect as the transducer moves across the defect.

For the 0.020-inch specimens, a different ultrasonic instrument was necessary because of the short time interval between front-surface and defect echoes. For this work, a DC Erdman high-resolution Model 1177B, shown in Figure 42, was utilized. It has a large bandwidth and was used with Automation Industries 25 MHz transducers to achieve the desired frequency range necessary for the measurements in the 0.020-inch material. Calibration was not possible since the unit does not have any gradations on the gain control. The gain was fixed, therefore, at a particular value and measurements were made on all the cracks in the aluminum specimens, and then fixed at another value for the corresponding measurements on the titanium specimens. Only two values were recorded on the 0.020-inch specimens, the scan distance through the center of the defect and a scan length along the defect to indicate the crack length. These two values were correlated with defect depth and length respectively. The analog gate output voltage of this unit was utilized for these measurements as with the UM-700 unit. The transducer was a focused lithium-sulfate type with an approximate 0.040-inch diameter where the beam enters the specimen.

A variation in the single transducer pulse-echo technique was necessary for the weld specimens where the defects were not surface connected. For the surface-connected defects, the ultrasonic wave returns to the sending transducer from direct reflection from the defect or indirect reflection from the opposite plate face (or the beam path may be the reverse of this), as illustrated in Figure 43a. When the defect is not near a surface and a small diameter transducer is used, some of the signal is missed, since the smooth incomplete penetration interface acts as a mirror and the wave is not reflected back in the range of the transducer as illustrated in Figure 43b. However, a second transducer can be inserted to record the defect signal with both transducers tied to a common base. The use of a small diameter transducer to receive improves resolution of the defect.

2) Shear-Wave Test Results

The shear-wave test results on the 0.020-inch fatigue-cracked specimens are listed in Table XV. In all but one of the specimens, the cracks extended through the full thickness of material. Although the crack lengths generally correlate with the actual measured values, some of these cracks appeared on the radiographs to be split or forked at the extremities so that some of the crack would not have the same orientation to the ultrasonic beam along the entire crack length.

The results of the shear-wave tests on the 0.125-inch specimens are listed in Table XVI. For specimens having almost identical dimensions such as 2014-1 and 3B, the gain settings to achieve an 80 percent signal height were vastly different. There was also a large variation in the readings between the different alloys in both the titanium and aluminum specimens. None of the cracks went undetected in these specimens, but the precision of measurement was low.

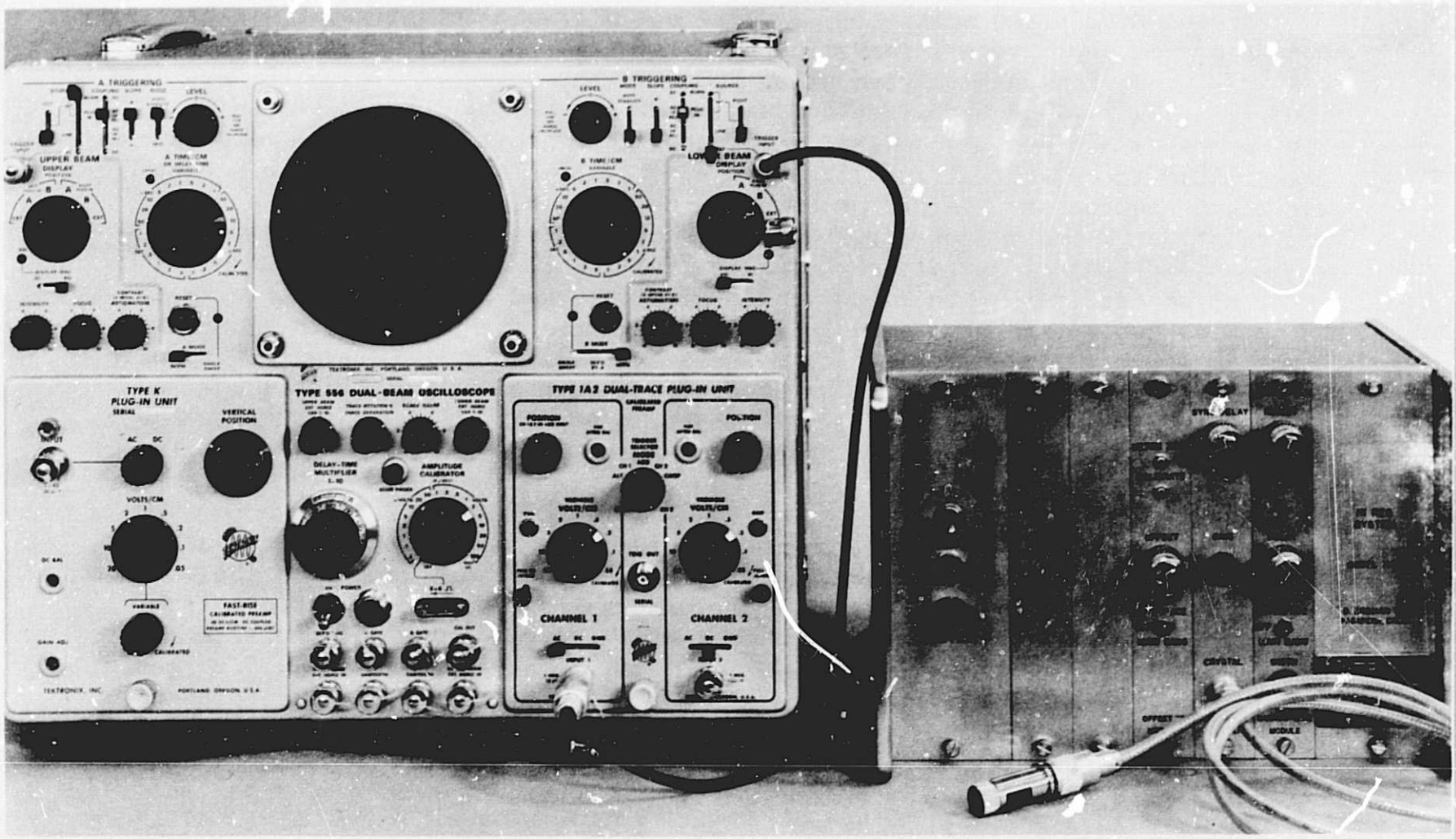

Figure 42. D.C. Erdman Model 1177 ultrasonic unit with Tektronix Model 556 Oscilloscope.

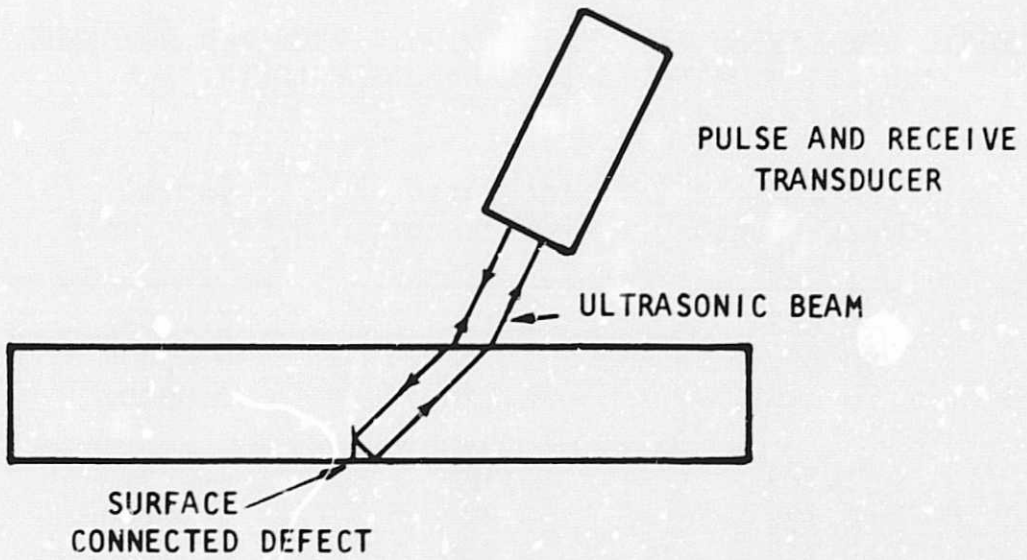

(a)

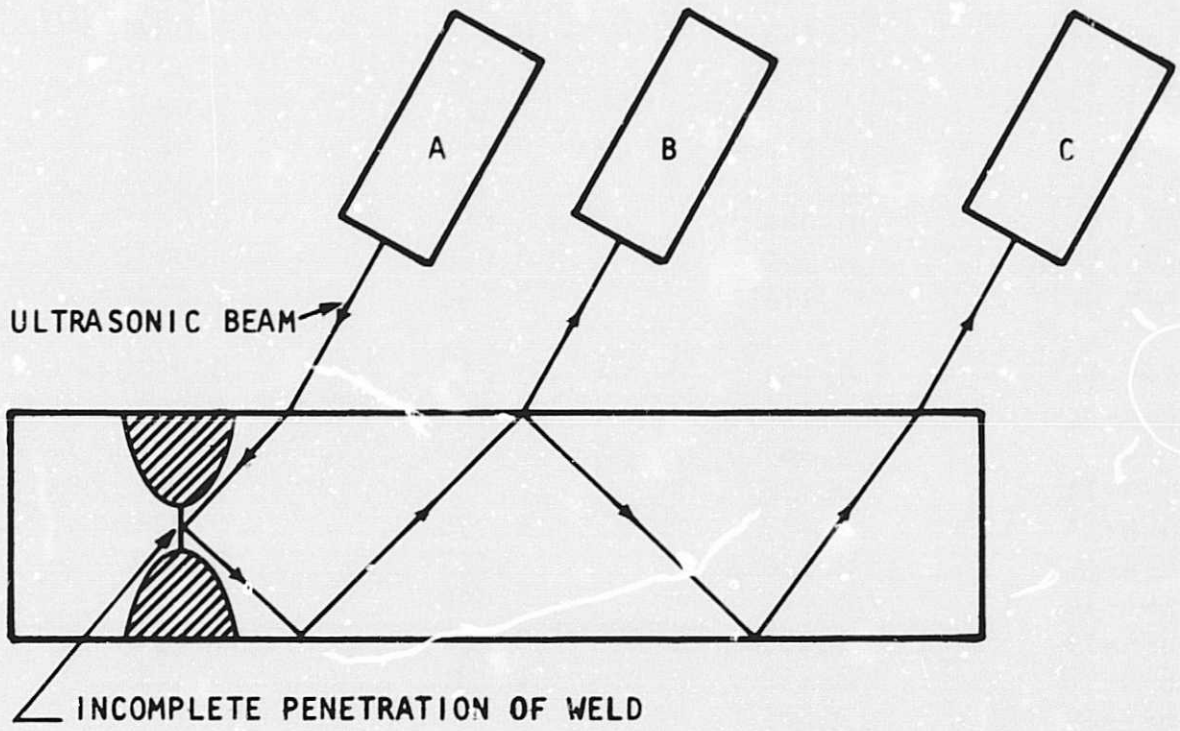

(b)

Figure 43. Reflection of ultrasonic waves from surface connected and internal defects.

5746 a

TABLE XV

ULTRASONIC SHEAR-WAVE TEST RESULTS ON 0.020-INCH ALUMINUM AND TITANIUM FATIGUE-CRACKED SPECIMENS

Specimen Identification	Actual Crack Length (inch)	Indicated Crack Length (inch)	Actual Crack Depth (inch)	Indicated Crack Depth (inch)
2014-1	0.088	0.120	0.0204*	0.120
2014-2	0.087	0.120	0.0200*	0.095
2014-1A	0.094	0.120	0.0200*	0.110
2219-1	0.189	0.190	0.0200*	0.105
2219-2	0.190	0.280	0.0220*	0.100
2219-3	0.138	0.180	0.0205*	0.090
2219-7	0.125	0.160	0.0215*	0.100
5-2.5-1	0.116	0.050	0.0215*	0.055
5-2.5-3	0.140	0.105	0.0220*	0.065
5-2.5-4	0.121	0.055	0.0215*	0.055
5-2.5-6	0.121	0.120	0.0220*	0.050
5-2.5-7	0.112	0.065	0.0215*	0.075
5-2.5-8	0.062	0.030	0.0055	0.055
5-2.5-9	0.087	0.085	0.0215*	0.065
5-2.5-10	0.075	0.065	0.0210*	0.055
5-2.5-12	0.116	0.150	0.0220*	0.065
6-4-1	0.261	0.275	0.0220*	0.090
6-4-2	0.118	0.145	0.0220*	0.060
6-4-3	0.067	0.060	0.0220*	0.080
6-4-11	0.172	0.175	0.0215*	0.100
6-4-13	0.137	0.175	0.0220*	0.090
6-4-15	0.130	0.125	0.0220*	0.085
6-4-16	0.077	0.100	0.0220*	0.085
6-4-17	0.085	0.100	0.0220*	0.090
6-4-18	0.112	0.130	0.0220*	0.075
6-4-19	0.082	0.090	0.0215*	0.085

* - Specimen Thickness

TABLE XVI

ULTRASONIC SHEAR-WAVE TEST RESULTS ON 0.125-INCH ALUMINUM AND TITANIUM FATIGUE-CRACKED SPECIMENS

Specimen Identification	Actual Crack Length (inch)	Indicated Crack Length Normalized Increment (Inch x10^{-6})	Actual Crack Depth (Inch)	Indicated Crack Depth Integrated Area (Microvolt-Inch)	Indicated Crack Depth Normalized Increment (Inch x10^{-6})	Input Signal Level for 80% Screen Height (millivolt)
2014-1	0.062	1.7	0.030	8.5	2.7	0.120
2014-2	0.075	11.7	0.029	58.6	17.9	0.850
2014-3A	0.046	12.3	0.022	64.6	17.4	0.820
2014-3B	0.064	11.2	0.025	48.4	13.8	0.690
2014-4A	0.091	17.4	0.034	74.6	22.7	1.070
2014-4B	0.063	15.8	0.026	84.8	24.9	1.060
2219-1	0.075	7.5	0.034	44.4	12.8	0.545
2219-2	0.082	18.8	0.036	82.2	26.6	1.250
2219-3	0.064	17.2	0.034	90.1	32.8	1.220
2219-4	0.077	9.2	0.032	47.5	15.1	0.675
2219-5	0.040	18.8	0.025*	91.1	28.1	1.250
2219-6	0.035	18.8	0.017*	90.6	28.1	1.220
5-2.5-1A	0.098	20.0	0.034	75.0	22.5	1.000**
5-2.5-2	0.058	6.6	0.024	12.6	10.8	0.480
5-2.5-3	0.054	4.2	0.020	2.8	4.2	0.210
5-2.5-4	0.222	31.6	0.047	95.5	19.4	1.150
5-2.5-7	0.200	30.2	0.041	60.9	20.1	1.150
5-2.5-8	0.075	3.3	0.025	4.4	3.8	0.200
6-4-1	0.077	2.5	0.023	14.5	3.6	0.180
6-4-1B	0.054	10.2	0.021	43.3	13.1	0.580
6-4-3	0.062	2.9	0.021	1.9	4.1	0.180
6-4-4	0.158	9.7	0.045	33.6	15.2	0.480
6-4-5***	0.065		0.024			
6-4-6	0.158	8.5	0.037	14.0	10.9	0.480

* - Possibly no crack-notch only. ** - Data recorded not at same time as others.
*** - Specimen pulled early in program - test not performed.

Some trends can be seen in the shear-wave data for the 0.500-inch fatigue cracked specimens as listed in Table XVII. It appears from these data that defect signal heights were affected significantly by acoustic impedance differences between alloys in each of the groups. However, some of the differences arising in the aluminum alloys were attributed to the fatigue crack propagation in che 2219 aluminum alloy. In several of the cracks in the 0.500-inch thickness, delaminations occurred at or near the tip of the fatigue crack. This may have caused the ultrasonic beam to indicate a deeper crack in some instances. The length indications did not correlate well between the titanium alloys, except for a trend established for various dimensions of the three samples of 6Al-4V alloy. The results of the shear-wave tests on the 1.0-inch aluminum samples in Table XVIIIshowed trends similar to the 0.5-inch specimens. There also were delaminations in the 2219 alloy at the 1.0-inch section thickness.

The large number of defects in the aluminum weld specimens made the shear-wave results on these specimens extremely difficult to interpret. Since a two transducer test was necessary because of the variation in response to surface and internal defects, no direct correlation was possible between the results of these tests and the fatigue crack data. The length of the defect in weld 2219-0.5-5A was measured ultrasonically to be approximately 1.2 inches, since this specimen had only a few pores in addition to the incomplete penetration. However, the incomplete penetration condition in weld 2219-0.5-5B was not detected at any gain setting on the ultrasonic unit. The fracture surfaces for these two welds are shown in Figures 28 and 29. Tests on welds are in general more difficult because, the relative position and angle of the defect has a large influence on response to the ultrasonic beam, and the weld zone adds a different grain structure with its own acoustic attenuation characteristics.

Defect signals were observed on the two 0.5-inch titanium weldments, specimens 5-2.5-0.5-13 and 14, but there were no observable defects in the fracture surfaces of these welds. The signal strength was larger in magnitude in specimen 13. However, since these two welds were made with a different filler metal, acoustic impedance differences in the structure of the weld may have caused the signals, as the transition from a fine to coarse grain was evident in both welds. The results of the ultrasonic tests on the four 0.020-inch welded titanium specimens are listed below.

Weld Specimen Identification	Actual Defect Length (inch)	Indicated Defect Length (inch)
6-4-1W	0.044	0.180
6-4-2W	0.058	0.140
5-2.5-3W	*	0.190
5-2.5-4W	0.084	0.140

* - could not be determined.

TABLE XVII

ULTRASONIC SHEAR-WAVE TEST RESULTS ON 0.500-INCH ALUMINUM AND TITANIUM FATIGUE-CRACKED SPECIMENS

Specimen Identification	Actual Crack Length (inch)	Indicated Crack Length Normalized Increment (Inch x10^{-6})	Actual Crack Depth (Inch)	Indicated Crack Depth Integrated Area (Microvolt-Inch)	Indicated Crack Depth Normalized Increment (Inch x 10^{-6})	Input Signal Level for 80% Screen Height (Millivolt)
2014-1	0.589	1060	0.176	1656	460	16.0
2014-2	0.554	1406	0.161	2428	687	25.0
2219-1	0.386	712	0.133	1891	510	17.0
2219-2	0.313	624	0.115	2249	576	19.2
2219-3	0.323	1096	0.119	2531	675	27.0
2219-4	0.334	645	0.123	1930	516	17.2
2219-5	0.299	570	0.113	1626	440	16.0
2219-6	0.354	880	0.122	2173	605	22.0
2219-7	0.340	683	0.117	2465	656	21.0
2219-8	0.612	1265	0.185	2318	632	22.0
2219-9	0.600	1402	0.182	1659	536	19.5
2219-1A	0.482	1540	0.148	2765	797	29.0
2219-1E	0.486	1462	0.142	2392	650	26.0
5-2.5-2	0.188	101	0.088	377	82.5	3.000
5-2.5-4	0.243	121	0.113	420	101	3.600
5-2.5-5	0.246	120	0.126	315	99.0	3.300
5-2.5-6	0.121	17	0.069	76	20.6	0.610
5-2.5-7	0.140	6	0.053	31.6	10.9	0.255
5-2.5-8	0.155	59	0.068	244	66.6	1.950
5-2.5-9	0.103	19.5	0.044	106	26.7	0.82
5-2.5-10	0.062	6.5	0.032	28.2	8.5	0.26
5-2.5-11	*	7.1	*	40.5	11	0.315
6-4-1	0.095	42.8	0.043	253	66.5	1.90
6-4-3	0.121	66.5	0.054	289	80.5	2.80
6-4-12	0.147	115	0.071	509	135	4.00

* - Data not available - specimen broke outside of crack.

TABLE XVIII

ULTRASONIC SHEAR-WAVE TEST RESULTS ON 1.0-INCH ALUMINUM FATIGUE-CRACKED SPECIMENS

Specimen Identification	Actual Crack Length (inch)	Indicated Crack Length Normalized Increment (Inch x 10^{-6})	Actual Crack Depth (Inch)	Indicated Crack Depth Integrated Area (Microvolt-Inch)	Indicated Crack Depth Normalized Increment (Inch x 10^{-6})	Input Signal Level for 80% Screen Height (Millivolt)
2014-1	0.567	788	0.190	3295	910	14.0
2014-2	0.550	928	0.185	3257	911	13.5
2219-1	0.543	638	0.191	2296	587	10.2
2219-2	0.617	612	0.205	2564	636	9.6
2219-3	0.530	613	0.195	3484	980	14.0
2219-4	0.473	473	0.167	2739	803	12.6

These defect lengths were determined with the identical techniques used for the fatigue crack specimens. Since, all of these weld specimens broke outside of the weld zone, measurements of the defect area were difficult to make; one of the measurements was not possible because of the condition of the specimen after the tensile test. The indicated dimensions were larger than the actual values, which is to be expected since the ultrasonic beam has a finite width and records information as long as some portion of the beam reflects from the defect. The response from these defects is larger than that expected from similiar fatigue-crack defects, due to the idealized reflecting surfaces, and possibly to the weld bead providing spurious signals in some of the welds.

b. Delta Inspection

From the evaluation performed at Automation Industries, the "delta technique" parameters were established. The basic delta configuration was used for the evaluations on the welded and fatigue-cracked specimens.

1) Inspection Technique

The angled pulse sending transducer for the delta tests was a 5 MHz 3/16-inch diameter long-focus lithium-sulfate unit. The test angle for this transducer was fixed at 23 degrees. Notched calibration standards were utilized to determine the transducer spacings for the initial setup on the fatigued-crack specimens. The sending transducer was used in pulse-echo operation to establish the proper relationship between this transducer and the defect. The receiving transducer, a 5 MHz 1/2-inch diameter focused lithium-sulfate unit, was then positioned at the point over the defect where maximum signal strength was received. Both transducers were operated with a 5N Pulser-Receiver on the Sperry Products UM-700, with gated output being recorded on a standard C-scan recorder.

For the weld defects in the 1.0-inch aluminum specimens, a slightly different setup was required. A special calibration standard was fabricated which had a 4/64-inch flat bottom hole drilled parallel to the plate surfaces in the middle of the plate, 1/2-inch deep. The receiving transducer was placed directly over the bottom of the hole and the optimum separation distance between the two transducers was then determined by adjusting the location of the pulsing transducer for maximum received signal. This calibration hole was used when each of the weld specimens was inspected.

The length and depth of the defect dimensions were measured from the recorded C-scans. The depth was measured in one direction across the center of the C-scan, and the width at right angles where the indicated width was largest on the recording.

2) Delta Inspection Results

The delta inspections were not performed on the 0.020-inch material since this thickness probably would have resulted in Lamb-wave formation. Delta technique is not recommended for materials under 0.100-inch in thickness. The results of the delta tests on the 0.125-inch fatigue crack specimens, as listed in Table XIX, show that several of the defects were not detected in the aluminum specimens, and therefore produced a smaller response than the 0.020 by 0.020-inch calibration notch. The response of the tests to

TABLE XIX

ULTRASONIC DELTA INSPECTION RESULTS ON THE 0.125-INCH ALUMINUM AND TITANIUM FATIGUE-CRACK SPECIMENS

Specimen Identification	Actual Crack Length (inch)	Indicated Crack Length (inch)	Actual Crack Depth (inch)	Indicated Crack Depth (inch
2014-1	0.062	0.140	0.030	0.120
2014-2	0.075	0.080	0.029	0.100
2014-3A	0.046	0.130	0.022	0.130
2014-3B	0.064	0.120	0.025	0.080
2014-4A	0.091	0.080	0.034	0.090
2014-4B	0.063	*	0.026	*
2219-1	0.075	*	0.034	*
2219-2	0.082	*	0.036	*
2219-3	0.064	0.140	0.034	0.140
2219-4	0.077	*	0.032	*
2219-5**	0.040	0.130	0.025	0.130
2219-6**	0.035	0.100	0.017	0.120
5-2.5-1A	0.098	0.120	0.030	0.060
5-2.5-2	0.058	0.080	0.024	0.050
5-2.5-3	0.054	0.070	0.020	0.050
5-2.5-4	0.222	0.200	0.047	0.170
5-2.5-7	0.200	0.270	0.041	0.260
5-2.5-8	0.075	0.100	0.025	0.100
6-4-1	0.077	0.120	0.023	0.110
6-4-1B	0.054	0.090	0.021	0.120
6-4-3	0.062	0.070	0.021	0.040
6-4-4	0.158	0.190	0.045	0.210
6-4-5	0.065	0.140	0.024	0.160
6-4-6	0.158	0.120	0.037	0.240

* - Defect response smaller than that from 0.020x0.020-inch calibration notch.

** - Possibly no crack - notch only.

titanium defects was better than the aluminum, with all defects being detected. The titanium cracks had a larger range of length and depth than those in the aluminum specimens.

On the 0.500-inch specimens, all but one crack was recorded, as tabulated in Table XX, at the gain settings used. The range of crack depths and lengths was small for the aluminum alloys, and hence the depth and length responses were nearly constant. The crack values and measurement values had a greater range of variation for the titanium alloys. The measured values and actual values for the delta tests of the 1.0-inch aluminum alloys are listed in Table XXI.

The delta-test results on the weldments were affected by the many extraneous defects that affected the shear-wave tests. In the 0.500-inch 5Al-2.5Sh titanium weldments, a large area of the C-scan of the weld showed defect indications for welds 13 and 14. However, the calibration standard of 0.020-inch width by 0.020-inch depth used to set the gating signal level was evidently smaller in equivalent area than much of the grain structure in the weld. At reduced gain settings, these welds also produced indications which could not be traced to any gross defects. The incomplete penetration defects in the welds in aluminum specimens 2219-0.5-5A and 5B were not detected in 5A, the larger defect, but many indications appeared across the 5 inches of weld in 5B. These indications did not appear to be attributable to the incomplete penetration, since at lower gain recordings, distinct porosity-like dots appeared.

The delta-tests on the 1.0-inch aluminum weldments displayed a variety of results. The defects present in weld samples 2014-1.0-2A and 2B and 2219-1.0-4A and 4B were not detected. No indications could be seen on the recordings for these samples even though the 4/64-inch diameter calibration hole appeared as a 1/4-inch diameter indication on the recordings. Various defects had been noted previously for these welds in the radiographic tests. The largest of the defects were incomplete penetrations at the center of the weld zone. For the other 1.0-inch thick welds in the aluminum alloys, better results were obtained. Extensive indications were obtained on weld 2014-1.0-3D which contained a tungsten inclusion, as well as, lack of fusion and incomplete penetration. A delta-scan recording for specimen 2014-1.0-3D is shown in Figure 44 with a photograph of the fracture surface of the weld. (The recordings were made on a wide sample which was subsequently machined for tensile testing). The response is quite variable along the weld as indicated by the recording. In Figure 45, a delta-scan recording of weld specimen 2219-1.0-3B is shown along with the fracture surface of the weld. The large white area in the recording appears to correlate with the incomplete penetration but does not reveal all of this defect. The white dot above the figure caption in Figure 45 is a recording of the 4/64-inch diameter calibration hole. Large defects were also noted in C-scans of welds 2014-1.0-3A and 3C. Only indications comparable to the 4/64-inch calibration hole were all that were visible in welds 2014-1.0-3B and 2219-1.0-3A.

B. Defect-Stress Evaluations

In order to determine the effect of stress on defect detectability, an experiment was performed where five aluminum and one titanium fatigue-cracked specimens were loaded in bending. These defect specimens were loaded in a cantilever beam arrangement so that the cracks received various stress levels transverse to the crack. The previously described immersion shear-wave tests were

TABLE XX

ULTRASONIC DELTA INSPECTION RESULTS ON THE 0.500-INCH ALUMINUM AND TITANIUM FATIGUE-CRACKED SPECIMENS

Specimen Identification	Actual Crack Length (inch)	Indicated Crack Length (inch)	Actual Crack Depth (inch)	Indicated Crack Depth (inch)
2014-1	0.589	0.340	0.176	0.580
2014-2	0.554	0.440	0.161	0.500
2219-1	0.386	0.360	0.133	0.540
2219-2	0.313	0.340	0.115	0.550
2219-3	0.323	0.450	0.119	0.510
2219-4	0.334	0.430	0.123	0.510
2219-5	0.299	0.380	0.113	0.510
2219-6	0.354	0.320	0.122	0.520
2219-7	0.340	0.300	0.117	0.540
2219-8	0.612	0.540	0.186	0.530
2219-9	0.600	0.480	0.182	0.480
2219-1A*	0.482	0.530	0.148	0.630
2219-1E*	0.486	0.530	0.142	0.570
5-2.5-2	0.188	0.210	0.088	0.330
5-2.5-4	0.243	0.240	0.113	0.450
5-2.5-5	0.246	0.240	0.126	0.270
5-2.5-6	0.121	0.070	0.069	0.075
5-2.5-7	0.140	0.230	0.053	0.275
5-2.5-8	0.155	0.180	0.068	0.260
5-2.5-9	0.103	***	0.044	***
5-2.5-10	0.062	0.050	0.032	0.075
5-2.5-11	**	***	**	***
6-4-1	0.095	0.150	0.043	0.275
6-4-2	0.121	0.170	0.054	0.290
6-4-12	0.147	0.150	0.071	0.260

* - Recorded on different instrument.
** - Data not available - specimen broke outside of crack.
*** - Crack not recordable.

TABLE XXI

ULTRASONIC DELTA INSPECTION RESULTS ON THE 1.0-INCH ALUMINUM FATIGUE-CRACKED SPECIMENS

Specimen Identification	Actual Crack Length (inch)	Indicated Crack Length (inch)	Actual Crack Depth (inch)	Indicated Crack Depth (inch)
2014-1	0.567	0.550	0.190	0.680
2014-2	0.550	0.700	0.185	0.690
2219-1	0.543	0.410	0.191	0.680
2219-2	0.617	0.640	0.205	0.630
2219-3	0.530	0.530	0.195	0.630
2219-4	0.473	0.410	0.167	0.630

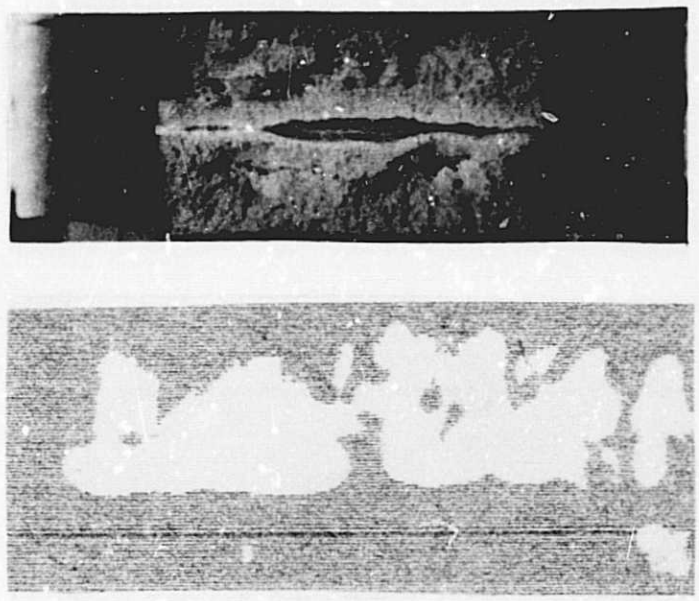

Figure 44. Delta scan recording and fracture surface of weld 2014-1.0-3D at IX.

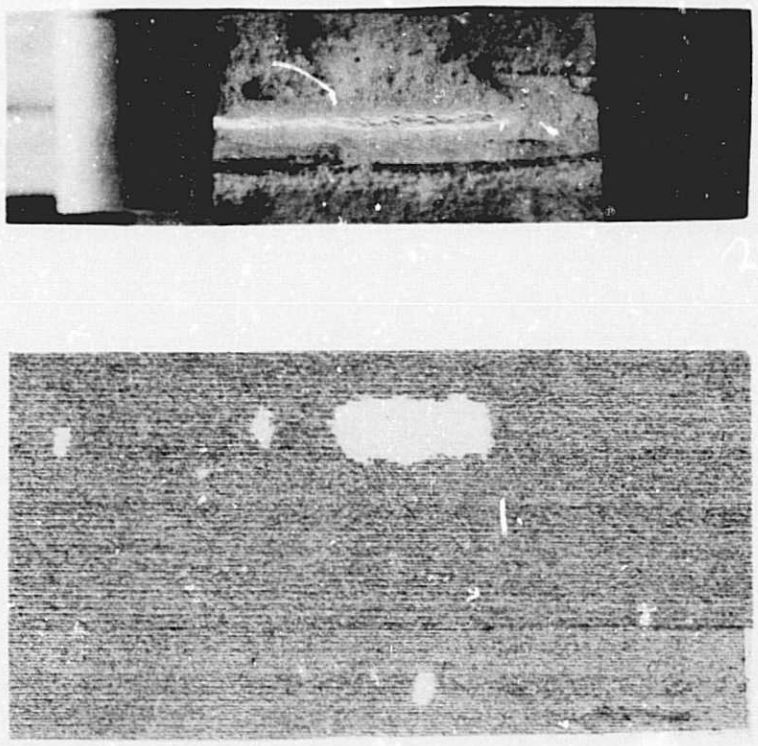

Figure 45. Delta scan recording and fracture surface of weld 2219-1.0-3B at IX with calibration hole trace. (4/64-inch calibration hole is eliptical indication towards bottom of page).

5817 B

performed at each load increment. The test specimen and external load application are depicted in Figure 46.

The maximum fiber stress in a box beam is calculated by the following equation (25).

$$S = \frac{6M}{bd^2}$$

where S = maximum fiber stress at surface,

M = moment,

b = width of beam,

d = depth of beam.

The moment M at the crack is the load times the moment arm which was 2.5 inches. The width of the aluminum sampies was 1.0 inches, while that for the titanium sample was 0.6-inch. The maximum fiber stresses at the surface of the test specimen at the crack are shown for various loads in Table XXII. Care had to be taken in loading the specimens so that the yield stress of the alloy was not exceeded at the maximum moment point where the beam was supported, hence, the maximum load applied to the specimens was limited to 30 pounds.

The test data recorded for two aluminum samples are shown in Figure 47, where the maximum signal voltage at a particular gain setting is shown for the two 2014 aluminum specimens as a function of the maximum compressive fiber stress at the crack. (The fiber stresswas figured for the maximum surface fiber stress). Figure 48 illustrates the effect of various compressive fiber stresses on three 2219 cracks. A rapid decrease in the ultrasonic instrument's signal strength resulted from increases in compressive stress. The larger fiber stresses causedthe defects to appear smaller and at approximately 25,000 psi, the defect indications disappeared from the oscilloscope screen for the particular instrument gain settings used.

The effect of the compressive fiber stress on the detectability of the crack depth as indicated by the sum of the area under the shear-wave scans is illustrated in Figures 49 and 50. For these specimens, the crack depth indications decreased sharply to small values at about half of the room-temperature yield-stress levels. Also plotted in these figures are the signal strength levels for several artificial calibration notches which were 0.020-inch wide and from 0.005 to 0.030-inches deep. The effect of the compressive stress was to make the cracks appear at approximately the same signal level as the 0.005-inch-depth notch when the cracks were stressed to 50 percent yield stress. Estimates of the size of the cracks varied greatly as a function of the stress level and may account for some of the variations in the actual measured crack parameters on the fatigue-cracked specimens. Another observation worthy of comment is the discrepancy between the size of the cracks and the size of the notches. The notches such as notch A which had a depth comparable to the crack depth in specimen 2014-0.125-2, produced a signal comparable in strength to that from the fatigue crack even though the crack is almost 3 times as long as the notch. Other variables such as the stress on and roughness of the crack surface may account for the similarity in the original signal levels.

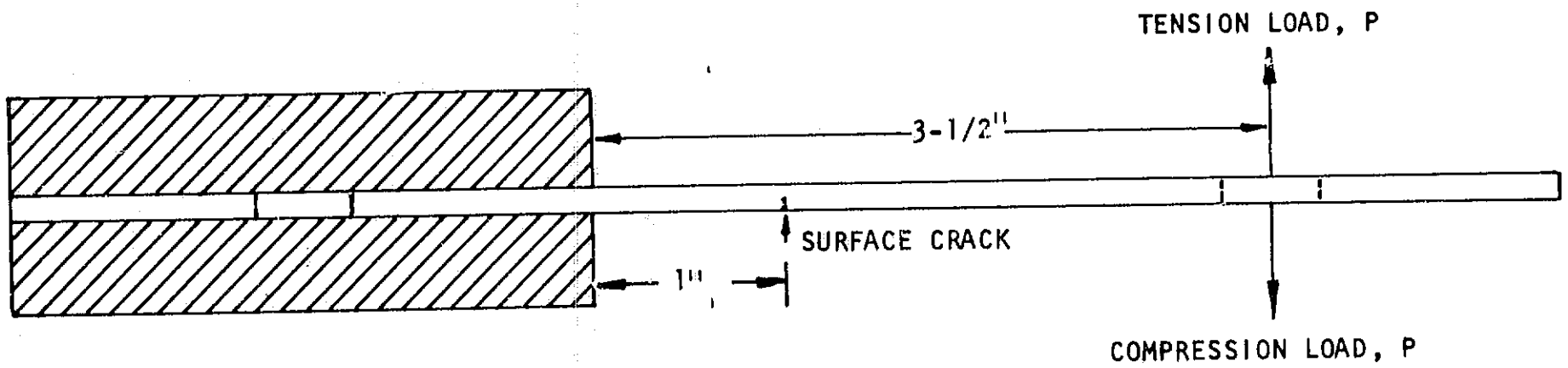

Figure 46. Cantilever beam arrangement for placing horizontal stresses on fatigue cracks.

TABLE XXII

CALCULATED MAXIMUM SURFACE FIBER STRESSES
IN THE TITANIUM AND ALUMINUM CRACK SPECIMENS FOR VARIOUS LOADS

	Shear Stress (psi)	
Load P (lbs.)	Aluminum (0.125 inch)	Titanium (0.120 Inch)
1	990	1,730
5	4,950	8,650
10	9,900	17,300
15	14,850	26,000
20	19,800	34,600
25	24,750	43,300
30	29,700	52,000

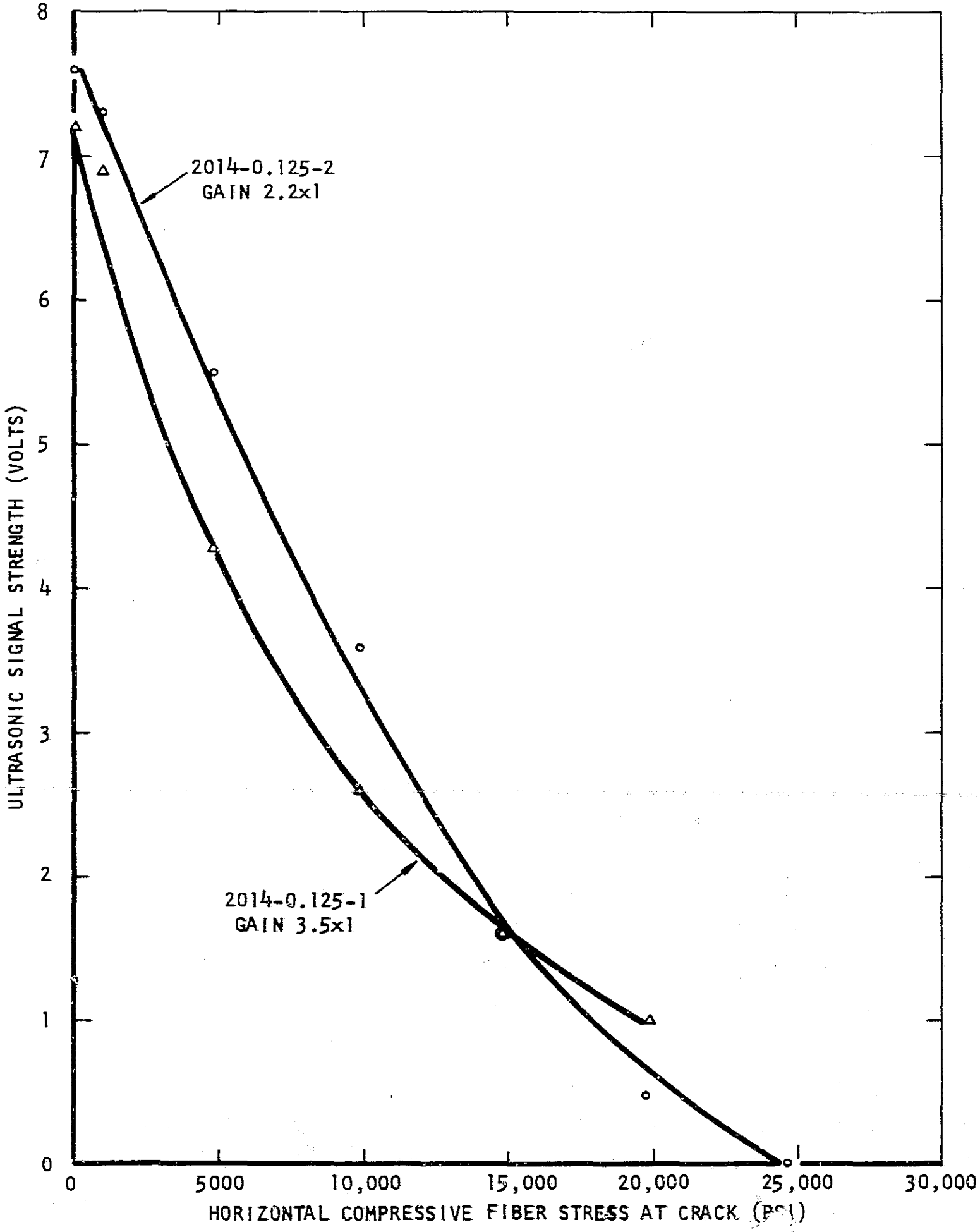

Figure 47. Ultrasonic shear wave signal strength as a function of a horizontal compressive fiber stress applied to two cracks in 0.125-inch 2014 aluminum.

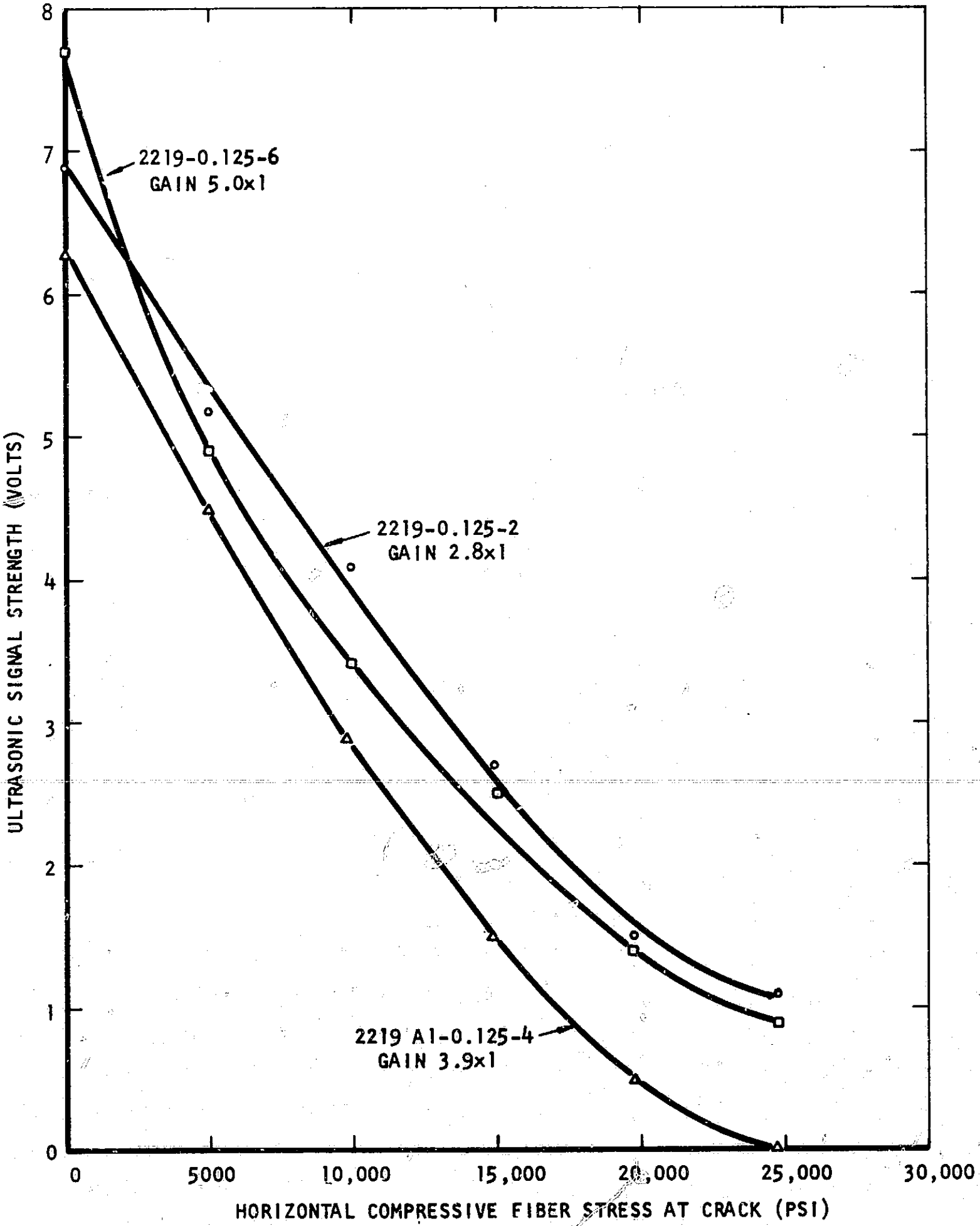

Figure 48. Ultrasonic shear wave signal strength as a function of a horizontal compressive fiber stress applied to three cracks in 0.125-inch 2219 aluminum.

5820 B

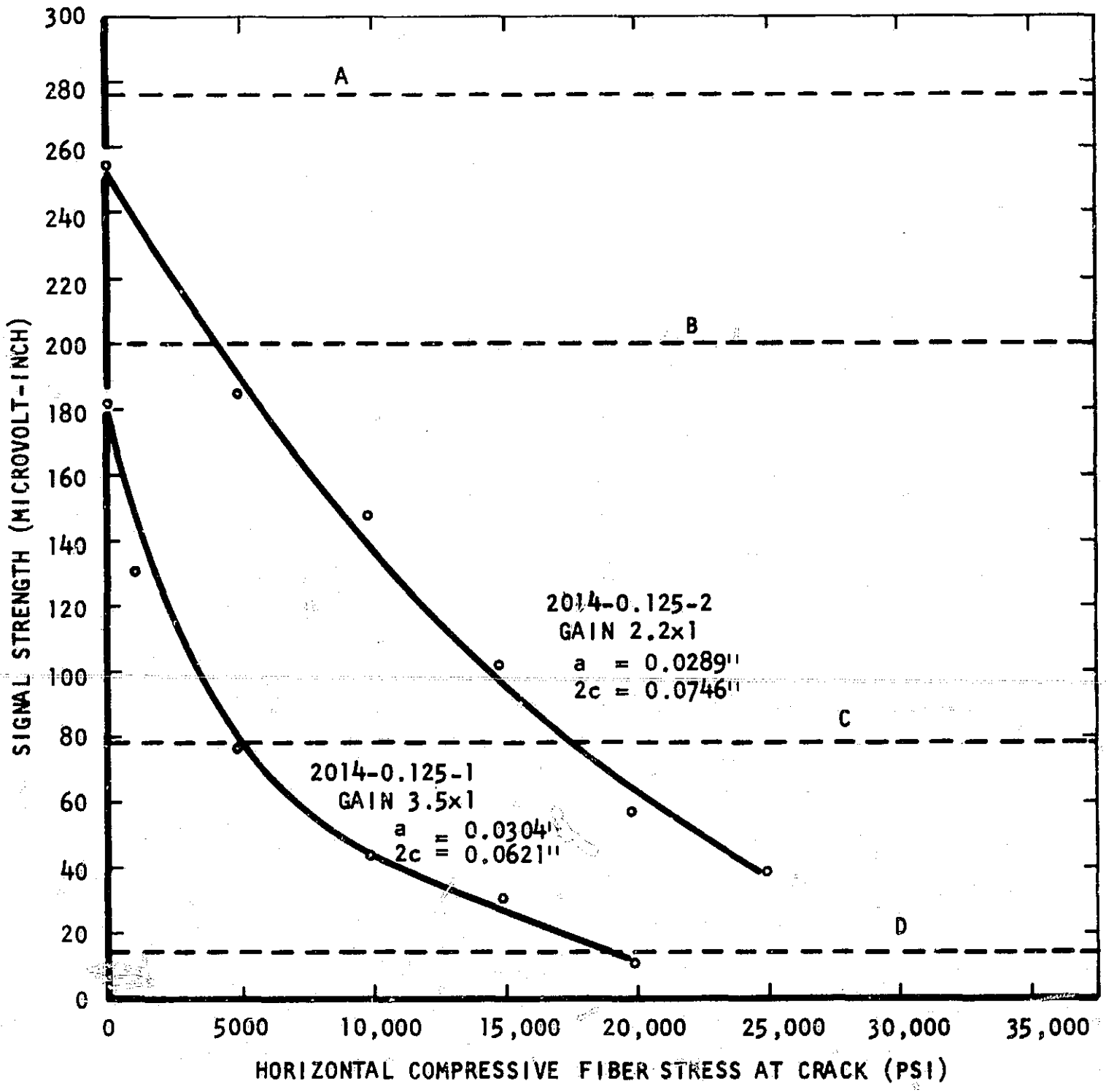

Figure 49. Ultrasonic shear wave signal strength as measured by the amplitude-distance integration technique as a function of a horizontal compressive fiber stress applied to cracks in 2-2014 aluminum specimens.

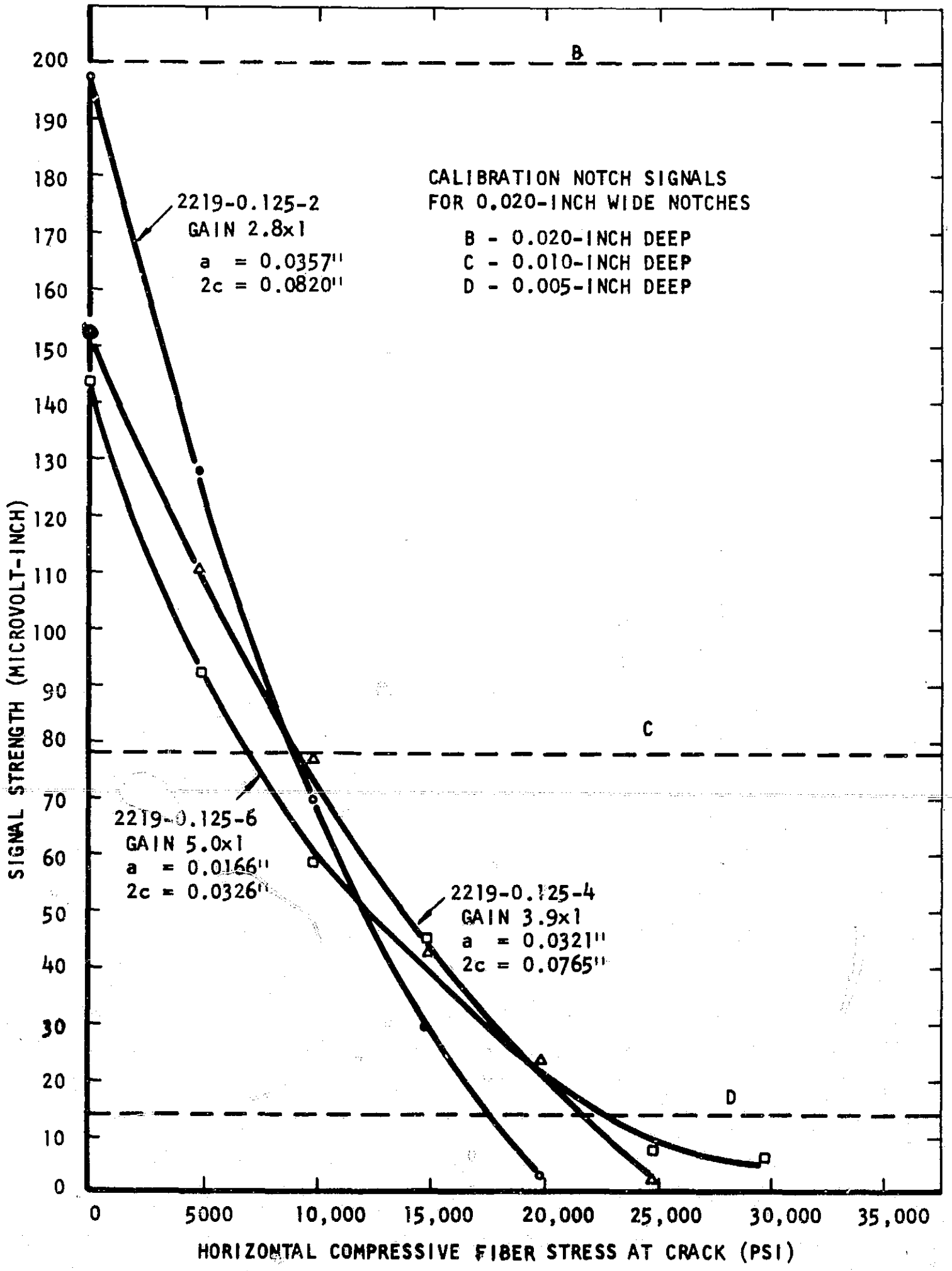

Figure 50. Ultrasonic shear wave signal strength as measured by the amplitude-distance integration technique as a function of a horizontal compressive fiber stress applied to cracks in 3-2219 aluminum specimens.

The above investigation into compressive-stress effects prompted a further study of both tensile and compressive effects on the defect surface. In this additional work, the 0.125-inch thick 5-2.5-0.125-4 titanium specimen was used. The stress evaluations were performed as before with the calculated stress levels, as shown in Table XXII. The actual crack depth in this specimen was 0.047-inch, while the actual crack length was 0.222-inches. Figure 51 shows both the tension and compression data summed through the point on the crack where the highest signal level was generated. The range of observed signal strengths was too large over the full range of tensile and compressive strengths for the use of one gain switch setting. Hence, separate curves were originally generated for tension and compression which did not meet at the zero-stress level. There is probably a degree of error in the assumption that the integrated values are valid over the entire measurement range. This is particularly true at the low defect signal levels. To obtain the curve in Figure 51, the tension load was applied at the maximum value in order to adjust the instrument gain to an 80-percent screen height. As the load was released, the measurement of the signal strength in the gate circuit becomes less accurate. By changing the gain to a higher value, the zero stress-level signal was measured with restored accuracy. An attempt was made to normalize the data by multiplying the tension data by the difference in the zero point values. The non-linear signal amplification inherent in the ultrasonic unit probably produced the zero point mismatch.

A second effort at determining the defect signal strength as a function of the stress state on the crack was made by measuring the signal voltage after one stage of amplification in the radio frequency amplifiers of the Sperry UM-700 unit. The highest signal generated by the crack as a function of stress is shown in Figure 52. This plot is similar to Figure 51 but does not show as large a range of signal variation. Both plots show an extremely rapid rise in signal strength with a small tensile load and region where further increases in tension do not greatly affect the signal strength. The compressive portions of the curve are linear on both semi-log plots and would therefore follow an exponential relationship.

Since the specimens were stressed in bending, it was thought that the deflection at the crack might produce sufficient change in the shear-wave angle to result in changes in the signal level. For the aluminum specimens, however, the deflection rate at the crack was calculated to be 0.0009 inch per pound, or 0.027 inch at the maximum load of 30 pounds. This corresponds to an approximate 1.5 degree change in the incident shear-wave angle. Although the effect on the change in actual signal intensity was negligible, a shift in the location of the signal peak was noted. For the titanium specimen, the higher modulus resuits in a deflection of 0.0198 inches for a 30 pound load to give an approximate 1.15 degree change in the incident shear-wave angle. This deflection in all cases could be disregarded.

C. Tensile Tests

Two types of tensile tests were performed on this program. The first were on non-defect specimens for several thicknesses of each alloy to determine the ultimate and yield stresses of the aluminum alloys at room temperature and the titanium alloys at -320 degrees F. The second were on the defect specimens at the previously used temperatures to reveal the defect dimensions and to develop fracture toughness data for the specimens.

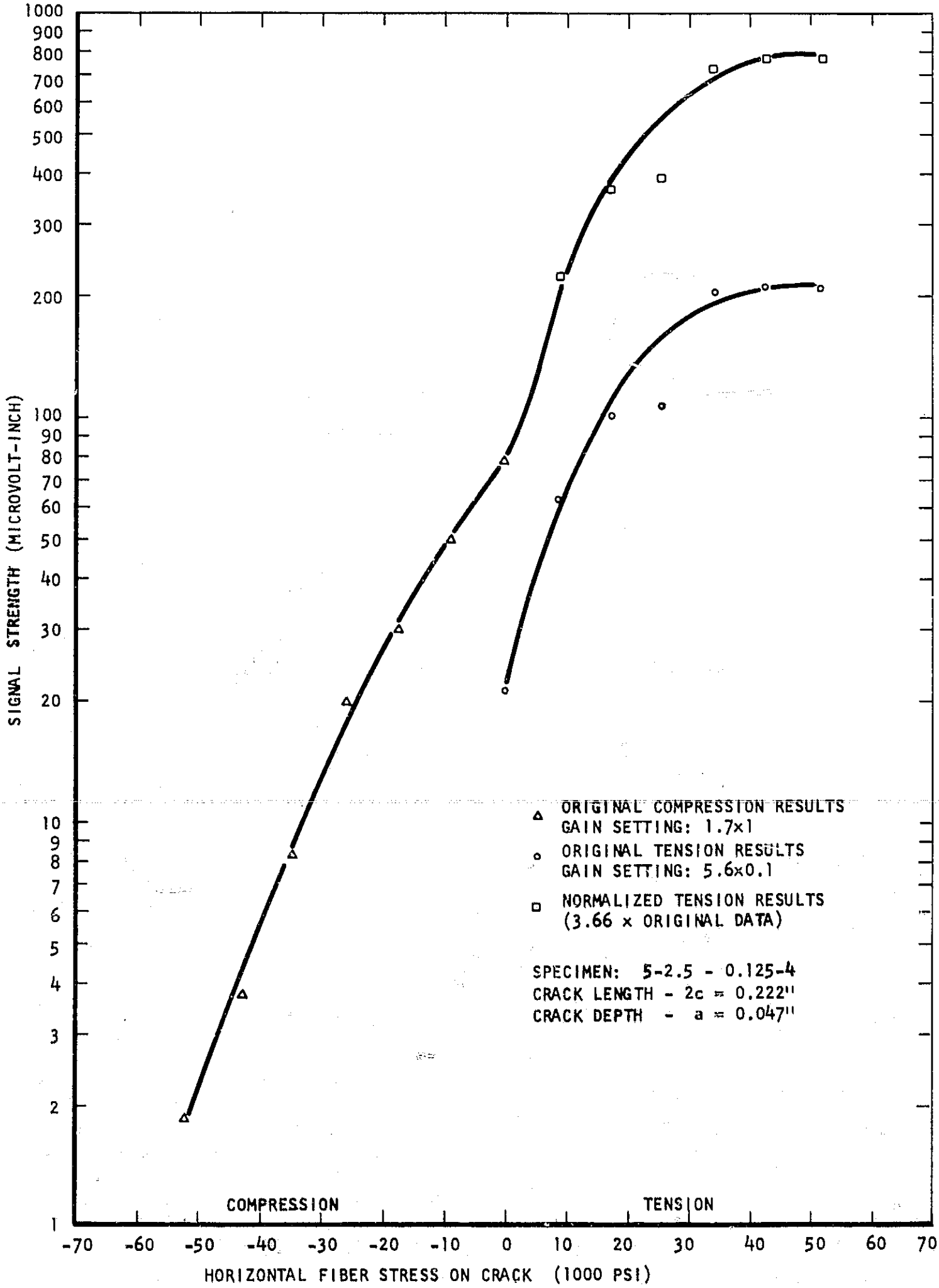

Figure 51. Ultrasonic shear wave signal strength as measured by the amplitude-distance integration technique as a function of a horizontal fiber stress applied to the crack in specimen 5-2.5-0.125-4.

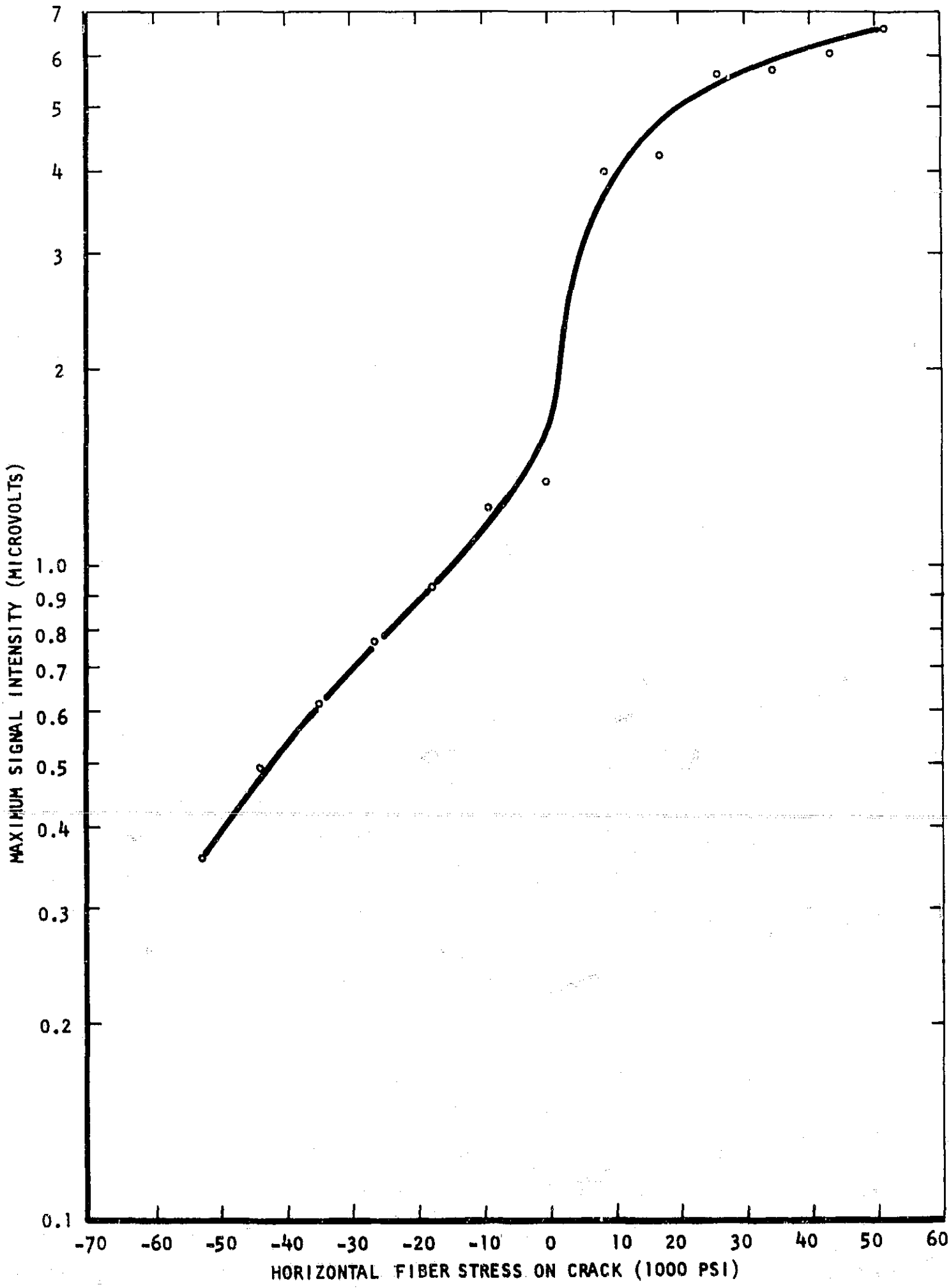

Figure 52. Ultrasonic shear wave signal intensity as measured after one radio frequency amplification stage as a function of a horizontal fiber stress applied to the crack in specimen 5-2.5-0.125-4.

1. Non-Defect Specimens

Non-defect tensile specimens were fabricated from the various thicknesses of each alloy, except for the 0.020-inch 2219 aluminum specimens. The 0.020-inch 2219 aluminum tensile specimens were fabricated from 0.125-inch plate samples which were machined to the smaller thickness. The results of the tensile tests and the specimen dimensions for the flat specimens are listed in Table XXIII. The yield strength values were used in the calculations for fracture toughness. Only the 0.125-inch titanium values were applicable since the critical crack depths are larger than the specimen thickness for all 0.020-inch materials and the 0.125-inch aluminum alloys. The variation in some of the values are quite large and in some instances differ from handbook values. However, the values with large variations were not necessary for any K_Q calculations.

Round-specimen tensile-test bars were machined from the 0.5 and 1.0-inch nominal thickness plates. A summary of the tensile-test data on these specimens is listed in Table XXIV. The values for the yield and ultimate tensile stress measured on the round specimens show less variability and better agreement with handbook values. These data were not generated to establish design values, but were used to establish the yield-stress values for the particular materials from which the fatigue-cracked specimens were fabricated.

2. Defect Specimens

Tensile tests were performed on the defect specimens to determine the failure stress values for the cross section of the specimen including the crack. From the stress and crack dimension data, K_Q values were calculated for the fatigue-cracked specimens. No attempt was made to determine values for the weld specimens since they contained too many defects and the yield stress values for the welds had not been determined.

The results of the tensile tests and the defect dimensions for all 0.020-inch defect specimens are listed in Table XXV. The failure-strength values of the specimens are quite variable depending on the size of the crack. Corresponding results for the defect tensile tests on the 0.125-inch specimens are listed in Table XXVI, including K_Q and $^a/_Q$ values calculated for the titanium specimens. The failure stress for the aluminum specimens all exceeded the 0.2 percent offset yield stress as expected. One titanium specimen, 5-2.5-0.125-4, had too small a width for valid K_Q and $^a/_Q$ calculations. The crack lengths and depths in the titanium specimens appeared to range above and below critical size for both alloys.

The results of the tensile tests on the 0.500-inch specimens are listed in Table XXVII. The two cracks in 2014 aluminum were larger than critical, while the majority of the cracks in the 2219 alloy were subcritical. The two weld specimens in 2219 aluminum had failure-stress levels below 30 ksi, with the specimen containing the smaller incomplete penetration defect having the lower failure stress. Five of the 5Al-2.5Sn titanium specimens were pulled at room temperature. Critical and near critical defects were in other specimens of this alloy pulled at the -320°F temperature. The 6Al-4V titanium cracks are all above critical defect size.

The defect tensile-test results on the 1.0-inch aluminum alloys are listed in Table XXVIII. All the fatigue cracks except in specimen 2219-1.0-4 were at or larger than the critical defect size. The failure-stress values for the

TABLE XXIII

FLAT-SPECIMEN TENSILE-TEST DATA FOR 2014 and 2219 ALUMINUM AND ELI 5Al-2.5Sn and 6Al-4V TITANIUM

Specimen Identification	Thickness (inch)	Width (inch)	Area ($inch^2$)	Ultimate Load (lbs.)	0.2% Offset Yield Load (lbs.)	0.2% Offset Yield Stress (psi)	Average 0.2% Offset Yield Stress (psi)	Ultimate Stress (psi)	Average Ultimate Stress (psi)
2014-A	0.0203	0.2509	0.0051	355	333	65,294	-	69,608	-
2014-B	0.0204	0.2508	0.0051	350	347	68,039	-	68,627	-
2014-C	0.0203	0.2507	0.0051	350	325	63,725	65,686	68,627	68,954
2014-D	0.1280	0.2509	0.0321	2325	1597	49,750	-	72,430	-
2014-E	0.1285	0.2502	0.0322	2205	1510	46,894	-	68,478	-
2014-F	0.1287	0.2508	0.0323	2295	1578	48,854	48,499	71,053	70,653
2219-G	0.1243	0.2501	0.0311	1965	1555	50,000	-	63,183	-
2219-H	0.1241	0.2505	0.0311	1960	1556	50,032	-	63,023	-
2219-J	0.1238	0.2502	0.0310	1960	1546	49,871	49,871	63,225	63,144
6-4-K	0.0249	0.2513	0.0063	1285	1269	201,429	-	203,968	-
6-4-L	0.0233	0.2508	0.0058	1255	1249	215,345	-	216,379	-
6-4-M	0.0233	0.2511	0.0059	1255	1211	205,254	207,342	212,712	211,020
6-4-N	0.1240	0.2500	0.0310	6740	6640	214,194	-	217,419	-
6-4-O	0.1238	0.2516	0.0311	6720	6580	211,576	212,885	216,077	216,748
5-2.5-P	0.0220	0.2509	0.0055	1000	932	169,455	-	181,818	-
5-2.5-Q	0.0231	0.2512	0.0058	1025	950	163,793	-	176,724	-
5-2.5-R	0.0223	0.2512	0.0056	1025	932	166,429	166,559	183,036	180,526
5-2.5-S	0.1194	0.2510	0.0300	5620	5340	178,000	-	187,334	-
5-2.5-T	0.1198	0.2511	0.0301	5690	5370	178,405	178,203	189,037	188,186

All aluminum alloys pulled at room temperature and all titanium alloys at -320°F in liquid nitrogen.

TABLE XXIV

ROUND-SPECIMEN TENSILE-TEST DATA FOR 2014 AND 2219 ALUMINUM AND ELI 5Al-2.5Sn and 6Al-4V TITANIUM ALLOYS

Specimen Identification	Plate Thickness (Inch)	Specimen Diameter (Inch)	Area ($Inch^2$)	Ultimate Load (lbs.)	0.2% Offset Yield Load (lbs.)	0.2% Offset Yield Stress (psi)	Average 0.2% Offset Yield Stress (psi)	Ultimate Stress (psi)	Average Ultimate Stress (psi)
2014-A	1.0	0.2530	0.05027	3600	3290	65,447	-	71,613	-
2014-B	1.0	0.2540	0.05067	3630	3313	65,384	-	71,640	-
2014-C	1.0	0.2530	0.05027	3600	3295	65,546	65,459	71,613	71,622
2014-D	0.5	0.2520	0.04988	3415	3182	63,793	-	68,464	-
2014-E	0.5	0.2530	0.05027	3445	3205	63,756	-	68,530	-
2014-F	0.5	0.2530	0.05027	3420	3178	63,219	63,589	68,033	68,342
2219-G	1.0	0.2525	0.05008	3480	2863	57,169	-	69,489	-
2219-H	1.0	0.2530	0.05027	3490	2863	56,952	-	69,425	-
2219-J	1.0	0.2530	0.05027	3500	2877	57,231	56,997	69,624	69,513
2219-K	0.5	0.2520	0.04988	3435	2810	56,335	-	68,865	-
2219-L	0.5	0.2520	0.04988	3420	2790	55,934	-	68,565	-
2219-M	0.5	0.2525	0.05008	3455	2798	55,871	56,046	68,990	68,807
6-4-N	0.5	0.2520	0.04988	10940	10430	209,102	-	219,326	-
6-4-O	0.5	0.2515	0.04968	10760	10170	204,710	-	216,586	-
6-4-P	0.5	0.2515	0.04968	10820	10200	205,314	206,375	217,794	217,902
5-2.5-Q	0.5	0.2515	0.04968	9230	8720	175,523	-	185,789	-
5-2.5-R	0.5	0.2520	0.04988	9290	8845	177,326	-	186,247	-
5-2.5-S	0.5	0.2515	0.04968	9260	8810	177,335	176,728	186,393	186,143

All aluminum alloys pulled at room temperature and all titanium alloys at -320°F in liquid nitrogen.

TABLE XXV

DEFECT TENSILE TEST RESULTS ON THE 0.020-INCH SPECIMENS

Specimen Identification	Test Temp. (°F)	Specimen Thickness (Inch)	Specimen Width (Inch)	Specimen Area ($Inch^2$)	Crack Depth, (a) (Inch)	Crack Length, (2c) (Inch)	Failure Load (K-lbs)	Failure Stress (KSI)
2014-1	+ 70	0.0204	0.312	0.00636	0.0204	0.088	0.255	40.06
2014-1A	+ 70	0.0200	0.266	0.00532	0.0200	0.094	0.215	40.41
2014-2	+ 70	0.0200	0.336	0.00672	0.0200	0.087	0.295	43.90
2219-1	+ 70	0.0200	0.670	0.01340	0.0200	0.189	0.520	38.81
2219-2	+ 70	0.0220	0.673	0.01481	0.0220	0.190	0.530	35.80
2219-3	+ 70	0.0205	0.673	0.01380	0.0205	0.138	0.590	42.76
2219-7	+ 70	0.0215	0.673	0.01447	0.0215	0.125	0.660	45.61
5-2.5-1	-320	0.0215	0.382	0.00821	0.0215	0.116	0.995	121.19
5-2.5-3	-320	0.0220	0.382	0.00840	0.0220	0.140	1.050	125.00
5-2.5-4	-320	0.0215	0.382	0.00821	0.0215	0.121	1.045	127.28
5-2.5-6	-320	0.0220	0.382	0.00840	0.0220	0.121	1.045	124.40
5-2.5-7	-320	0.0215	0.379	0.00815	0.0215	0.112	1.185	145.40
5-2.5-8	-320	0.0220	0.379	0.00834	0.0055	0.062	1.410	169.06
5-2.5-9	-320	0.0215	0.675	0.01451	0.0215	0.087	*	-
5-2.5-10	-320	0.0210	0.380	0.00798	0.0210	0.075	1.205	151.00
5-2.5-12	-320	0.0220	0.380	0.00836	0.0220	0.116	1.070	127.99
6-4-1	-320	0.0220	0.377	0.00829	0.0220	0.261	0.370	44.63
6-4-2	-320	0.0220	0.378	0.00832	0.0220	0.118	1.170	140.63
6-4-3	-320	0.0220	0.381	0.00838	0.0220	0.067	1.485	177.21
6-4-11	-320	0.0215	0.380	0.00817	0.0215	0.172	.870	106.49
6-4-13	-320	0.0220	0.381	0.00838	0.0220	0.137	1.075	128.28
6-4-15	-320	0.0220	0.380	0.00836	0.0220	0.130	1.115	133.37
6-4-16	-320	0.0220	0.381	0.00838	0.0220	0.077	1.405	167.66
6-4-17	-320	0.0220	0.380	0.00836	0.0220	0.085	1.375	164.47
6-4-18	-320	0.0220	0.379	0.00834	0.0220	0.112	1.260	151.08
6-4-19	-320	0.0215	0.379	0.00815	0.0215	0.082	1.375	168.71

* Pulled out of pin hole.

TABLE XXVI

DEFECT TENSILE-TEST RESULTS ON THE 0.125-INCH SPECIMENS

Specimen Identification	Test Temp. (°F)	Specimen Thickness (Inch)	Specimen Width (Inch)	Specimen Area ($Inch^2$)	Crack Depth, (a) (Inch)	Crack Length, (2c) (Inch)	Failure Load (K-lbs)	Failure Stress (KSI)	K_Q (KSI $\sqrt{Inch}$)	a/Q (Inch)
2014-1	+ 70	0.1245	0.9974	0.1242	0.030	0.062	8.61	69.34	-	-
2014-2	+ 70	0.1238	1.0070	0.1247	0.029	0.075	8.58	68.82	-	-
2014-3A	+ 70	0.1243	1.0068	0.1260	0.022	0.046	8.80	69.84	-	-
2014-3B	+ 70	0.1241	1.0070	0.1250	0.025	0.064	8.69	69.54	-	-
2014-4A	+ 70	0.1245	1.0075	0.1254	0.034	0.091	8.40	66.97	-	-
2014-4B	+ 70	0.1247	1.0065	0.1255	0.026	0.063	8.68	69.16	-	-
2219-1	+ 70	0.1234	1.0050	0.1240	0.034	0.075	7.69	62.01	-	-
2219-2	+ 70	0.1235	1.0080	0.1245	0.036	0.082	7.60	61.05	-	-
2219-3	+ 70	0.1240	1.0057	0.1247	0.034	0.064	7.77	62.31	-	-
2219-4	+ 70	0.1235	1.0070	0.1244	0.032	0.077	7.78	62.56	-	-
2219-5	+ 70	0.1242	0.9965	0.1238	0.025	0.040	7.80	63.02	-	-
2219-6	+ 70	0.1235	0.9760	0.1205	0.017	0.035	7.81	64.79	-	-
5-2.5-1A	-320	0.1221	0.9988	0.1220	0.031	0.098	21.59	177.03	50.07	0.0210
5-2.5-2	-320	0.1202	0.9975	0.1199	0.024	0.058	22.50	187.66	41.90	0.0131
5-2.5-3	-320	0.1231	0.6024	0.0742	0.020	0.054	13.62	183.67	39.30	0.0120
5-2.5-4	-320	0.1240	0.6013	0.0746	0.047	0.222	11.40	152.89	59.07	0.0393
5-2.5-7	-320	0.1184	0.9975	0.1181	0.041	0.200	19.87	168.24	62.07	0.0358
5-2.5-8	-320	0.1194	0.9974	0.1191	0.025	0.075	22.10	185.57	46.49	0.0165
6-4-1	-320	0.1230	0.6034	0.0742	0.023	0.077	15.86	213.69	53.45	0.0165
6-4-1B	-320	0.1231	0.6002	0.0739	0.021	0.054	16.18	218.99	47.09	0.0122
6-4-3	-320	0.1205	0.6032	0.0727	0.021	0.062	15.95	219.44	50.15	0.0137
6-4-4	-320	0.1196	0.9959	0.1191	0.045	0.158	20.04	168.25	58.05	0.0313
6-4-5	-320	0.1231	0.6030	0.0742	0.024	0.065	16.06	216.36	50.84	0.0145
6-4-6	-320	0.1230	0.6023	0.0741	0.037	0.158	13.12	177.10	59.09	0.0293

0.2% Offset Yield Stress at -320°F: 6Al-4V titanium = 206.4 KSI

5Al-2.5Sn titanium = 176.7 KSI

TABLE XXVII

DEFECT TENSILE TEST RESULTS ON THE 0.500-INCH SPECIMENS

Specimen Identification	Test Temp. (°F)	Specimen Thickness (Inch)	Specimen Width (Inch)	Crack Depth, (a) (Inch)	Crack Length, (2c) (Inch)	Failure Load (K-lbs)	Failure Stress (KSI)	K_Q (KSI $\sqrt{\text{Inch}}$)	a/Q (Inch)
2014-1	+ 70	0.5134	1.676	0.176	0.589	49.70	57.76	39.25	0.1215
2014-2	+ 70	0.5133	1.676	0.161	0.554	51.40	59.75	39.36	0.1142
2219-1	+ 70	0.5088	1.671	0.133	0.386	47.65	56.05	31.71	0.0842
2219-2	+ 70	0.5073	1.676	0.115	0.313	49.75	58.51	30.13	0.0697
2219-3	+ 70	0.5088	1.676	0.119	0.323	49.90	58.52	30.62	0.0720
2219-4	+ 70	0.5040	1.671	0.123	0.334	48.15	57.17	30.32	0.0740
2219-5	+ 70	0.5074	1.671	0.113	0.299	49.45	58.32	29.40	0.0669
2219-6	+ 70	0.5073	1.677	0.122	0.354	49.95	58.71	32.01	0.0782
2219-7	+ 70	0.5089	1.677	0.117	0.340	49.00	57.62	30.71	0.0747
2219-8	+ 70	0.5083	1.676	0.189	0.612	43.90	51.53	35.82	0.1271
2219-9	+ 70	0.5099	1.676	0.182	0.600	44.30	51.84	35.68	0.1246
2219-1A	+ 70	0.4880	3.349	0.148	0.482	94.00	57.52	36.08	0.1035
2219-1E	+ 70	0.4870	3.351	0.142	0.486	94.50	57.91	36.27	0.1032
2219-5A*	+ 70	0.4550	3.256	0.070	1.217	44.00	29.70	**	**
2219-5B*	+ 70	0.4560	3.256	0.048	0.951	43.00	28.96	**	**
5-2.5-2	+ 70	0.5460	0.997	0.088	0.188	61.50	112.98	**	**
5-2.5-4	+ 70	0.5490	0.997	0.113	0.243	59.90	109.44	**	**
5-2.5-5	+ 70	0.5470	0.997	0.126	0.246	59.65	109.38	**	**
5-2.5-6	-320	0.5460	0.370	0.069	0.121	35.65	176.47	56.80	
5-2.5-7	-320	0.5480	0.371	0.053	0.140	36.10	175.20	60.05	0.0309
5-2.5-8	-320	0.5497	0.370	0.068	0.155	34.80	171.01	61.77	0.0343
5-2.5-9	-320	0.5446	0.373	0.044	0.103	36.80	180.36	53.41	0.0231
5-2.5-10	-320	0.5477	0.375	0.032	0.062	37.15	180.88	41.60	
5-2.5-11	-320	0.5455	0.365	-	-	36.60	183.82	Broke outside of crack	
5-2.5-13*	+ 70	0.5380	0.997	No defect		59.10	110.18	**	**
5-2.5-14*	+ 70	0.5285	0.998	No defect		75.95	144.00	**	**
6-4-1	-320	0.5498	0.375	0.043	0.095	40.30	195.39	55.16	0.0210
6-4-3	-320	0.5530	0.374	0.054	0.121	34.00	164.39	51.67	0.0260
6-4-12	-320	0.5482	0.376	0.071	0.147	34.00	165.01	57.17	0.0316

* - Weld Specimens

** - Not computed for room temperature and/or weld specimens.

0.2% Offset Yield Stress: At + 70°F — 2014 Al = 63.59 KSI; 2219 Al = 56.00 KSI

At -320°F — 6Al-4V-Ti = 206.4 KSI; 5Al-2.5Sn-Ti = 177.0 KSI

TABLE XXVIII

DEFECT TENSILE-TEST RESULTS ON THE 1.0-INCH SPECIMENS

Specimen Identification	Test Temp. (°F)	Specimen Thickness (Inch)	Specimen Width (Inch)	Crack Depth, (a) (Inch)	Crack Length, (2c) (Inch)	Failure Load (K-lbs)	Failure Stress (KSI)	K_Q (KSI$\sqrt{\text{Inch}}$)	a/Q (Inch)
2014-1	+ 70	0.9925	1.676	0.190	0.567	85.50	51.40	34.28	0.1170
2014-2	+ 70	0.9921	1.676	0.185	0.550	91.05	54.76	36.18	0.1148
2014-2A*	+ 70	0.9770	3.255	-	-	96.00	30.19	**	**
2014-2B*	+ 70	0.9850	3.256	-	-	95.50	29.78	**	**
2014-3A*	+ 70	0.9840	1.677	-	-	45.98	27.86	**	**
2014-3B*	+ 70	0.9759	1.637	-	-	49.80	31.17	**	**
2014-3C*	+ 70	0.9973	1.675	-	-	41.95	25.11	**	**
2014-3D*	+ 70	0.9930	1.677	-	-	24.60	14.77	**	**
2219-1	+ 70	0.9924	1.676	0.191	0.543	94.70	56.94	38.28	0.1189
2219-2	+ 70	0.9984	1.676	0.205	0.617	92.10	55.04	39.06	0.1325
2219-3	+ 70	1.0040	1.673	0.195	0.530	95.00	56.55	37.67	0.1167
2219-4	+ 70	0.9915	1.673	0.167	0.473	99.98	60.27	38.13	0.1053
2219-3A*	+ 70	0.9692	1.673	-	-	44.30	27.32	**	**
2219-3B*	+ 70	0.9657	1.617	-	-	36.70	23.50	**	**
2219-4A*	+ 70	0.9730	3.250	-	-	86.75	27.43	**	**
2219-4B*	+ 70	0.9630	3.252	-	-	81.25	25.94	**	**

* - Weld Specimens

** - Not computed for weld specimens

0.2% Offset Yield Stress at + 70°F: 2014 Al = 65.5 KSI

2219 Al = 57.0 KSI

welds varied greatly with only two being above 30 ksi. The weld with the lowest tensile strength, 2014-1.0-3D, had a tungsten inclusion, as well as numerous areas of lack of fusion, porosity and incomplete penetration.

IV - DISCUSSION OF RESULTS

In any investigation of measurement methods, two parameters must be evaluated: 1) the relationship of the measured value to the actual value; and 2) the repeatability of the observed relationship. The first value defines the sensitivity of the test method, while the second defines its accuracy. Both are interrelated, since they are obtained from the same data. It is important to point out that the measured value does not have to be numerically the same as the actual value, but only need be related to the actual value. In addition, a calibration standard may be used only to achieve the proper sensitivity in the nondestructive test, although the standard's dimensions may not correlate with the actual measured values.

Standard statistical analysis techniques were used to correlate the measured NDT values with the actual defect dimensions. This section of the report will detail the data correlation and accuracies of the various tests on the four alloys and four material thicknesses.

A. Nondestructive Test-Defect Correlations

The data generated for each of the four nondestructive tests and the corresponding defect dimensions revealed by the tensile tests have been listed in the previous section of this report. There are several possible sources for any inaccuracies in these measurements; i.e., limitations of the technique, operator errors and the physical variability of the specimens. In the section on defect stress evaluations, for example, differences were shown in the response of the ultrasonic shear-wave test to tensile and compressive stresses on the defect. Residual stress states, defect surface texture and defect orientation are only a few of the sources of measurement inaccuracies directly relatable to specimen variability. Some of these variables will be discussed with particular sets of data. The specific test results will be discussed for each thickness group in the sections that follow.

1. 0.020-Inch Specimens

Linear regression analysis techniques were applied to the data generated for crack-length measurements in the radiographic, ultrasonic and penetrant tests. The analysis of the radiographic data on the 0.020-inch thick aluminum alloys indicated that no correlation existed even though several of the measured values were near the actual length. For the penetrant data analysis, shown in Figure 53 for the aluminum alloys, an equation was obtained predicting the probable value of actual crack length with the listed 3σ ($\pm 99.7\%$) variation. Projection of the $+3\sigma$ limit to the X-axis indicates that an indicated length of zero can mean that a crack might be larger than 0.040-inch, 1.5 times out of 1000 measurements. For the ultrasonic shear-wave test results, shown in Figure 54, the 3σ variation is ± 0.0621-inch which is larger than the ± 0.036 value for the penetrant tests. However, the largest possible crack that might exist for a zero indicated length will not be larger than 0.048-inch, more than 1.5 times out of 1000 measurements. The penetrant test gives the most precise length determination of any of the three NDT tests performed on the 0.020-inch aluminum specimens.

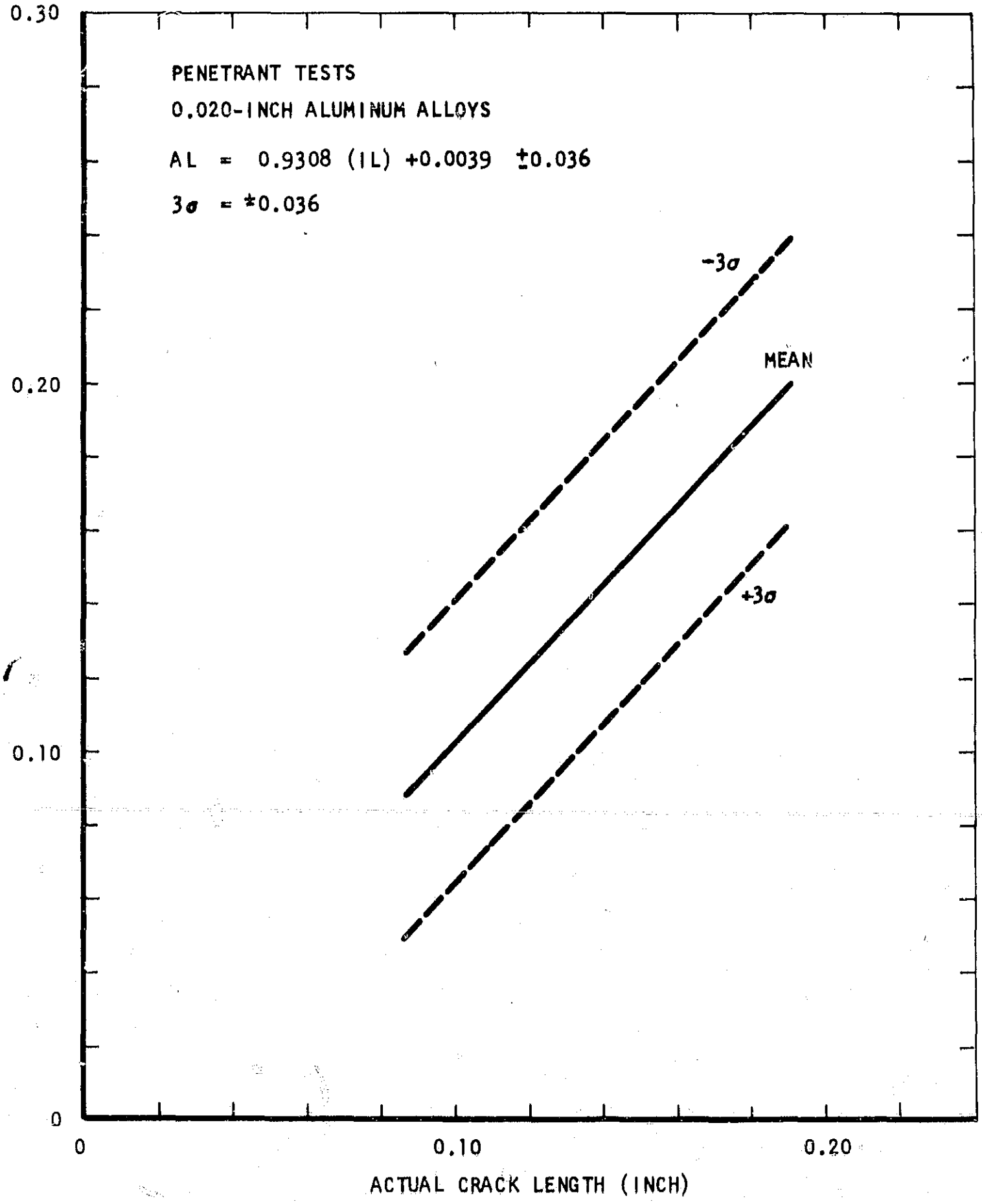

Figure 53. Indicated crack length for fluorescent penetrant tests as a function of actual crack length for fatigue cracks in 0.020-inch aluminum alloys.

5825 a

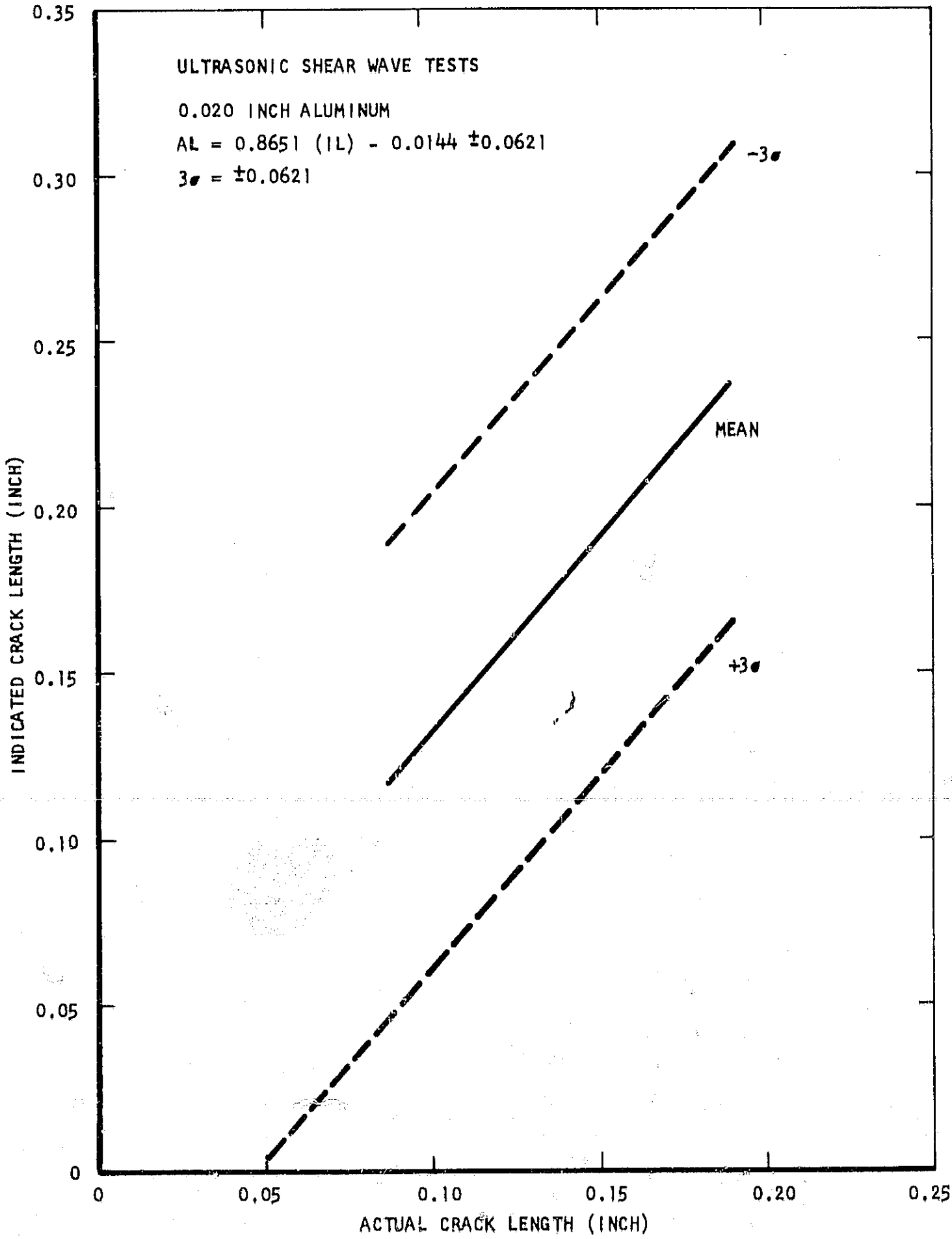

Figure 54. Indicated crack length for ultrasonic shear wave tests as a function of actual crack length for fatigue cracks in 0.020-inch aluminum alloys.

5326 B

A plot of the radiographic test results on the 0.020-inch thick titanium alloys is illustrated in Figure 55. The 3σ variation is ±0.0508-inch with a maximum actual crack length of approximately 0.069-inch for a zero indicated crack length. Statistically, this means that cracks as large as 0.069-inch in length might not be detected radiographically. The chance of a crack with dimensions exceeding this value not being detected radiographically will occur no more than in 0.15 percent of the time. The penetrant test results on the titanium alloys are presented in Figure 56. The lower 3σ limit (±0.027-inch) allows a maximum crack length of approximately 0.032-inch for a zero indicated crack length, a value much smaller than that for the radiographic tests. For the ultrasonic shear-wave tests, the results plotted in Figure 57 give a 3σ value of ±0.0844-inch, the largest for the three test methods. Since titanium alloys are known to exhibit high acoustic attenuation coefficient variation, the crack length data were analyzed for each alloy. The 5Al-2.5Sn titanium measurements correlated very poorly with the actual crack lengths. The 6Al-4V titanium measurements, however, produced much improved correlations, as shown in Figure 58, with a 3σ variation of ±0.0394-inch and a maximum actual crack length for zero indicated length of approximately 0.028-inch. Compared to the penetrant tests, this 3σ limit for the shear-wave tests is a little larger, but the maximum crack length at zero indicated length is smaller. Overall, the penetrant test was the most accurate for the 0.020-inch titanium alloys.

2. 0.125-Inch Specimens

The radiographic results on the 0.125-inch aluminum specimens showed that no cracks were resolved. The results of the penetrant tests for the aluminum alloys are illustrated in Figure 59. The 3σ limit was calculated to be ±0.032-inch, with the maximum crack length at a zero indicated length of 0.029-inch. Both the delta and shear-wave ultrasonic tests failed to produce any significant correlations with the actual measured crack depths and lengths. The penetrant test again provided the most accurate crack-length measurement, while the depth of the cracks was not determined accurately in this aluminum thickness.

Radiographic test results on the 0.125-inch titanium alloys, plotted in Figure 60, show the maximum crack length at zero indicated crack length to be approximately 0.130-inch, while the 3σ limit is ±0.086-inch. The penetrant test results, illustrated in Figure 61, gives a 3σ limit of 0.067-inch, with a maximum crack length at zero indicated crack length of 0.050-inch. These results are more accurate than those of the radiographic tests. The shear-wave test results on the 6Al-4V titanium alloy showed that there were no significant correlations between the measured values and the actual values of crack length and depth. The evaluation of the test data for the 5Al-2.5Sn alloy, however, revealed the following equations and 3σ values:

Values in Inch Units

Crack Length	AL = 0.00601(IL)+0.0218±0.0696
Crack Depth (Area Integration)	AD = 0.00165(ID)+0.0091±0.0241
Crack Depth (Increment)	AD = 0.00029(ID)+0.0190±0.0146

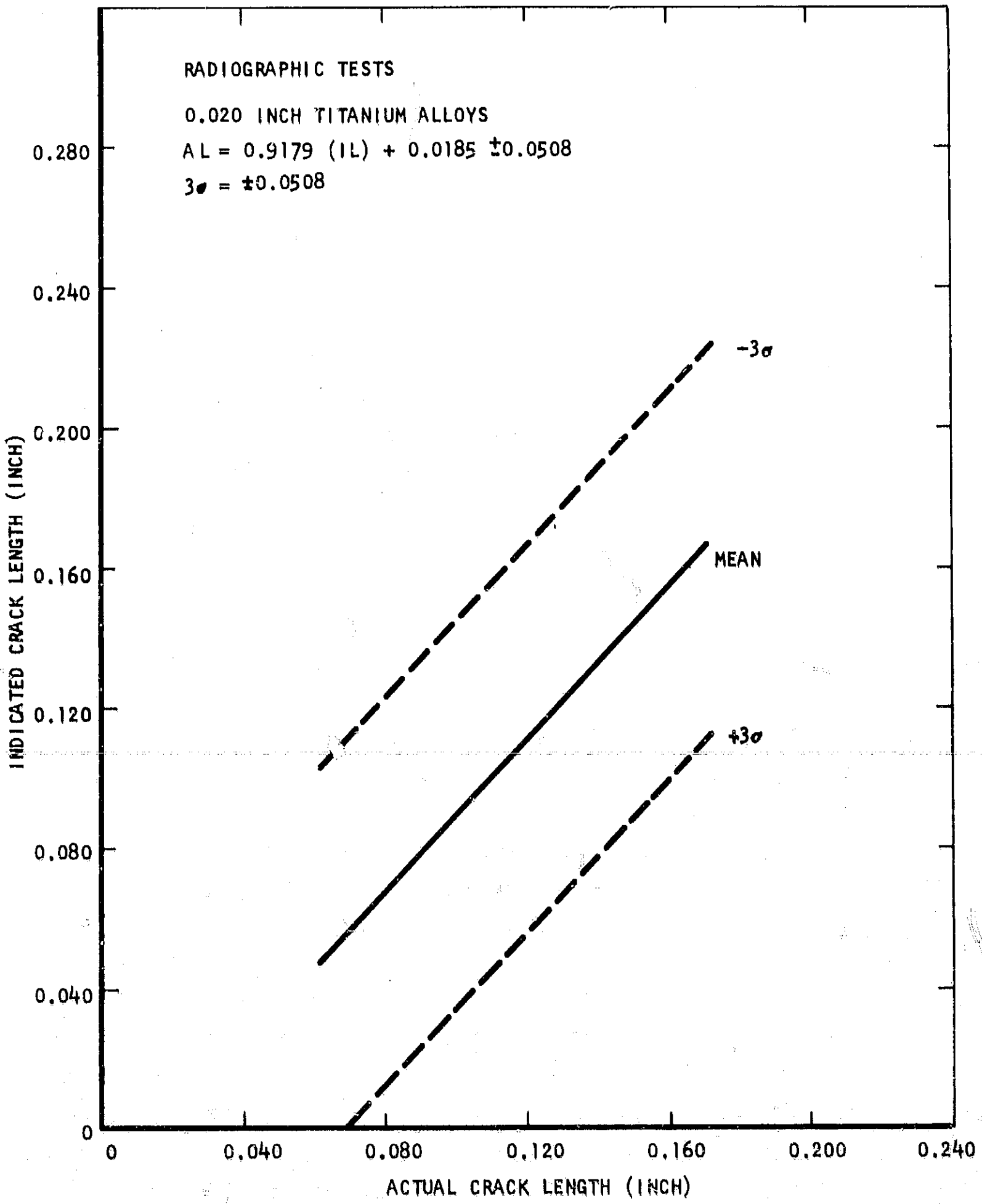

Figure 55. Indicated crack length for radiographic tests as a function of actual crack length for fatigue cracks in 0.020-inch titanium alloys.

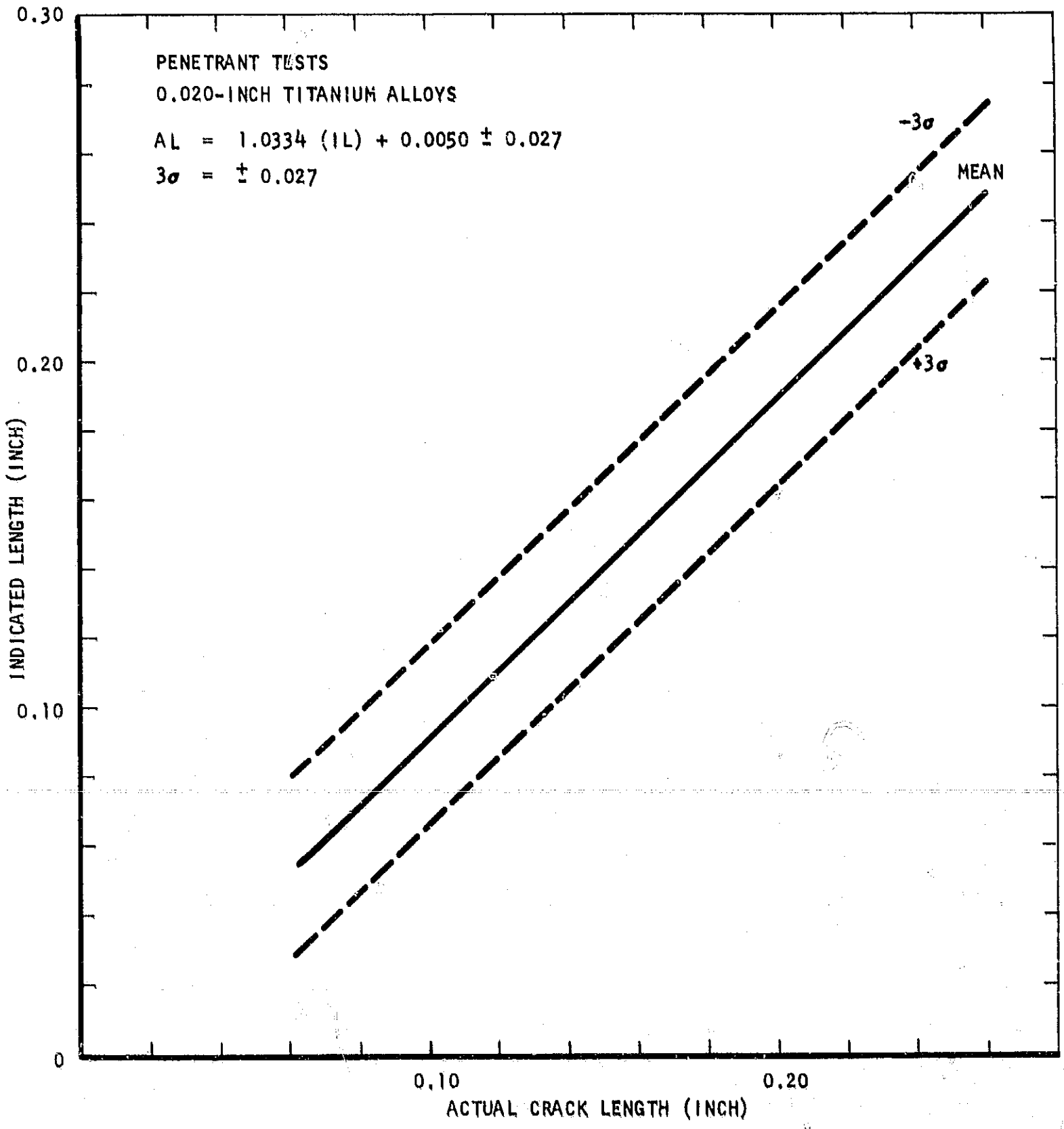

Figure 56. Indicated crack length for fluorescent penetrant tests as a function of actual crack length for fatigue cracks in 0.020-inch titanium alloys.

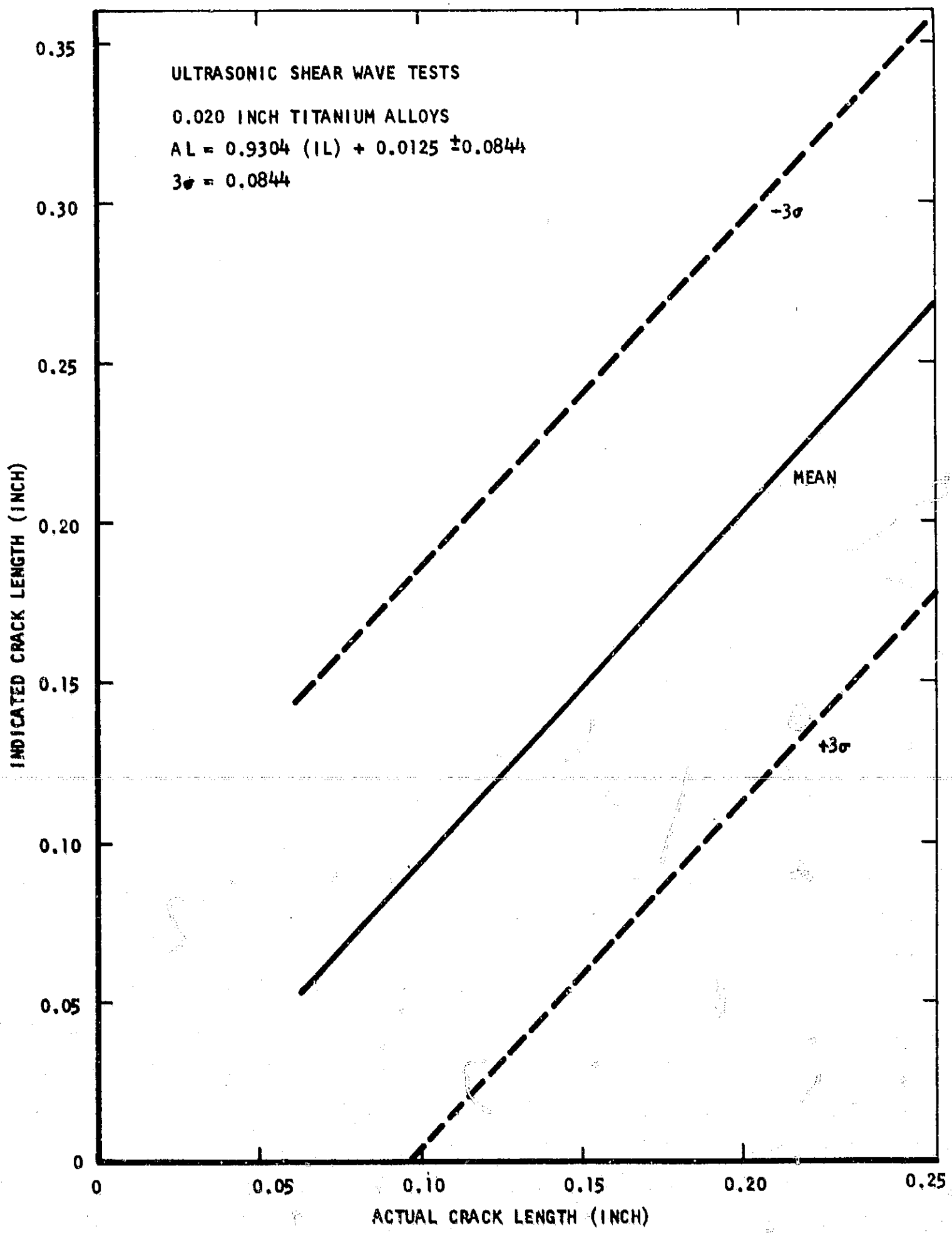

Figure 57. Indicated crack length for ultrasonic shear wave tests as a function of actual crack length for fatigue cracks in 0.020-inch titanium alloys.

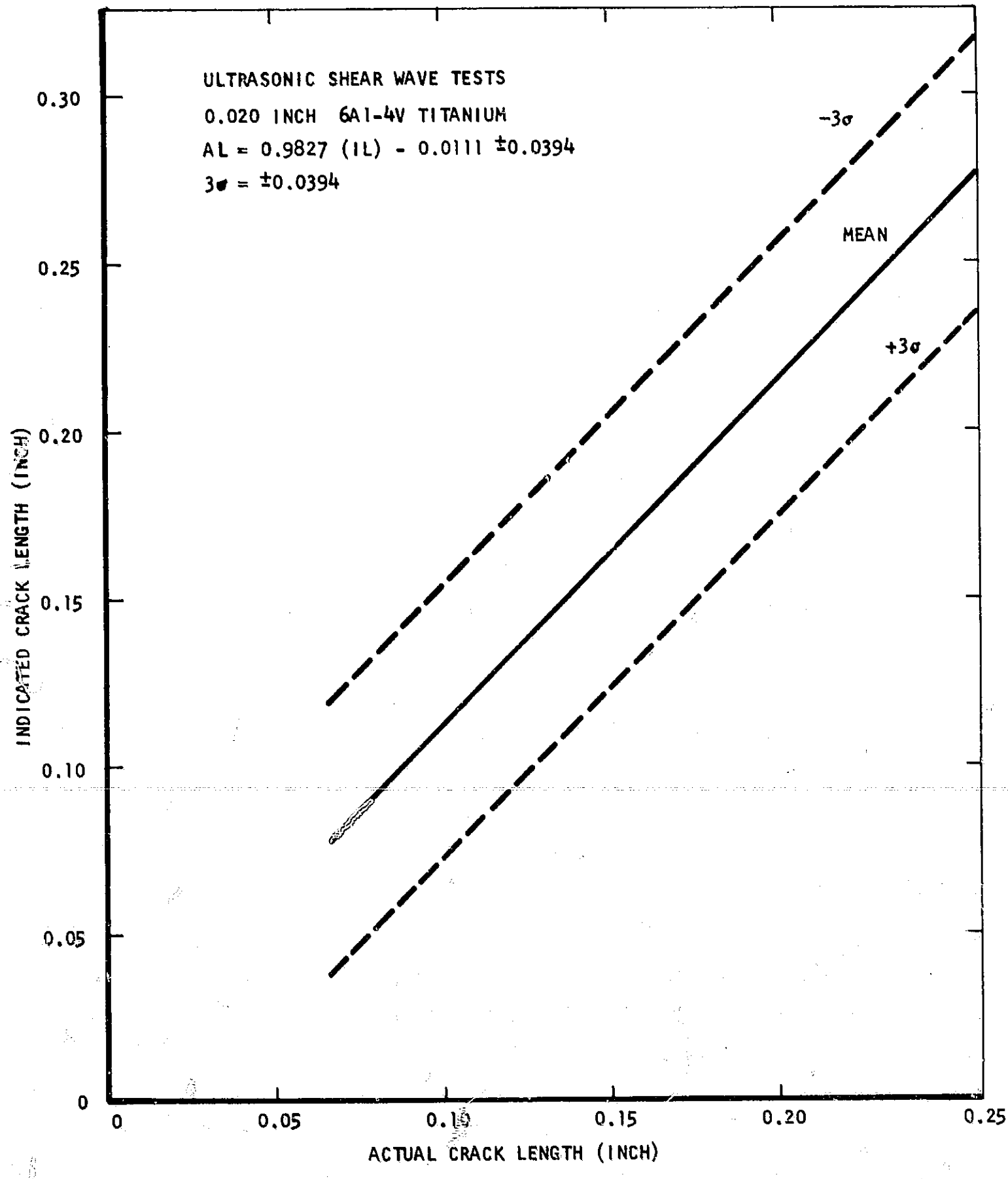

Figure 58. Indicated crack length for ultrasonic shear wave tests as a function of actual crack length for fatigue cracks in 0.020-inch 6A1-4V titanium.

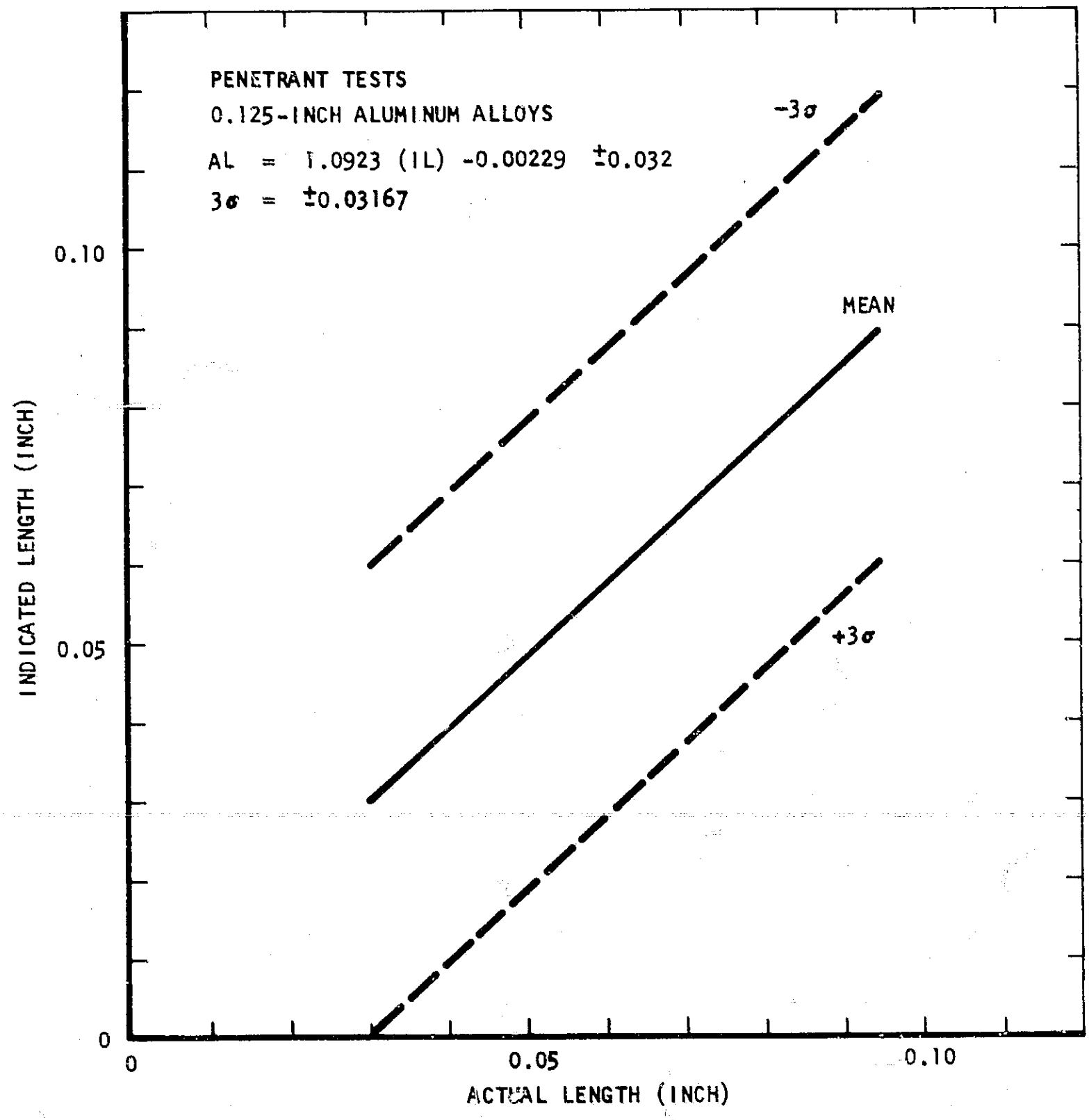

Figure 59. Indicated crack length for fluorescent penetrant tests as a function of actual crack length for fatigue cracks in 0.125-inch aluminum alloys.

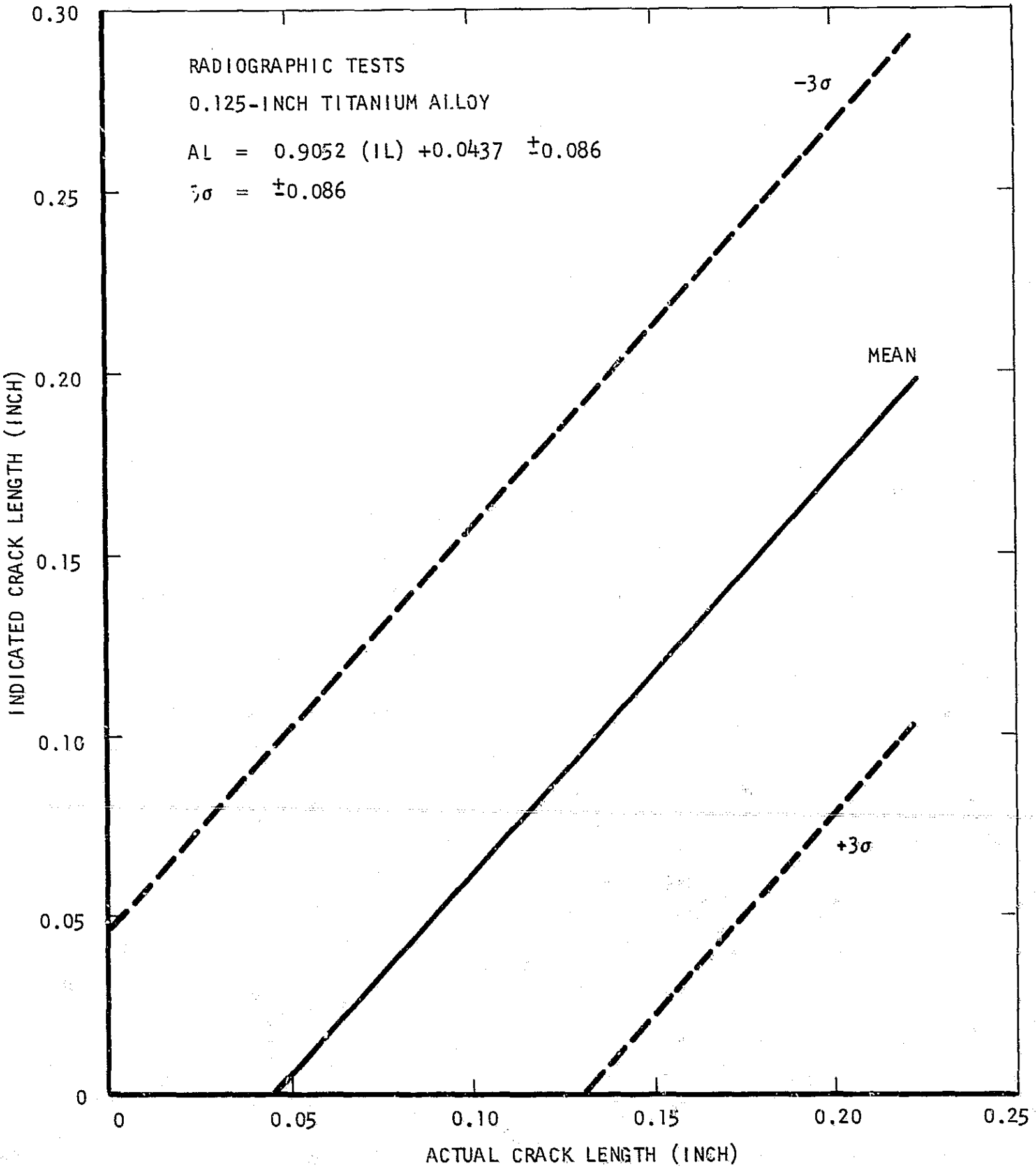

Figure 60. Indicated crack length for radiographic tests as a function of actual crack length for fatigue cracks in 0.125-inch titanium alloys.

5833 a

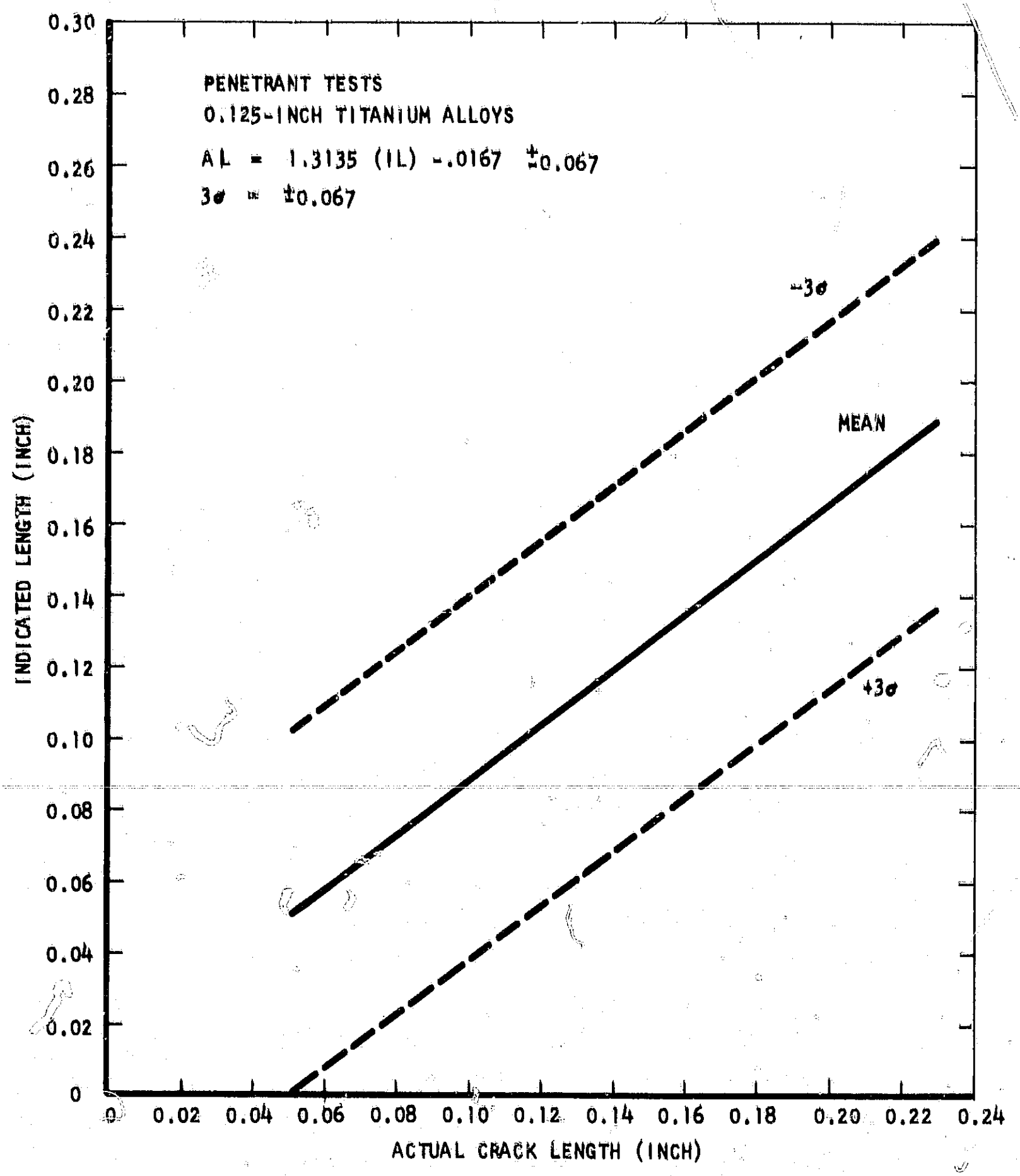

Figure 61. Indicated crack length for fluorescent penetrant tests as a function of actual crack length for fatigue cracks in 0.125-inch titanium alloys.

The crack-length accuracy determinations for this latter alloy are comparable to the best results achieved with the penetrant tests, although the penetrant test has a lower maximum crack-length value for a zero indicated crack-length. Crack-length data for the ultrasonic shear-wave tests on 5Al-2.5Sn titanium alloy are plotted in Figure 62, and crack-depth results in Figure 63 for the increment measurement. The accuracy of the depth measurement is ±0.015-inch with a maximum actual crack-depth at zero indicated crack-depth of 0.034-inch.

Delta tests results correlated with the actual crack-length for both alloys and for the 5Al-2.5Sn alloy alone, and for crack-depth in the 6Al-4V alloy, as tabulated below:

Crack Length, both Ti Alloys	Al = 1.168(IL)-0.046±0.105
Crack Length, 5Al-2.5Sn	AL = 1.014(IL)-0.024±0.081
Crack Depth, 6Al-4V	AD = 0.170(ID)+0.004±0.020

Although the maximum crack-lengths detectable at a zero indicated value are approximately the same in both instances, better results were obtained for crack-length measurements in the other nondestructive tests at this thickness. The crack-depth measurement in the 6Al-4V alloy, however, is the only measurement with any accuracy. Some property of the material such as variable acoustic attenuation appears to be affecting the ultrasonic test results. The 5Al-2.5Sn titanium alloy does not appear to be affected as much as the 6Al-4V alloy.

A summary of the results of the NDT tests on the 0.125-inch materials is shown in Table XXIX. The best test for crack length appears to be the penetrant test in both materials. No method provides reliable results for crack depth in the aluminum alloys. The ultrasonic shear-wave increment measurement produces the best results in the measurement of crack depth in the 5Al-2.5Sn titanium alloy, and the delta test in the 6Al-4V alloy.

The use of the data presented in the previous figures should be discussed at this point. By reference to Table V for the 0.125-inch thick 5Al-2.5Sn titanium alloy and Table XXIX for the measurement correlations, at an aspect ratio of 0.1, the critical crack depth is 0.022-inch while the corresponding length is 0.222-inch. Since the maximum crack depth for an indicated zero reading is 0.034-inch from Figure 63, this test cannot adequately resolve cracks of critical depth.

The critical defect parameter must revert back to the minimum crack length for a maximum crack depth. From Table V, the minimum crack length for a 0.5 aspect ratio is 0.098-inch. To insure that all cracks above 0.098-inch are detected, from Figure 61, only indicated penetrant crack lengths below approximately 0.040-inch can be tolerated in this alloy for operating conditions at -423°F. Different environments, which change the critical crack lengths and depths, will permit the use of other maximum defect lengths. Since no accurate method for crack-depth measurement exists in either of the titanium alloys, the smallest critical crack length must be chosen. For the 6Al-4V alloy, the 0.077-inch minimum crack length from Table V allows cracks giving indications smaller than 0.020-inch to be tolerated at the -423°F temperature. Designers may want to establish some additional safety factors, and this discussion is only intended to show how these data would be used. It will be necessary to establish test results on a large number of samples before these tests can be applied in practice.

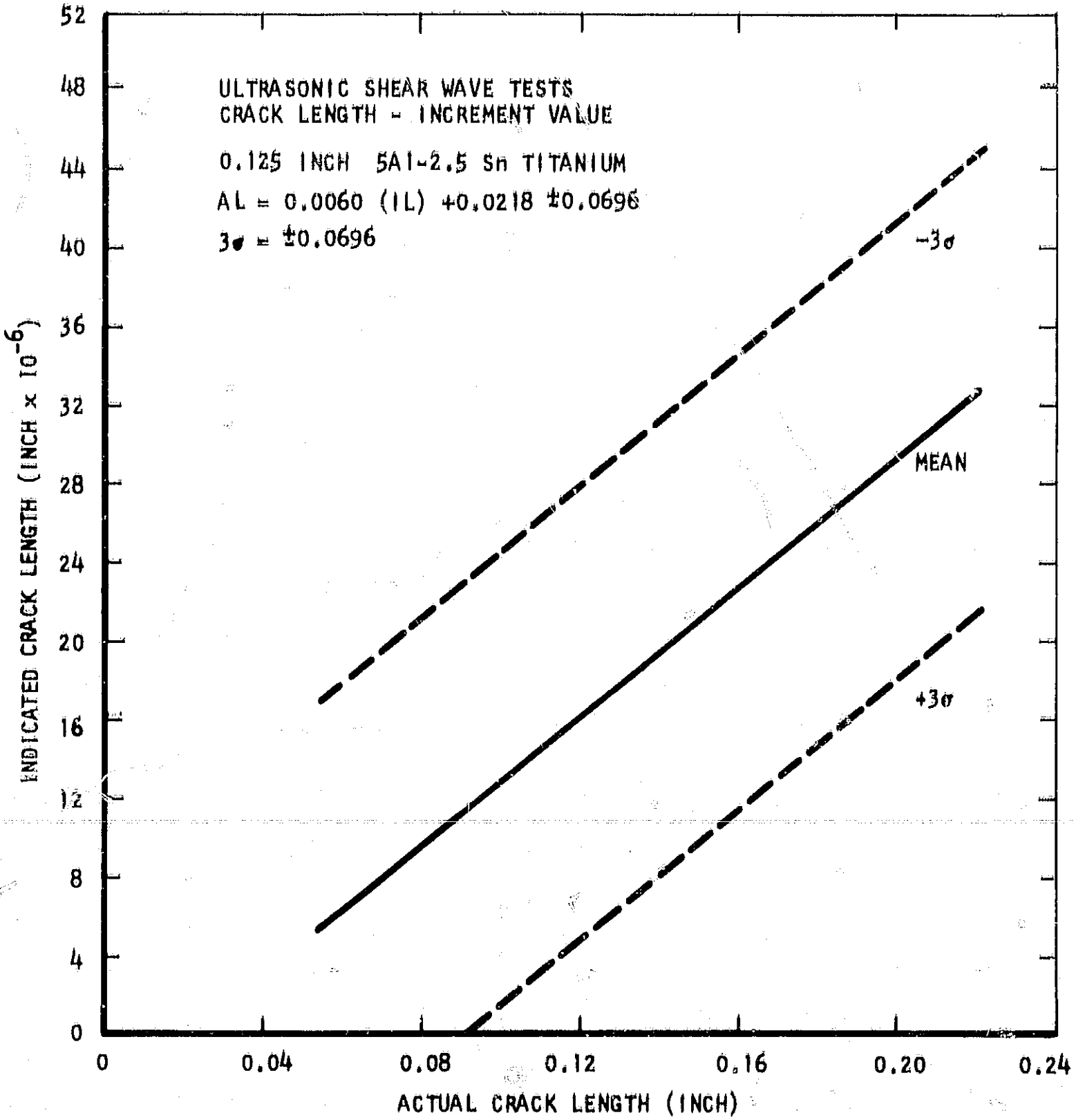

Figure 62. Indicated crack length for ultrasonic shear wave tests as a function of actual crack length for fatigue cracks in 0.125-inch 5Al-2.5Sn titanium.

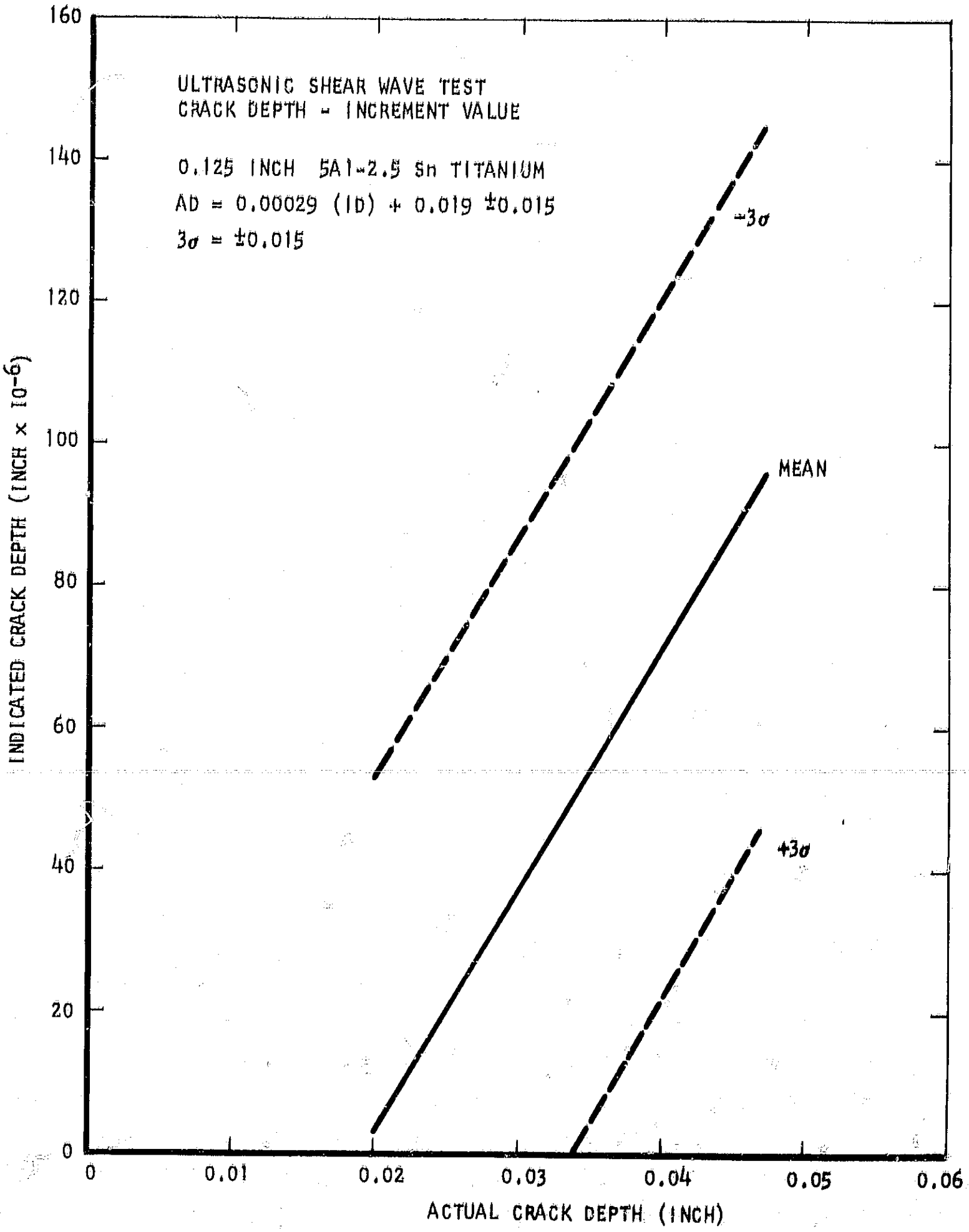

Figure 63. Indicated crack depth for ultrasonic shear wave tests as a function of actual crack depth for fatigue cracks in 0.125-inch 5Al-2.5Sn titanium.

TABLE XXIX

SUMMARY OF NONDESTRUCTIVE TEST CRACK MEASUREMENTS
ON 0.125-INCH SPECIMENS

Test Method	Material	Crack Measurement	Equation (Inch)	3σ Limit (Inch)
Radiography	Aluminum	L	No correlation	-
	Titanium	L	AL=0.9052(IL)+0.044	±0.086
Penetrant	Aluminum	L	AL=1.0923(IL)-0.002	±0.032
	Titanium	L	AL=1.3135(IL)-0.017	±0.067
Ultrasonic Shear Wave	Aluminum	L	No correlation	-
		D	No correlation	-
	Titanium 6Al-4V	L	No correlation	-
		D	No correlation	-
	5Al-2.5Sn	L	AL=0.00601(IL)+0.022	±0.070
(Increment)		D	AD=0.00029(ID)+0.019	±0.015
(Area Value)		D	AD=0.00165(ID)+0.009	±0.024
Delta Ultrasonic	Aluminum	L	No correlation	-
		D	No correlation	-
	Titanium	L	AL=1.168(IL)-0.046	±0.105
		D	No correlation	-
	6Al-4V	L	No correlation	-
		D	AD=0.170(ID)+0.004	±0.020
	5Al-2.5Sn	L	AL=1.014(IL)-0.024	±0.081
		D	No correlation	-

L = Length
D = Depth
AL = Actual Length
IL = Indicated Length
AD = Actual Depth
ID = Indicated Depth

3. 0.500-Inch Specimens

The penetrant tests on the 0.500-inch thick aluminum specimens were unsuccessful with none of the cracks being detected. The radiographic crack-length measurements as correlated with the actual crack-length data are plotted in Figure 64. The maximum actual crack length for a zero indicated crack length is approximately 0.460-inch with a 3σ limit from the mean of ±0.237-inch. The only shear-wave measurement which showed any correlation was the crack-length measurement illustrated in Figure 65. The 3σ limit is approximately the same as for the radiographic tests but the maximum crack-length at zero indicated crack length is 0.278-inch. The only delta test with a significant correlation for the aluminum alloy defect measurements was also on crack length. The 3σ variation for the 2219 aluminum alloy is ±0.319-inch as illustrated in Figure 66. More significant, however, the delta test data imply that the lower 3σ limit does not have a positive maximum actual crack-length for zero indicated length. The limited test data for crack lengths from 0.3 to 0.6-inch do not justify projecting the -3σ limit much lower than the 0.3-inch actual crack length.

For the penetrant test results on the 0.500-inch titanium, plotted in Figure 67, the 3σ limit is ±0.021-inch while the maximum crack length for zero indicated crack length is 0.025-inch. In the radiographic tests, the results were poor with none of the fatigue cracks being detected. The results of ultrasonic shear-wave tests indicated that again the two titanium alloys should be analyzed separately. However, since there were only three 6Al-4V titanium specimens, no significant correlations could be developed for this alloy. The results of the ultrasonic shear-wave tests for determining crack length in 5Al-2.5Sn titanium specimens are plotted in Figure 68. Also plotted are the actual data points for this alloy and three points for the 6Al-4V alloy. The 6Al-4V data established a trend of their own and fall either outside or near the +3σ limit. The 3σ variation for this test on the 5Al-2.5Sn alloy is ±0.073-inch, while the maximum crack length at zero indicated length is 0.150-inch. A correlation of input signal strength for an 80 percent screen height to actual crack length produced comparable results to the measured increment results.

To analyze the defect depth measurements, three quantities were correlated with actual depth with the results listed below:

AD IN INCH UNITS

(INCREMENT)	AD = 0.000914(ID) + 0.027 ±0.042
(AREA VALUE)	AD = 0.000245(ID) + 0.025 ±0.058
(INPUT SIGNAL)	AD = 0.025575(ID) + 0.030 ±0.042

The increment value, shown in Figure 69, has a slight preference because of the lower maximum actual crack depth (0.069-inch) at zero indicated depth. These results are not as accurate as those on the 0.125-inch titanium specimens.

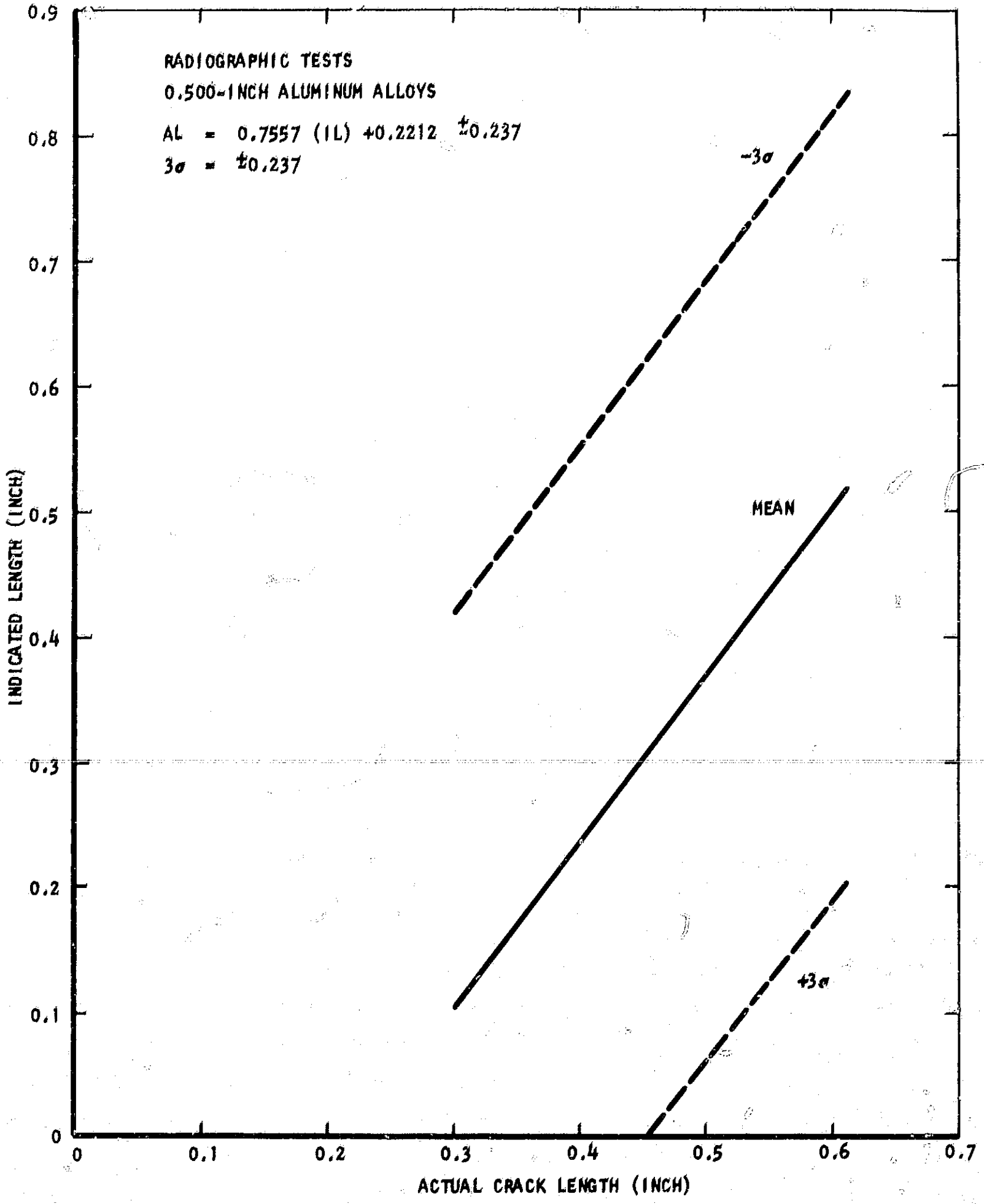

Figure 64. Indicated crack length for radiographic tests as a function of actual crack length for fatigue cracks in 0.500-inch aluminum alloys.

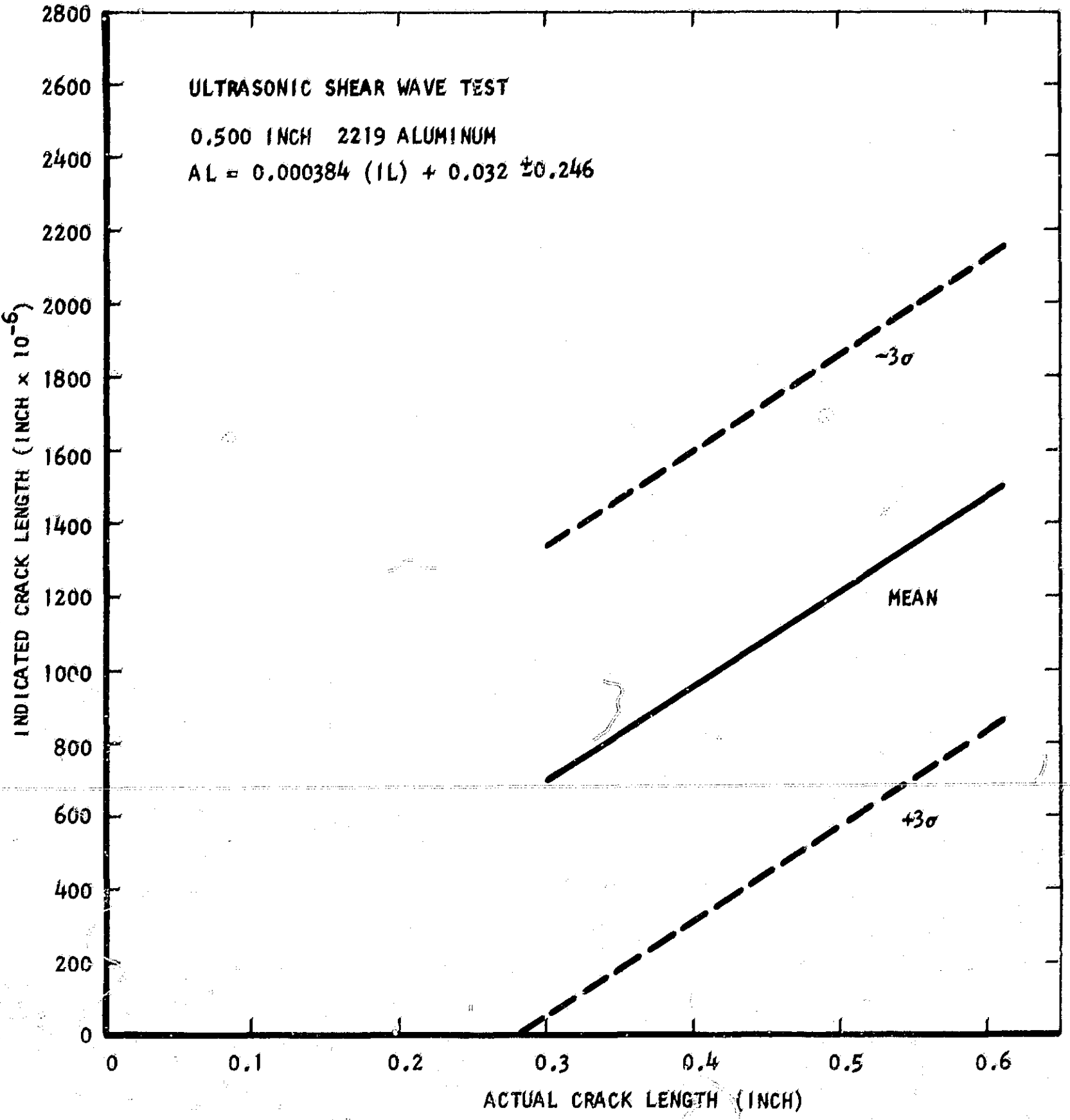

Figure 65. Indicated crack length for ultrasonic shear wave tests as a function of actual crack length for fatigue cracks in 0.500-inch 2219 aluminum.

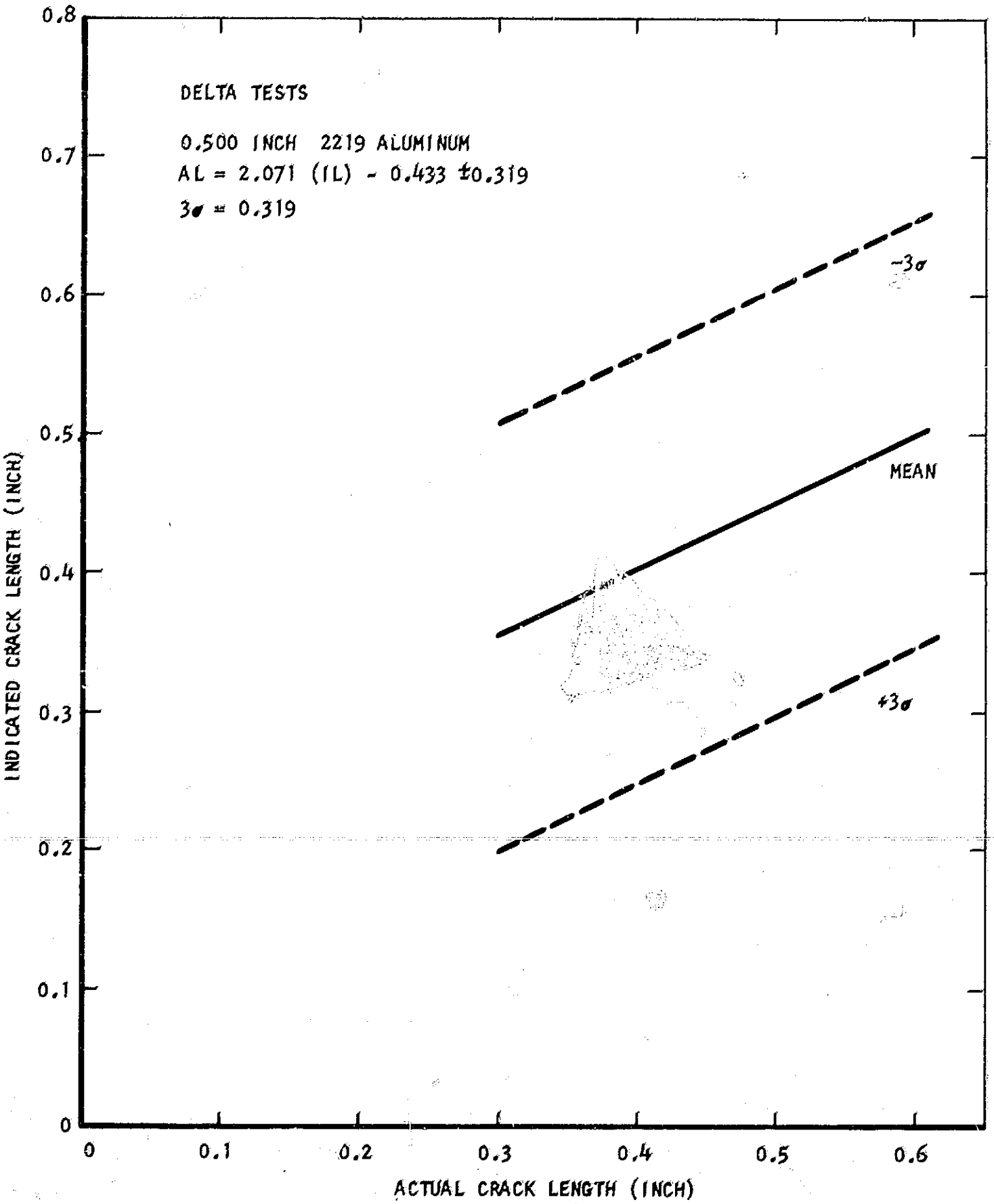

Figure 66. Indicated crack length for delta tests as a function of actual crack length for fatigue cracks in 0.500-inch 2219 aluminum.

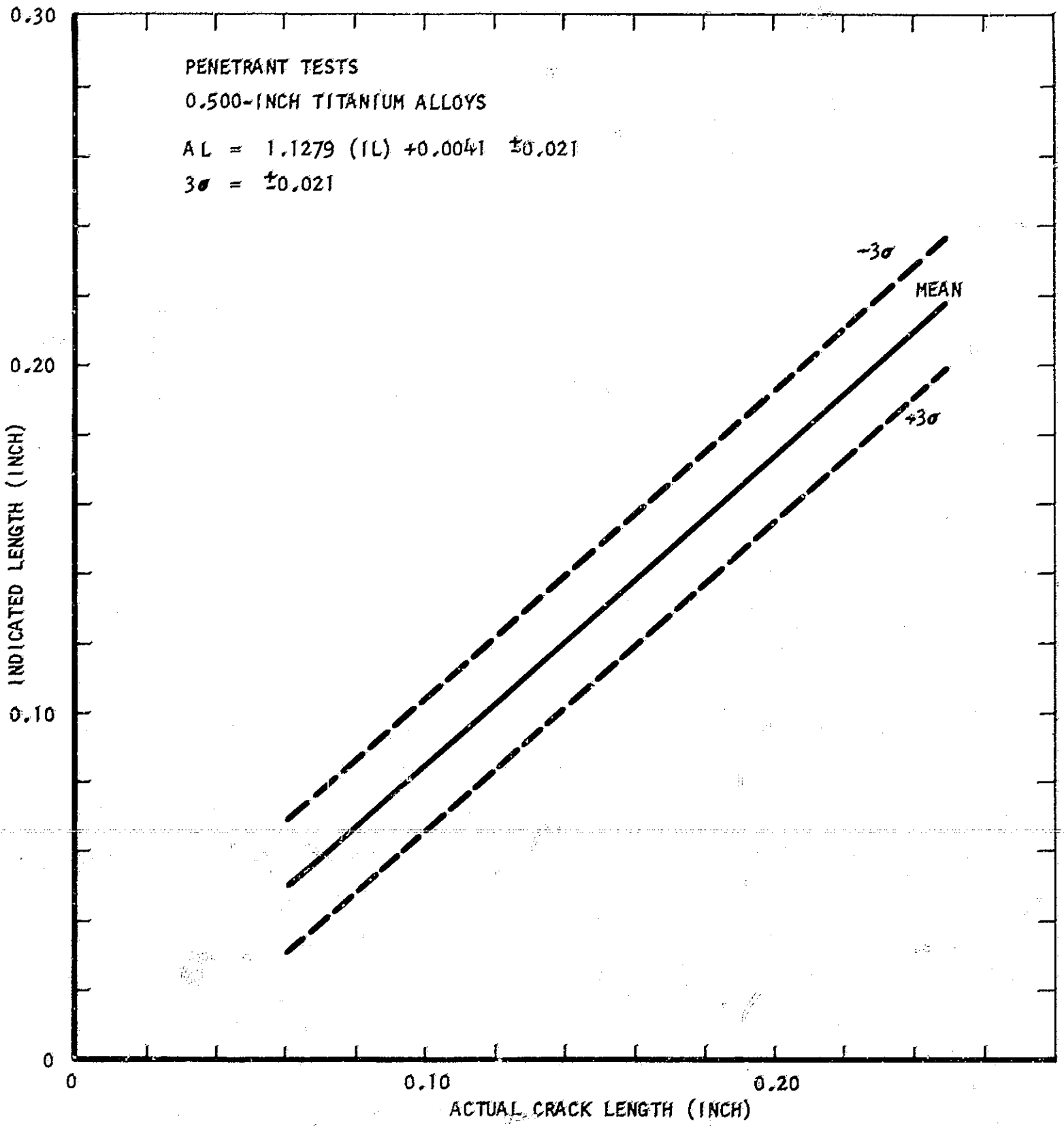

Figure 67. Indicated crack length for fluorescent penetrant tests as a function of actual crack length for fatigue cracks in 0.500-inch titanium alloys.

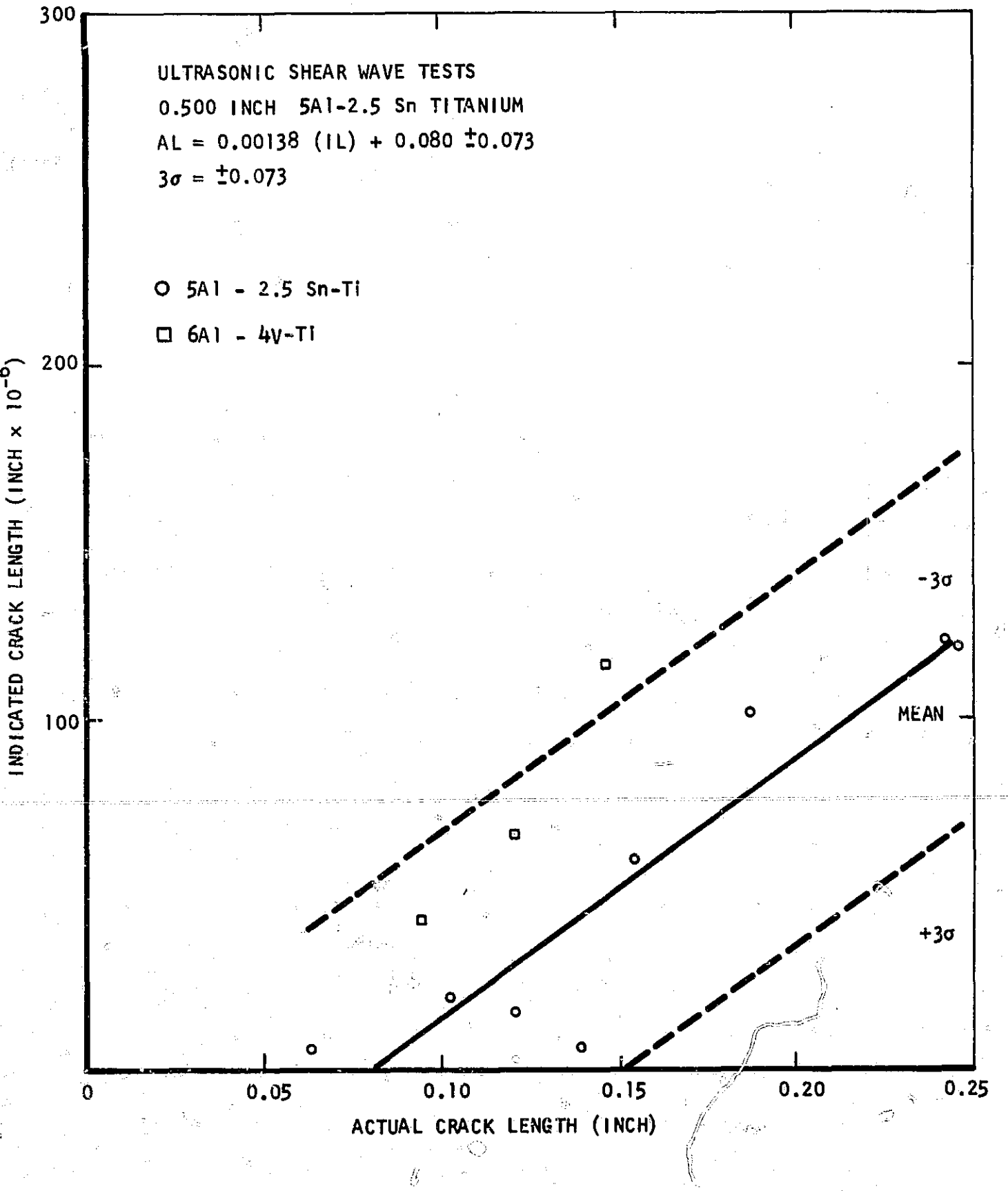

Figure 68. Indicated crack length for ultrasonic shear wave tests as a function of actual crack length for fatigue cracks in 0.500-inch 5Al-2.5Sn titanium.

5828 B

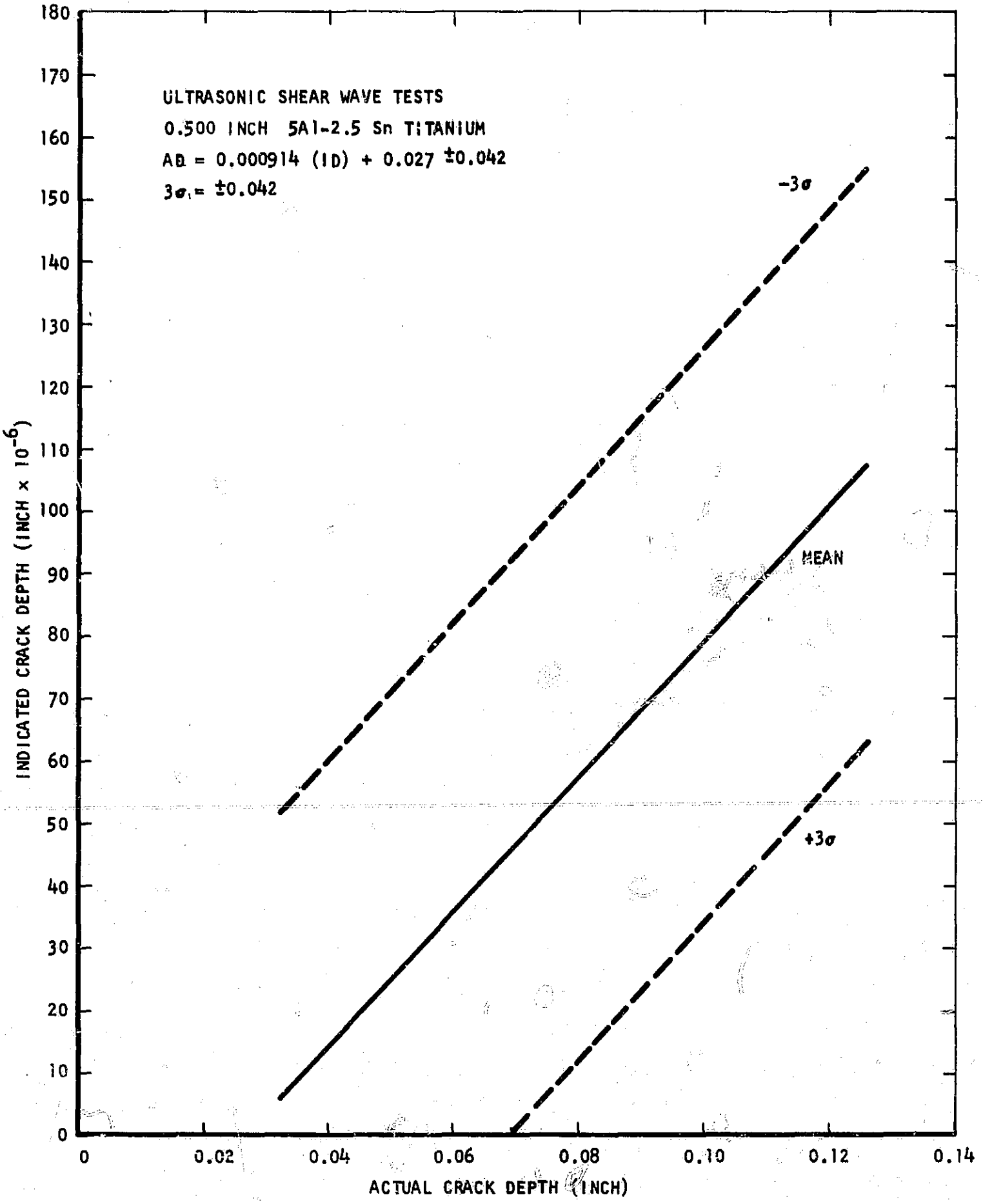

Figure 69. Indicated crack depth for ultrasonic shear wave tests as a function of actual crack depth for fatigue cracks in 0.500-inch 5Al-2.5Sn titanium.

The delta-test results as correlated for actual crack length on all 0.500-inch titanium alloys, produced comparable results to data generated for the 5Al-2.5Sn alloy alone. Defect depth data for the 5Al-2.5Sn alloy correlated significantly with actual defect depth as listed below:

All Titanium Alloys	$AL = 1.105(IL) - 0.035 \pm 0.125$
5Al-2.5Sn Ti	$AL = 0.813(IL) + 0.033 \pm 0.125$
5Al-2.5Sn Ti	$AD = 0.302(ID) + 0.009 \pm 0.090$

Although the length measurements have comparable 3σ variations, the maximum crack length at zero indicated crack length is only 0.090-inch for the correlation based on all the titanium alloy specimens. This is an improvement over the accuracy of the shear-wave tests. The crack-length data for the delta tests are plotted in Figure 70 for all titanium alloys, while the depth data are presented in Figure 71 for the 5Al-2.5Sn alloy only.

The results of the nondestructive tests performed on the 0.500-inch fatigue crack specimens are summarized in Table XXX. Both delta and shear-wave tests appear capable of resolving the actual crack lengths in the aluminum alloys. From Table IV, the critical crack length for operation at -423°F is approximately 0.520-inch for both alloys at an 0.5 aspect ratio. With the scatter band present for the ultrasonic tests of the 2219 aluminum alloy, much smaller cracks would be rejected part of the time in order to insure that cracks of 0.520-inch or larger would be rejected. The delta tests show about the same results as the radiographic tests. The accuracy of the tests for aluminum are not good and need improvement, however, the good fracture toughness of these alloys compensates for the poor measurement accuracy. One of the sources of error in the measurement undoubtedly is traceable to the cracks themselves. Most of the 2219 alloy cracks delaminated near the tip of the crack and this effect undoubtedly affected the response of the two ultrasonic test methods. The delaminated condition is shown for three aluminum alloy fatigue cracks in Figure 72. Two cracked specimens showing the delamination are of 2219 aluminum, while the third specimen is of 2014 aluminum.

For the titanium alloys, the crack-depth measurements are again poor. Therefore, the minimum crack length, 0.098-inch as given in Table V for 5Al-2.5Sn titanium must be used as the rejection criteria. Since the penetrant tests for titanium had the best accuracy, penetrant indicated crack lengths below 0.060-inch are acceptable while actual crack lengths above 0.056-inch must occasion- alloy be rejected because of the 3σ limits. For 6Al-4V alloys, a 0.077-inch minimum crack length is acceptable so that indicated crack lengths below 0.046-inch can be tolerated; this will result in some instances in actual crack lengths as small as 0.035-inch being rejected because of the measurement variability.

4. 1.000-Inch Specimens

The penetrant tests on the 1.0-inch fatigue-crack samples did not detect any cracks. The radiographic test results, plotted in Figure 73 show a 3σ variation of ±0.164-inch, while the zero indicated crack-length reading may mean actual cracks as long as 0.210-inch. The test data are limited since only six fatigue-crack specimens were made at this thickness and the

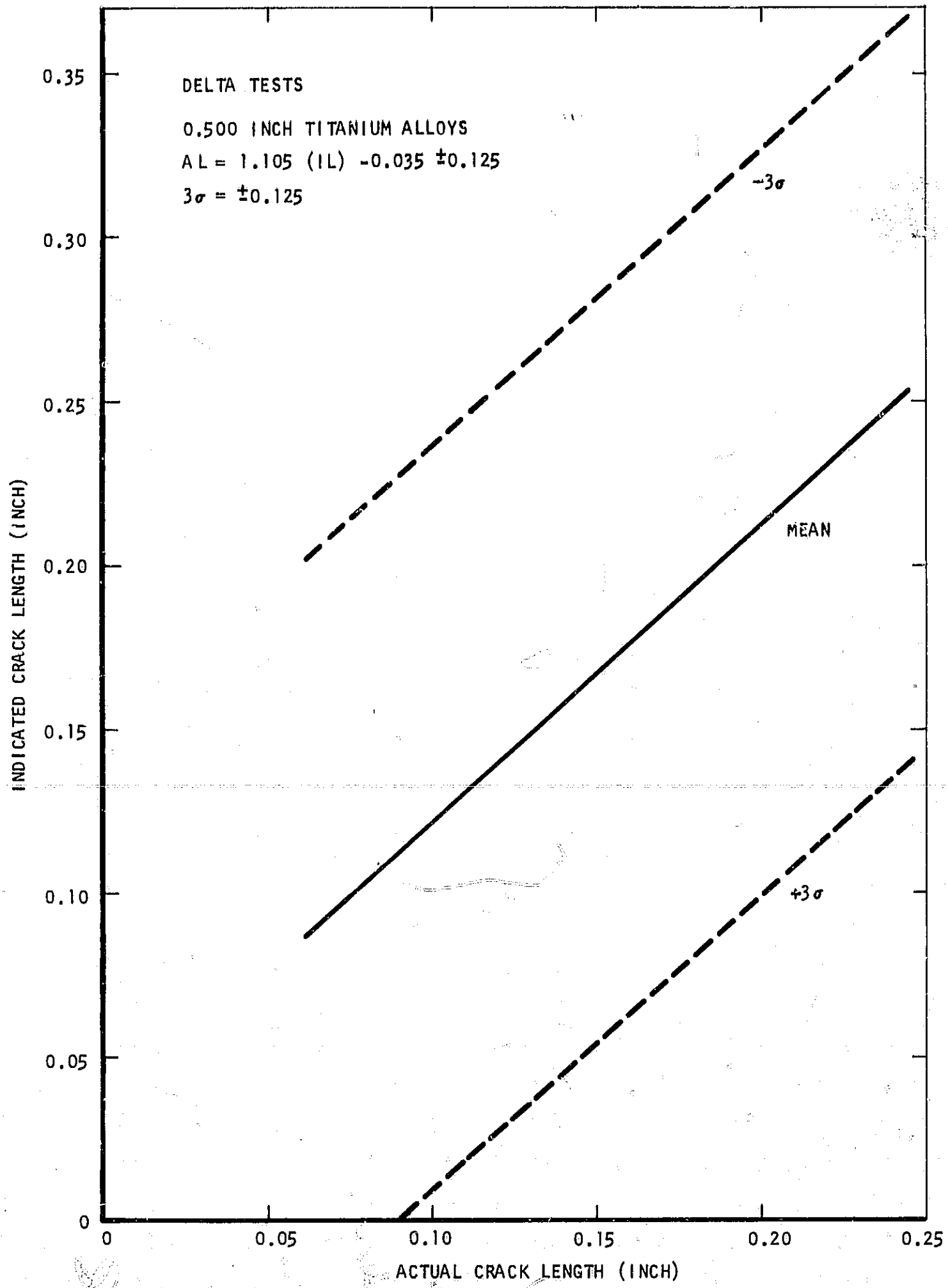

Figure 70. Indicated crack length for delta tests as a function of actual crack length for 0.500-inch titanium alloys.

5843 B

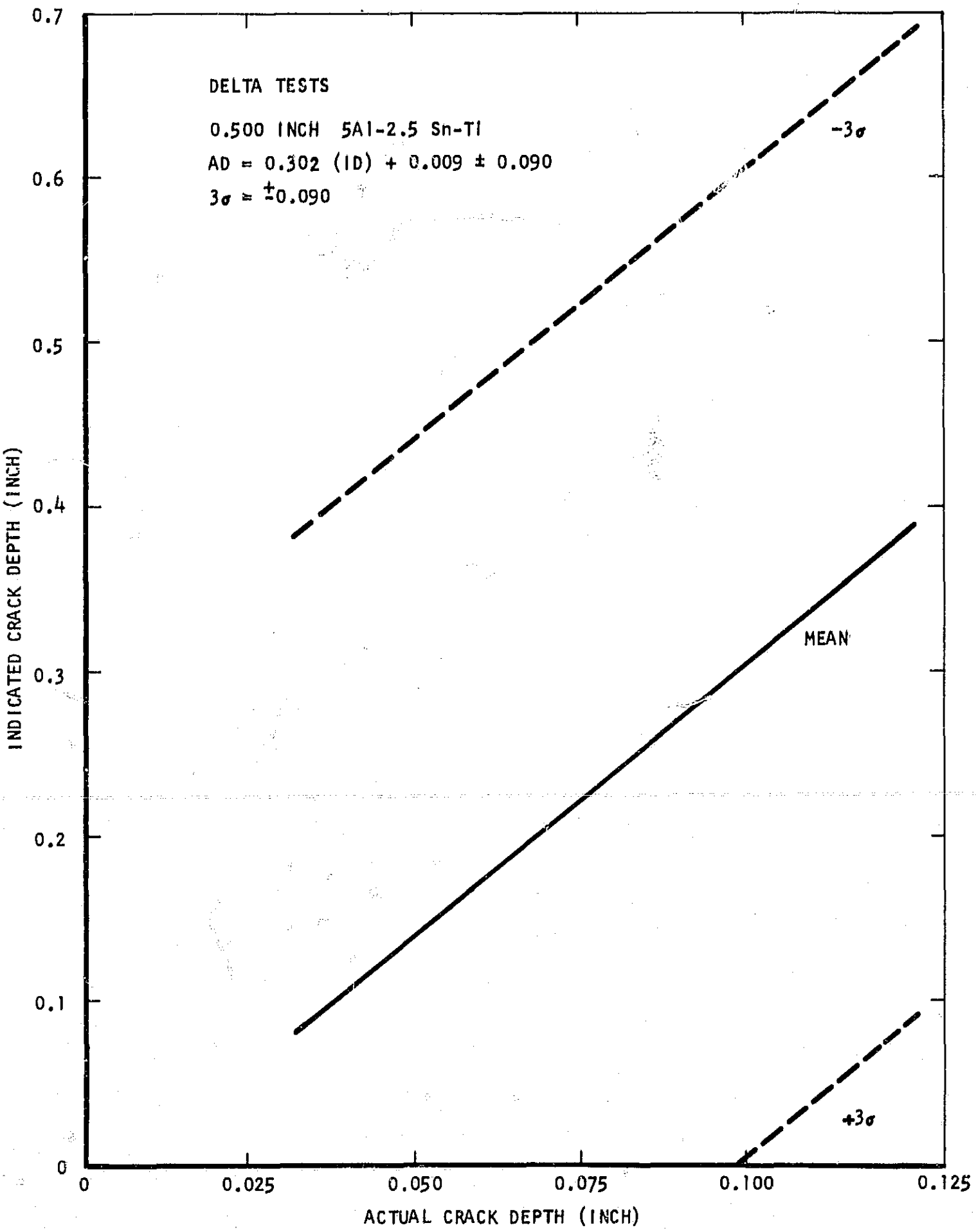

Figure 71. Indicated crack depth for delta tests as a function of actual crack depth for 0.500-inch 5Al-2.5V titanium.

5842 8

TABLE XXX

SUMMARY OF NONDESTRUCTIVE TEST CRACK MEASUREMENTS
ON 0.500-INCH SPECIMENS

Test Method	Material	Crack Measurement	Equation (inch)	3σ Limit (inch)
Radiography	Aluminum	L	AL=0.7557(IL)+0.221	±0.237
	Titanium	L	No Indicated Data	-
Penetrant	Aluminum	L	No Indicated Data	-
	Titanium	L	AL=1.1279(IL)+0.004	±0.021
Ultrasonic Shear Wave	Aluminum-2219	L	AL=0.000384(IL)+0.032	±0.246
		D	No correlation	-
	-2014	L&D	Insufficient Number of Specimens	
	Titanium			
(Increment)	5Al-2.5Sn	L	AL=0.00138(IL)+0.080	±0.073
(Input Signal)		L	AL=0.05021(IL)+0.071	±0.079
(Increment)		D	AD=0.000914(ID)+0.027	±0.042
(Area Value)		D	AD=0.000245(ID)+0.025	±0.058
(Input Signal)		D	AD=0.025575(ID)+0.030	±0.042
	6Al-4V	L&D	Insufficient Number of Specimens	
Delta Ultrasonic	Aluminum-2219	L	AL=2.071(IL)-0.433	±0.319
		D	No correlation	
	-2014	L&D	Insufficient Number of Specimens	
	Titanium	L	AL=1.105(IL)-0.035	±0.125
	5Al-2.5Sn	L	AL=0.813(IL)+0.033	±0.125
		D	AD=0.302(ID)+0.009	±0.090
	6Al-4V	L&D	Insufficient Number of Specimens	

L = Length
D = Depth
AL = Actual Length
IL = Indicated Length
AD = Actual Depth
ID = Indicated Depth

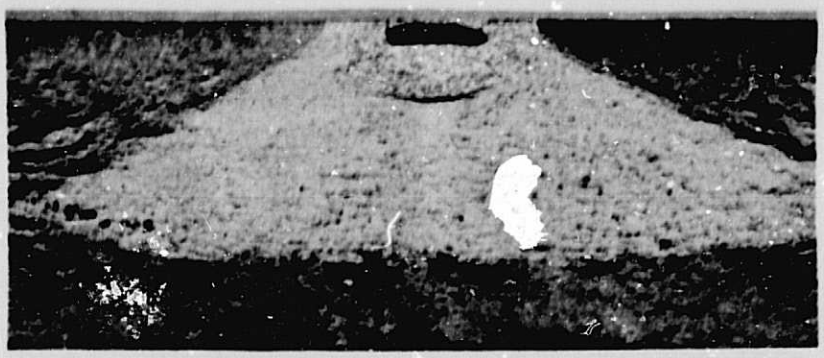

a

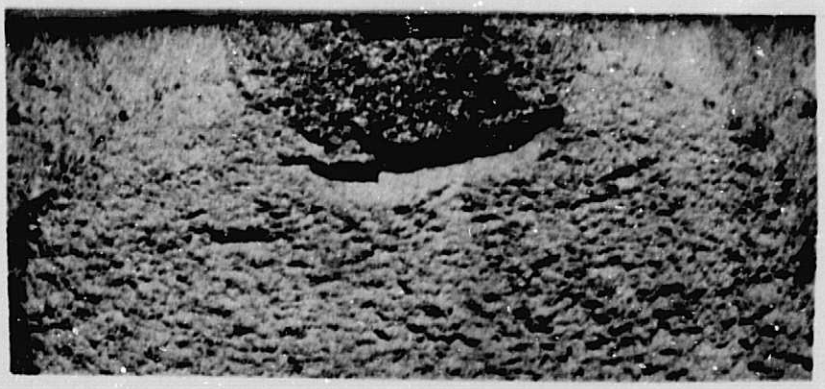

b

c

Figure 72. Macrographs of fracture surfaces of specimens 2219-0.5-3(a), 2219-1.0-3(b) and 2014-0.5-2(c) at 3X.

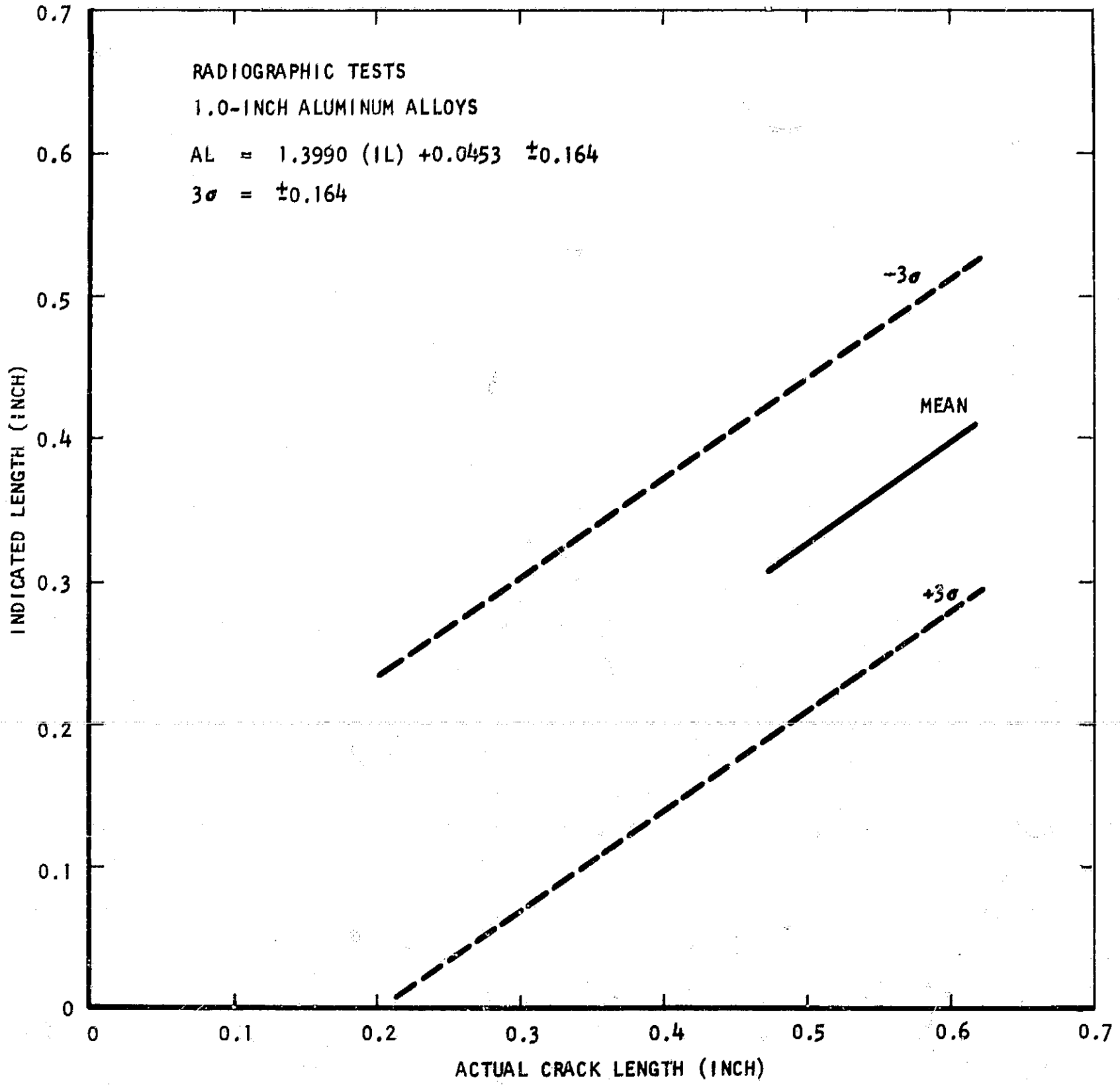

Figure 73. Indicated crack length for radiographic tests as a function of actual crack length for 1.0-inch aluminum alloys.

defect lengths ranged from 0.45-inch to slightly over 0.6-inch. Neither the delta nor the shear-wave tests provided any significant correlations.

The minimum critical crack length from Table IV of 0.52-inch would mean that cracks having indicated lengths smaller than 0.230-inch could be tolerated, while actual crack lengths as low as 0.2-inch would be rejected part of the time. Better accuracy tests are definitely needed for the aluminum alloys.

B. Discussion

The results of the ultrasonic shear-wave tests on the detection of defects under stress may provide a partial explanation for the results, in general, of the ultrasonic tests. Variable stress conditions cause rather large differences in the signal levels and therefore in the determination of defect dimensions. Improved measurement methods are necessary for the accurate determination of crack depth in both aluminum and titanium alloys, and of crack length in the aluminum alloys. Stress conditions on the defect will affect both the shear-wave and delta test results. To further complicate things, the delamination problems in the 2219 aluminum fatigue cracks create additional measurement inaccuracy.

New or improved test methods are necessary whose responses are not sensitive to stress and reflection conditions at an interface. For example, the shear-wave test results were quite complicated on weld specimens because of the defect locations and because of the intimate contact of base metal surfaces in the incomplete penetration defects. A test is necessary which measures the defect dimensions independent of location and which also provides an accurate definition of defect location. Such a test may be possible with a through-wave ultrasonic test. Additional work appears necessary on this measurement approach.

The limitations in the accuracy of the present ultrasonic test might be improved by a different approach to the measurement. From the data analysis, it appears that the integration measurement was not as good as the increment measurement. Fixed signal levels might be better to use in judging the length and depth measurements rather than attempting to put the crack data in absolute units. In addition, some method will be necessary to compensate for attenuation differences between specimens of the same alloy. Separate analyses of crack measurements were necessary for ultrasonic tests on titanium alloys.

The penetrant test results provided the most accurate length measurement correlations on titanium, and 0.020 and 0.125-inch aluminum fatigue-crack specimens. However, the test accuracy on the aluminum specimens became unacceptably poor as section thickness increased. Cracks were not resolved by the penetrant test in the 0.5 and 1.0-inch thicknesses.

Other accurate methods of crack length and depth measurement are desirable so that two or more measurements can confirm the dimensions of a crack. The radiographic tests, although not accurate enough in most of the specimens, did provide measurement data for the 0.5 and 1.0-inch aluminum specimens where other test methods were ineffective. The radiographic tests were not sensitive to the delamination problem in the aluminum alloys since the delaminations occur parallel to the plate surfaces and do not present any change of thickness or density to the radiation beam.

The data generated in the defect correlations on the various specimen thicknesses and alloys aresummarized in Table XXXI for defect length and in Table XXXII for defect depth. The data can be compared directly in these tables without having to refer to the main text. When satisfactory comparative data were generated for a particular group of alloys; i.e., either aluminum or titanium, it was not necessarily repeated for the individual alloys within the group in these tables.

TABLE XXXI

SUMMARY OF MAXIMUM CRACK LENGTHS POSSIBLE FOR ZERO INDICATED CRACK LENGTHS AND TEST ACCURACIES FOR THE VARIOUS NONDESTRUCTIVE TESTING TECHNIQUES ON THE FOUR ALLOYS AND FOUR SECTION THICKNESSES*

		Maximum Crack Length for Zero Indicated Length and ± 3 σ Limit*							
		Radiographic		Penetrant		Ultrasonic Shear		Ultrasonic Delta	
Thickness	Alloy	MCL	± 3 σ	MCL	± 3 σ	MCL	± 3 σ	MCL	± 3 σ
0.020	2014 & 2219 Al	* *	* *	0.040	0.036	0.048	0.062	-	-
0.020	6-4 & 5-2.5 Ti	0.069	0.051	0.032	0.027	0.097	0.084	-	-
0.020	6Al-4V-Ti	-	-	-	-	0.051	0.039	-	-
0.125	2014 & 2219 Al	* *	* *	0.029	0.032	* *	* *	* *	* *
0.125	6-4 & 5-2.5 Ti	0.130	0.086	0.050	0.067	-	-	0.061	0.105
0.125	6Al-4V-Ti	-	-	-	-	* *	* *	* *	* *
0.125	5Al-2.5Sn-Ti	-	-	-	-	0.092	0.070	0.057	0.081
0.500	2014 & 2219	0.458	0.237	* *	* *	-	-	-	-
0.500	2014 Al	-	-	-	-	***	***	***	***
0.500	2219 Al	-	-	-	-	0.278	0.246	-0.114	0.319
0.500	6-4 & 5-2.5-Ti	* *	* *	0.025	0.021	* *	* *	0.090	0.125
0.500	6Al-4V-Ti	-	-	-	-	***	***	***	***
0.500	5Al-2.5Sn-Ti	-	-	-	-	0.153	0.073	0.158	0.125
1.000	2014 & 2219 Al	0.210	0.164	* *	* *	* *	* *	* *	* *

* All dimensions in inches * * No correlation *** Insufficient sample

MCL - Maximum crack length at zero indicated length

TABLE XXXII

SUMMARY OF MAXIMUM CRACK DEPTHS POSSIBLE FOR ZERO INDICATED CRACK DEPTHS AND TEST ACCURACIES FOR THE ULTRASONIC SHEAR AND DELTA TESTING TECHNIQUES ON FOUR ALLOYS AND THREE SECTION THICKNESSES

		Maximum Crack Depth for Zero Indicated Depth and ± 3σ Limit*					
		Ultrasonic Shear (Increment)		Ultrasonic Shear (Area)		Ultrasonic Delta	
Thickness	Alloy	MCD	± 3 σ	MCD	± 3 σ	MCD	± 3 σ
0.125	2014 & 2219 Al	* *	* *	* *	* *	* *	* *
0.125	6Al-4V-Ti	* *	* *	* *	* *	0.024	0.020
0.125	5Al-2.5Sn-Ti	0.034	0.015	0.033	0.024	* *	* *
0.500	2014 Al	***	***	***	***	***	***
0.500	2219 Al	* *	* *	* *	* *	* *	* *
0.500	6-4 & 2.5 Ti	* *	* *	* *	* *	* *	* *
0.500	6Al-4V-Ti	***	***	***	***	***	***
0.500	5Al-2.5Sn-Ti	0.069	0.042	0.083	0.058	0.099	0.090
1.000	2014 & 2219 Al	* *	* *	* *	* *	* *	* *

* - All dimensions in inches

* * - No correlation

*** - Insufficient sample

MCD - Maximum crack depth at zero indicated length

V - CONCLUSIONS

Four nondestructive testing techniques have been evaluated for determining critical defect dimensions in 2014 and 2219 aluminum and ELI 5Al-2.5Sn and 6Al-4V titanium alloys. The most accurate nondestructive test to measure crack dimensions was shown to be the penetrant test for crack lengths in 0.020, 0.125 and 0.500-inch thick titanium, and in 0.020 and 0.125-inch thick aluminum alloys. The penetrant tests were not successful in revealing any defects in the 0.5 and 1.0-inch aluminum specimens. Radiographic and ultrasonic tests provided some defect measurement accuracy in the thicker aluminum alloys but this accuracy was not sufficient in view of the required critical defect measurements. Various measurement accuracies were achieved for each thickness, alloy and test method.

Since penetrants only provide information on the surface defect length, and no accurate methods were revealed for defect depth determinations, the minimum crack length determined from fracture toughness calculations must be used as the rejection criteria with these test methods. The accuracy of the ultrasonic tests for crack depth, as well as the maximum possible value of actual crack depths for zero indicated crack depths, limited their use for crack depth measurement. More accurate techniques of crack-depth measurement are necessary for both the titanium and aluminum alloys.

The evaluation of the effects of stress on crack detectability revealed that rather large differences can occur in the signal strength of the ultrasonic wave reflected from a defect as a function of various stress levels. Varying residual stresses in the vicinity of crack defects may account for the low accuracy of the ultrasonic tests for both crack depth and length measurements. Other sources of measurement variability probably can be attributed to acoustic attenuation differences due to the metallurgical structure in the titanium alloys and to the cracks themselves. The relative position of the flaw within the thickness of the material also provides a response variation to the ultrasonic tests. Test methods are necessary which are capable of measuring the defect dimensions unaffected by stress states on the defect and which provide this information independent of any corrections for the location of the defect. The position of the defect in the material must be accurately determined since its location in relation to the external surfaces will affect its fracture toughness criticality.

The use of present nondestructive tests is limited for critical crack measurements. Improved testing techniques are necessary in order to achieve better measurement accuracy. These test methods should provide for measurement of both the defect length and depth so that both values can be used in the determination of a particular defect's effect on a material's performance.

VI - REFERENCES

1. P.F. Packman, H.S. Pearson, J.S. Owens and G.B. Marchese, "The Applicability of Fracture Mechanics-Nondestructive Testing Design Criterion", AFML-TR-68-32, May 1968.

2. R.C. McMaster, editor, Nondestructive Testing Handbooks, Vols. I and II, Ronald Press, 1959.

3. C.E. Betz, Principles of Penetrants, Magnaflux Corporation, 1963.

4. W.E. Thomas, "Analytic Approach to Penetrant Performance", Materials Evaluation, Vol. 21, No. 6, 1963.

5. R.B. McCauley and Q. Van Winkle, "Research to Develop Methods for Measuring the Properties of Penetrant Flaw Inspection Materials", WADD-TR-60-520, Part III, February 1963.

6. H.N. Skoglund and C. Magdalin, "Gillespian Approach to Penetrability", Materials Evaluation, Vol. 26, No. 12, 1968.

7. W.B. Campbell and R.C. McMaster, "Derivation of Penetrant-Developer Resolution", Materials Evaluation, Vol. 25, No. 5, 1967.

8. E.O. Lomerson, "Statistical Method for Evaluating Penetrant Sensitivity and Reproducibility", Materials Evaluation, Vol. 27, No. 3, 1969.

9. M.L. Rhoten, "Research on Radiographic Techniques of Graphite Evaluation", ML-TDR-64-277, Air Force Materials Laboratory, November 1964.

10. Industrial Radiography, Agfa-Gevaert Company, 1966 Edition.

11. A.J. Stevens, "Effects of Source and Specimen Dimensions on Resolution in Gamma Radiography", Nondestructive Testing, Vol. 11, No. 8, 1953.

12. J.P. Mitchell, M.L. Rhoten and R.C. McMaster, "X-ray Image System for Nondestructive Testing of Solid Propellant Missile Case Walls and Weldments", Watertown Arsenal, WAL 142,5/1.5, August 1962.

13. T.H. Rogers, "Uses of Low Voltage X-ray Tubes with Thin Beryllium Windows", Vol. 11, No. 2, 1953.

14. J. and H. Krautkrämer, Ultrasonic Testing of Materials, Springer-Verlag, 1969.

15. F.A. Firestone, "Flaw detecting device and measuring instrument", United States Patent 2,280,226.

16. J. Krautkrämer, "Ultrasonic Weld Testing in Europe and the Attitude of Technical Control Authorities", Nondestructive Testing, Vol. 20, No. 5, 1962.

REFERENCES (Cont'd.)

17. F.C. Parker, "Ultrasonic Weldment Inspections Currently in Use", Nondestructive Testing, Vol. 20, No. 6, 1962.

18. J.E. Bobbin, "Ultrasonic Weld Inspection", Nondestructive Testing, Vol. 17, No. 1, 1959.

19. J.E. Bobbin, "Ultrasonic Weld Inspection - A Status Report", Nondestructive Testing, Vol. 18, No. 3, 1960.

20. A. DeSterke, "Weld Inspection by Ultrasonics", Materials Evaluation, Vol. 22, No. 1, 1964.

21. R.B. Socky, "The Use of Ultrasonics in Fatigue Testing", Materials Evaluation, Vol. 22, No. 11, 1964.

22. B.T. Cross and W.M. Tooley, "Advancement of Ultrasonic Techniques Using Re-radiated Sound Energies for Nondestructive Evaluation of Weldments", Automation Industries Report TR 67-53, AD 659033, August 30, 1967.

23. B.T. Cross, K.J. Hannah and W.M. Tooley, "The Delta Technique - A Research Tool; A Quality Assurance Tool", Automation Industries TR 68-11.

24. G.R. Irwin, "Crack Extension Force for a Part-Through Crack in a Plate", Journal of Applied Mechanics, 29, Trans. ASME, 84, December 1965.

25. J.E. Boyd and S.B. Folk, Strength of Materials, Fifth Edition, McGraw-Hill, 1950.